Development of Ag_2S/PEI Theranostic Nanoparticles

by

DİDAR AŞIK

A Thesis Submitted to the
Graduate School of Engineering
in Partial Fulfillment of the Requirements for
the Degree of

Master of Science
in
Materials Science and Engineering

Koc University

July 2015

Koc University

Graduate School of Sciences and Engineering

This is to certify that I have examined this copy of a master's thesis by

Didar Aşık

and have found that it is complete and satisfactory in all respects,
and that any and all revisions required by the final
examining committee have been made.

Committee Members:

_____

Havva Funda Yağcı Acar, Ph. D. (Advisor)

_____

Uğur Ünal, Ph. D.

_____

Devrim Gözüaçık, MD, Ph. D.

Date: _____

ABSTRACT

In this study, biocompatible, heavy metal free and cationic Ag_2S quantum dots (QDs) which luminesce in the medical range (700-900 nm) were synthesized with a mixed coating comprised of a small thiolated molecule such as 2-mercaptopropionic acid (2MPA) or L-Cyseine (Cys) and linear polyethyleneimine (PEI) at 2.5kDa and 25kDa molecular weights, instead of the branched 25kDa PEI, which is the golden standard for gene delivery, since it is less toxic.

QDs coated with only linear PEI do not luminesce. However, QDs with the mixed coating, benefit from a synergy and are more luminescent than the 2MPA coated Ag_2S which is known as one of the best luminescent Ag_2S QDs in the literature. Quantum yield of 2MPA/PEI coated Ag_2S QD (2MPA/PEI (2.5kDa): 20/80) is 310 % with respect to LDS 798 NIR dye. This is the highest quantum yield reported till today. Although a significant reduction in the luminescence intensity is observed over time, even after 8 months, the luminescence intensity is still quite high. Optical imaging studies of these QDs with HeLa cell line and C.elegans model organisms showed that these QDs can be strong optical labels and can be successfully used in optical imaging.

In this study, the effect of pH during and after the reaction was also investigated. The strongest luminescence was detected in an acidic (pH 5) and the weakest luminescence was seen in basic environment (pH 10). Changes in the pH did not cause any shift in the emission wavelength of the 2MPA/PEI coated QDs but Cys/PEI coated QDs experienced a shift towards longer wavelengths at acidic pH.

In vitro cytotoxicity of these cationic Ag_2S QDs were determined in HeLa, HCT116 (p53-) and HCT116WT cells. Overall, 2MPA/PEI coated quantum dots are less toxic than Cys/PEI coated ones and the onset of toxicity is 7.5 μg/mL Ag dose. Significantly toxic dose of Cys/PEI coated Ag_2S QDs is 7.5 μg/mL Ag in HeLa, 1.8 μg/mL Ag in HCT116WT and 18 μg/mL Ag in HCT116(p53-) cells. These doses are sufficient to test these particles in drug delivery and medical imaging studies. In

addition, the intracellular uptake of the QDs were determined and correlated with the toxicity data. Effect of particle size and surface charge on the intracellular uptake was also investigated.

Overall, strongly luminescent, cationic Ag_2S NIR QDs were successfully prepared with the mixed coating comprised of L-PEI/2MPA and L-PEI/Cys at both low and high molecular weights. QDs are small in size and colloidally stable, which is crucial for any *in vivo* application. They have been demonstrated as strong optical probes for medical imaging.

ÖZET

Bu çalışmada, gen tedavisi için, medikal bölgede ışıyabilen (700-900nm) ve ağır metal içermeyen, biyouyumlu ve katyonik Ag_2S kuantum noktacıkları 2MPA ve Cys gibi tiyol içeren küçük moleküller ile, altın standart olarak bilinen dallı 25kDa`luk dallı PEI yerine daha az toksik olan lineer PEI in hem yüksek (25kDa) hem de düşük (2.5kDa) moleküler ağırlıklarda karıştırılmasıyla elde edilmiştir.

Lineer PEI tek başına kullanıldığında ışımaya sahip KNlar üretememektedir. Ancak, karışık kaplamaların kuantum noktacıkların ışıma şiddetinde sinerjistik bir etki yarattığı ve bu parçacıkların literatürde yer alan ve en iyi ışıyan Ag_2S kuantum noktacıklarından biri olan 2MPA kaplı Ag_2S kuantum noktacıklarından bile şiddetli ışıdığı görülmüştür. 2MPA/PEI kaplı kuantum noktacığının (2MPA/PEI (2.5kDa): 20/80) kuantum verimi LDS 798 yakın kızılötesi boyası ile karşılaştırıldığında % 310 bulunmuştur. Bu şimdiye kadar görülmemiş derecede yüksek bir değerdir. Zaman geçtikçe bu ışıma şiddetinin düştüğü görülse de yaklaşık 8 ay sonrasında bile çok şiddetli ışımaya sahip oldukları gözlemlenmiştir. HeLa hücre hattı ve c.elegans model organizmaları ile yapılan optik görüntüleme çalışmaları geliştirilen bu Ag_2S kuantum noktacıklarının kuvvetli optik etiketler olabileceği ve optik görüntülemede başarılı olacağını göstermiştir.

Çalışmada sentez pH ı ve sentez sonrası ortam pH`ının optik özelliklere etkisi de incelenmiştir. Parçacıklardan en şiddetli ışıma asidik pH (5) ortamında, en zayıf ışıma ise bazik pH (10) da görülmüştür. 2MPA/PEI kaplı kuantum noktacıklarında pH değişimi floresan ışıma dalgaboyunda bir kayma yaratmazken, Cys/PEI kaplı kuantum noktacıklarında ise pH ın düşmesiyle yüksek dalgaboylarına kayma görülmüştür.

Geliştirilen kuantum noktacıklarının in vitro toksisite çalışmaları HeLa, HCT116(p53-) ve HCT116WT hücrelerinde test edildi. Genel olarak 2MPA/PEI kaplı kuantum noktacıklarının Cys/PEI kaplı olarlardan daha az toksik oldukları ve toksik etkinin 7.5 µg/mL Ag dozunda başladığı belirlendi. Cys/PEI kaplı kuantum

noktacıklarının önemli ölçüde toksik oluğu değerler ise HeLa hücre hattında 7.5 µg/mL Ag, HCT116(p53-) hücre hattında 1.8 µg/mL Ag ve HCT116WT hücre hattında 1 µg/mL Ag olarak tespit edildi. Bu dozlar, parçacıkların ilaç taşıma ve tıbbi görüntüleme çalışmaları için yeterli dozlardır. Ayrıca parçacıkların hücre içi alımları ICP metoduyla belirlenilerek, toksisite ile korelasyonu, parçacık büyüklüğü, yüzey yükü gibi değerlerin, hücre alımına etkileri incelendi.

Özet olarak, L-PEI/2MPA ve L-PEI/Cys karışık kaplaması olan katyonik ve yakın kızılötesi bölgesinde güçlü ışımaya sahip Ag_2S kuantum noktacıkları hem yüksek hem de düşük moleküler ağarlıklardaki L-PEI ile başarıyla sentezlenmiştir. Bu KN`lar küçük ve kolloidal olarak kararlıdır. Bu da her tür canlı çalışması için çok gerekli bir özelliktir. Bu nanoparçacıkların medical görüntülemede kuvvetli optic etiketler olarak kullnaılabileceği de gösterilmiştir.

DEDICATION

This thesis is dedicated to Kerem Acar and Şirin Acar
who gave me the happiness of being their big sister

ACKNOWLEDGEMENTS

There are special people without them this thesis is not possible. First of all, I would like to thank especially to my advisor Assoc. Prof. H. Funda Yağcı Acar. I am sure that without her I would not want to study or manage as much as I do. Since Organic Chemistry lecture, I have admired her mother hen character, executive group leadership, positive endless energy and teaching style. I felt very lucky to be in her group since the first day. In 2008, I left my family in Bursa. I got out of my comfort zone and started to Koç University. Then in 2011, I started to live with my other family because of her. It is so difficult to thank her, because she is not only my advisor also the part of my family.

In addition, I would like to thank my thesis committee Assoc. Prof. Uğur Ünal and Assoc. Prof Devrim Gözüaçık.

I would like to thank to Tubitak for funding and my project partners Dr. Rouhollah Khodadust for his academic experience and Fatma Demir for her perfect friendship and support when I needed.

I would thank to Assoc. Prof. Özgür Birer for the handmade PL instrument, Assist. Prof. Halil Bayraktar for microscopy training, Assist. Prof Funda Şar and Fatma Sevde Coşkun for c.elegans studies.

I am indebted to members of Funtech, especially to my big sister Yasemin Yar for being with me even at the most difficult times and when I became the most difficult person in the world. I would like to thank Emek Göksu Durmuşoğlu for giving me his positive energy every time and my thesis angel Özlem Ünal for her friendship and for the times that we have laughed for hours. I would like thank also to Dr. İbrahim Hocaoğlu for his support and friendship and Hande Öztürk for her mentorship during my firsy year in Funtech. Also, I would like to thank Enes Buz, İrem Ülkü, Pelin Turhan, Emre Köken, Emre Nakay and Çağnur Celaloğlu and all other members of Funtech. I will be always proud of being a member of Funtech.

I would also like to thank KUYTAM, especially to Dr. Barış Yağcı and Cansu Yıldırım for their patience and support.

I am indebted to my friends in MASE program, especially to Eylül Saraç, Dr Ceren Yılmaz, Sinem Ertaş and Armen Yıldırım for their friendship and coffee breaks.

I would like to thank science lounge team Ayşe Ruçoğlu and Pınar Akdeniz for their help and hot tea.

I would like to thank my helpmates Benay Uzer, Çiğden Altıntaş and Özge Soyoğul for their patience for seven years, for sisterhood, love and support all the time. Without them, everything would be much more difficult for me.

I am indebted to especially Kerem Acar and Şirin Acar. They gave me the happiness of being their big sister. They give me life energy and great motivation.

I would like to specially thank to my parents Hülya Aşık and Adnan Aşık and also all members of my big family for their endless love and support.

TABLE OF CONTENTS

LIST OF TABLES

LIST OF FIGURES

NOMENCLATURE

2MPA	2-Mercaptopropionic Acid
bp	Base pair
bPEI	Branch Polyethyleneimine
Cys	Cyseine
Da	Dalton
DAPI	Diamidino-2-phenylindole dihydrochloride
DLS	Dynamic light scattering
DMEM	Dulbecco's Modified Eagle Medium
DMSA	Dimercaptosuccinic acid
DMSO	Dimethyl sulfoxide
DNA	Deoxyribonucleic acid
DOX	Doxorubicin
EBR	Exciton Bohr Radius
Eqn	Equation
EtOH	Ethanol
FA	Folic Acid
FBS	Fetal Bovine Serum
FTIR	Fourier Transformed Infra-Red
FWHM	Full Width At Half Maximum
GFP	Green fluorescent protein
HCT116	Human colon carcinoma
HeLa	Human cervical carcinoma
Hz	Hertz

ICP-MS	Inductively Coupled Plasma – Mass Spectrometer
ICP-OES	inductively coupled plasma optical emission spectrometry
IR	infrared
KB	Human contaminant carcinoma
kDa	Kilo Dalton
LDS 798	4-[4-[4-(dimethylamino)phenyl]-1,3-butadienyl]-1-ethyl quinolinium perchlorate
lPEI	Linear Polyethyleneimine
MAA	Methacrylic Acid
MPA	Mercaptopropionic Acid
MTT	(3-(4,5-dimethylthiazol-2-yl)-2,5-diphenyltetrazolium bromide)
MW	Molecular weight
NIH3T3	Mouse Embryo Fibroblast Cell Line
NIR	Near-infrared
PBS	Phosphate buffered saline
PEG	Polyethylene glycol
PEI	Polyethyleneimine
PL	Photoluminescence
QDs	Quantum Dots
QY	Quantum Yield
si-RNA	Small interfering RNA
TAA	Thioacetamide
TEM	Transmission electron microscopy
TOPO	Trioctylphosphine oxide
UV-Vis	Ultraviolet-Visible-Near Infrared
WT	Wild type

Chapter 1

INTRODUCTION

1.1 Quantum Dots

Semiconductor quantum dots (QDs) with special optical and electronic properties are one of the most fascinating nanomaterials and therefore, heavily studied and used by the scientists and engineers over the past two decades.[1] Quantum dots were first discovered in 1981 in a glass matrix by Alexey Ekimov [2] and in colloidal solutions by Louis E. Brus in 1985.[3] Quantum Dots are usually made up of II-VI (i.e. CdS, CdTe, ZnSe, etc), III-V (i.e. GaAs, InP, etc) or IV-VI (i.e. PbS, SnTe, etc) elements with distinctly different chemical and physical properties from the elements that they are made up from.[3] The most widely studied QDs in the literature are the QDs made up of group II-VI (i.e. CdS, CdTe and ZnSe) or III-V (i.e. GaAs, InP) elements. The former set has luminescence in the visible range that is between 400-700 nm (Figure 1.1).

Figure 1.1 Ten different emission colors of visible CdSe/ZnS core/shell QDs under near UV excitation.[4]

Quantum dots are small enough to get into quantum confinement regime.[5] Into the radius of a tennis ball nearly 10 million QDs would fit end to end (Figure 1.2). Although usually they are less than 10 nm, the critical size changes from material to material.[6]

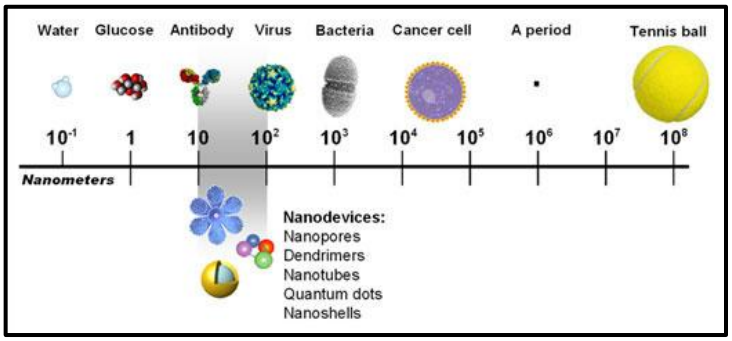

Figure 1.2 Comparative size scale of different molecules, virus, bacteria, a cancer cell, a tennis ball and a Quantum Dot. (http://nano.cancer.gov/media_backgrounder.asp)

Nanotechnology, in general, aim to utilize the unique properties of QDs and to create smart functional materials. Many properties of QDs are size dependent. [1] QDs are restricted in all three dimensions and are spherical. Large surface to volume ratio of these spherical particles becomes very beneficial when surface functionalization is required, especially for bioapplications.[7] Semiconductors with rod or tetrapod shapes have also been reported.[8]

1.2 Size Dependent Energy Band Gap and Fluorescence

The most important feature of the semiconductor materials is their band gap. The width of the band gap determines the type of the materials as a conductor, insulator or a semiconductor. Energy levels are so close to each other in a conductor that they are considered to have continuous energy levels. In semiconductor materials some energy levels are quantum mechanically forbidden and there exists a band gap. Energy levels that are below the band gap are described as the valence and energy levels above the

band gap are described as conduction bands (Figure 1.3). In an insulator material the band gap is large enough to prevent the electron jump from valance to conduction band. The band gap of semiconductor materials is in between the two extremes. In semiconductors, when an electron gains enough energy, it can cross the band gap and reach conduction band leaving a positive hole behind (Figure 1.4).

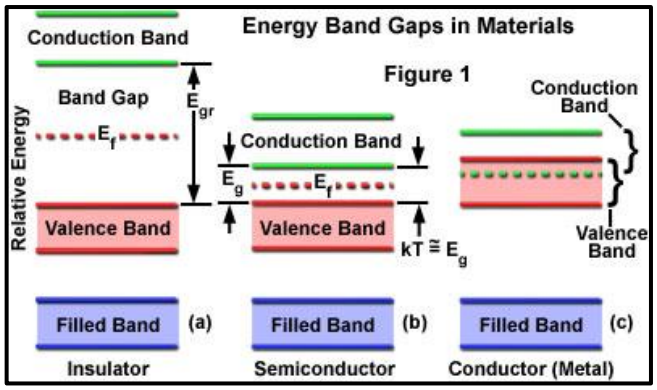

Figure 1.3 The electronic band description in solids (http://www2.warwick.ac.uk/fac/sci/physics/current/postgraduate/regs/mpags/ex5/bandstructure/)

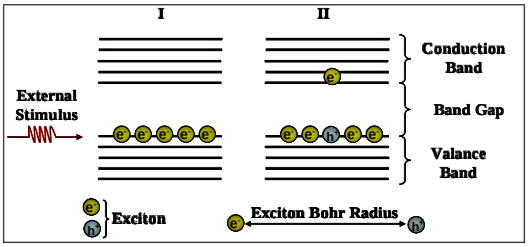

Figure 1.4 Scheme of excited electron in conduction band and the electron hole in valence band (www.evidenttech.com)

Electron excitation can be achieved by an external stimulus like photon flux, voltage or heat. Usually a photon flux is used and the key is that the incoming photon should have energy higher than the band gap energy so that the valance band electron can jump across the band gap. As a result, an electron-hole pair which is called as an

exciton is generated (Figure 1.4). The electron in the conduction band is not stable and relaxes back to the valance band. There are non-radiative and radiative events during this relaxation (Figure 1.5). Non-radiative decay mostly occurs with the loss of heat because of lattice vibrations. Radiative decay is also called as nuclear decay that occurs with photon generation from combination of the electron and the hole. This is called as the *fluorescence.* Due to the energy loss during the excited lifetime, emitted photons have lower energy than the absorbed ones and therefore, emitted photons are at longer wavelengths than the absorbed ones, which is called as the *Stokes Shift* (Figure 1.6).

The distance between the hole and the electron is called *Excitation Bohr Radius* (EBR) (Figure 1.4). To achieve quantum confinement, crystal size of the semiconductor material should not be larger than EBR. When the confinement happens in three dimensions, small semiconductor materials are defined as *quantum dots*. So, while bulk semiconductor materials have continues energy levels, quantum confined QDs have discontinuous energy levels with a size dependent band gap. The band gap of a QD is always larger than the band gap of the bulk form of the same composition and as the size decreases, the band gap of the QD increases (Figure 1.7). This allows size tunable absorption and emission properties, which are the most exploited properties of QDs (Figure 1.8).

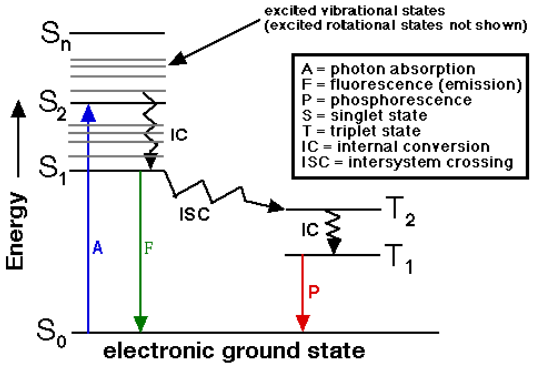

Figure 1.5 Jablonski energy diagram illustrating the absorbance and emission processes (http://www.shsu.edu/chm_tgc/chemilumdir/JABLONSKI.html)

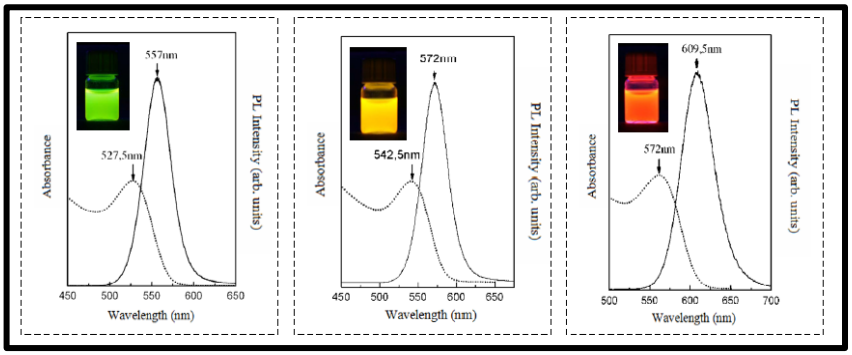

Figure 1.6 Absorption (dotted lines) and photoluminesence (solid lines) spectra of CdTe-MPA QDs showing the Stokes shift. [9]

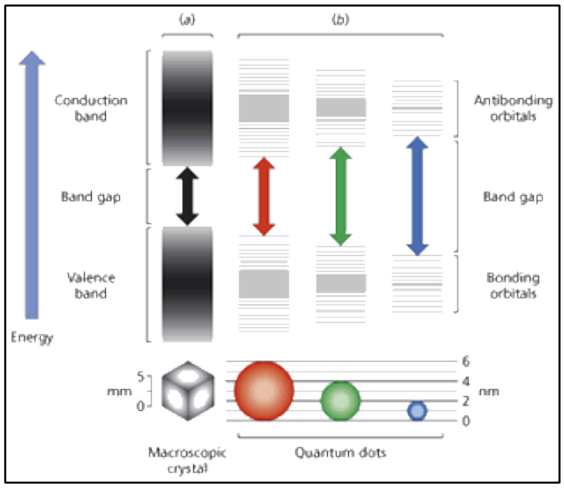

Figure 1.7 Size dependent energy band gap of QDs .[10]

QDs have broad absorption spectrum that allows excitation at any wavelength shorter than their absorption onset which allows excitation of different QDs at the same time at a single wavelength but create size dependent narrow emission peaks at different wavelengths (Figure 1.9). This is an exceptional opportunity when compared to organic fluorophores.

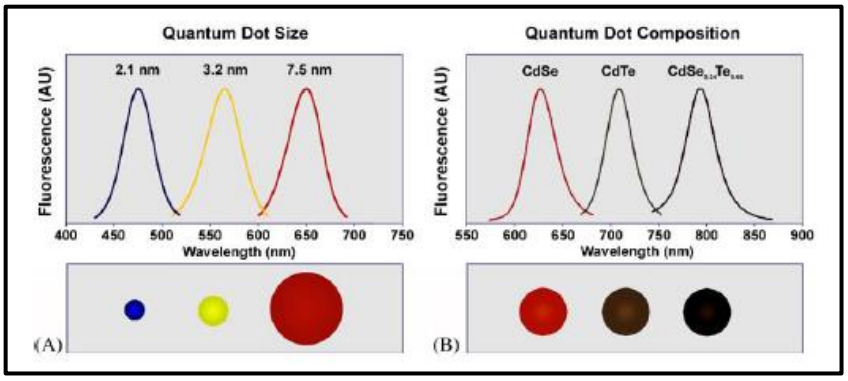

Figure 1.8 QD emission wavelength tunability because of changing nanoparticle size and composition of QDs (A) The emission range (450-650nm) depend on nanoparticle diameters between 2 and 7.5 (B) The emission range (610-800nm) depend on nanoparticle composition. [7]

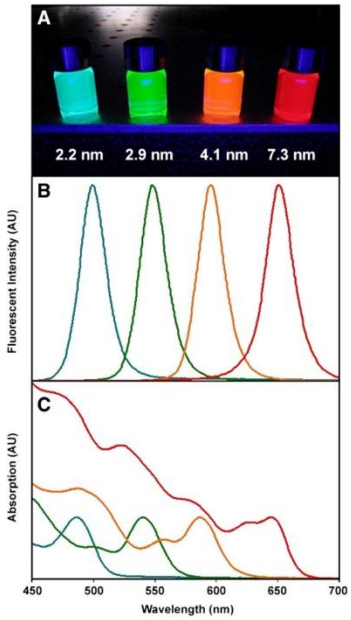

Figure 1.9 (A) Fluorescence image of CdSe (2.2-7.3nm) QDs under UV excitation, (B) Size dependent narrow emission and (C) absorbance spectra of CdSe QDs. [11]

1.3 Synthesis of Quantum Dots

QDs can be synthesized in organic or aqueous medium in the presence of surfactants. Hydrophobic quantum dots prepared in organic solvents at high temperatures are usually more preferred ones due to rather monodisperse size distribution and strong luminescence. [12] However, such hydrophobic QDs are not suitable for biological applications which usually means aqueous working environment. In 1998, the first water soluble QDs for biological labelling were prepared by surface modification of the hydrophobic CdSe/ZnS QDs with water soluble mercaptoacetic acid. [13] Exchange of the hydrophobic ligands with water soluble ones is the most widely used method to achieve aqueous QDs, but suffer from aggregation and loss of luminescence intensity due to surface perturbation. Alternatively, silica coating, attachment of hydrophilic molecules or polymers, growth of water soluble polymers from the QD surface or deposition of amphiphilic polymers are alternative routes (Figure 1. 10). Although, direct synthesis of QDs in the aqueous medium usually produces QDs with broader size distribution and lower quantum yield, due to the safer and simpler steps of the synthesis, becoming more and more popular.[14]

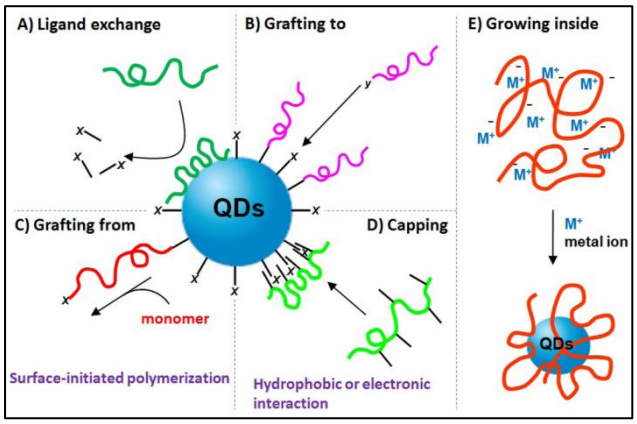

Figure 1.10 Different ways to produce aqueous QDs from hydrophobic ones (A-D) and directly in water (E). [15]

QDs are composed of the semicrystalline crystal core and an organic shell which makes the particle hydrophilic or hydrophobic. Organic shell is comprised of surfactants or ligands which have an affinity to crystal surface hence adsorb or bind to crystal surface and form a coating around it. Surfactants play a significant role in the control of particle growth during the synthesis. When they bound on the crystal surface, they prevent growth in that direction. Hence, prevent formation of the bulk material and further help to tune the crystal size. Also, an effective surface passivation by surfactants are essential for stability and strong luminescence, which usually balances the nonstoichiometric surfaces, eliminates dangling bonds, etc. Such surface defects usually results in non-radiative events and surface oxidation. So, the choice of the surfactant is important and a good surface passivation is essential for stable and good quality colloidal QDs.

Surfactants with thiol (S-H) groups are usually preferred for chalcogenides such as CdS, CdSe, PbS, Ag_2S. Yet, at least di-functional molecules are used for the preparation of aqueous QDs since hydrophilic groups are necessary in the organic coating to provide suspension of QDs in aqueous environments. Thioacetamide[16], Cyseine [17], 2-mercaptopropionic acid [14, 18] and DMSA [19] are some of the mostly used ligands for aqueous QDs, and the last two were developed by our group. Additionally, organic coating should be carefully chosen for bio-applications, since toxicity is an issue and many times, drugs, genes, proteins etc are desired to be loaded to such organic coatings for therapeutic or targeting purposes. So, a carefully designed aq. QD may act as a multifunctional nanoparticle (Figure 1.11).

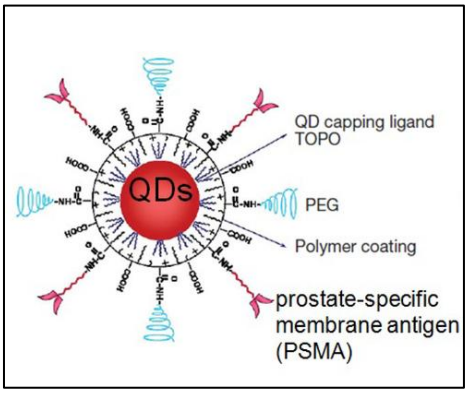

Figure 1.11 Schematic example to a multifunctional QD.[20]

1.4 Applicable Platforms for QDs

Unique optical and electronic properties of QDs make them attractive to many different technological platforms energy, electronics, biotechnology, optics and medicine. In optical labeling in biotechnology and optical imaging in medicine, they overcome the limitations of organic dyes as fluorescent probes. First of all, QDs are much more resistant to photo-bleaching which increases the experimental time dramatically and allows long monitoring time. In addition they have large molar extinction coefficient and usually high quantum yield which provides good signal at low doses. Thirdly, QDs have broad absorption spectra so they can be excited at different wavelengths, hence many different QDs can be excited at a single wavelength which is almost impossible with organic dyes. Plus, emission peaks are usually narrow which prevents mixed signals when different QDs are used simultaneously. Lastly by changing the size and or the composition, fluorescence from the UV through the near infrared can be achieved with QDs [1]. Due to these advantages of QDs, they are accepted as the new fluorophores to replace organic dyes for detection and labeling functions. QDs were first used in biological labeling in 1998. [11] They were mostly used in bio-analytical assays [21], coding [4], biological labeling and *in vivo* imaging. Bio-analytic uses

of QDs can be divided into two major subjects: immunoassays and biosensors. Availability of different emission wavelength and strong emission allows barcode generation with QDs that can be read at a single wavelength excitation. In the article of Han et al in 2001 [4], three QDs (red, green and blue) were used for barcode generation. For that study, polystyrene beads encapsulating QDs were conjugated to DNA. Each color represented different nucleic acid sequences and thus hybridized DNA could be detected by co-localization of the signal.[4] QDs are also promising materials or optical imaging in both in vitro and *in vivo* imaging studies.[22] With a careful choice of the organic shell, QDs may act as multifunctional, theranostic nanoparticles (Figure 1.12).

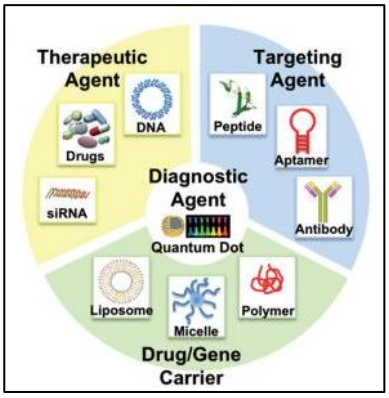

Figure 1.12 Available platforms for multifunctional QDs in medicine.[23]

Large Stokes shifts of QDs improve the detection sensitivity. Conversely organic dyes having usually small Stokes shifts are not so clearly detected because of autofluorescence. So, signals of QDs with large Stokes shifts are much more recognizable than organic dyes. This advantage of QDs is especially important in the *in vivo* studies. In Figure 1.13, image (II), due to large Stokes shifts of the QD, signals coming from tumor fluorescence and background fluorescence didn't overlap. In addition, QDs can be different colors so they can tag different molecules or proteins and it makes them very attractive materials as optical probes. [22]

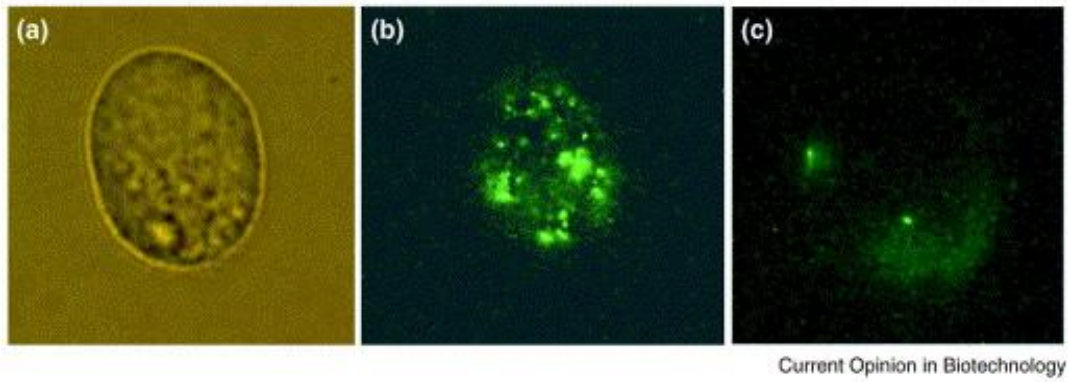

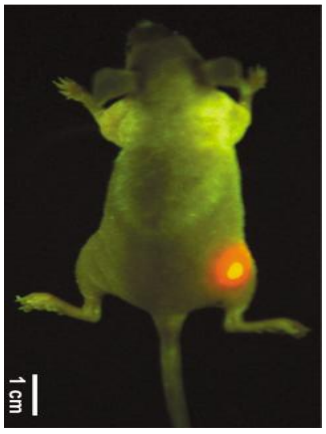

B.**Figure 1.13** (I) Cell internalization of folic acid tagged QDs (FA-QDs) in human KB carcinoma cell line (Ia) Bright-field image of control KB cell (Ib) KB cells incubated with FA-QDs (Ic) Internalization of bovine serum albumin tagged QDs in KB cell.[50] (II) *In vivo* tumor imaging with QD that was injected into right flank. Orange color represents the QD signal.[51]

1.5 NIR Ag_2S QDs in Biological Applications

Group II-VI visible range quantum dots such as CdS, CdSe, CdTe, ZnSe are excited in UV, luminesce in the visible range (400-700 nm) and are the most studied ones. Even though these quantum dots have high quantum yields, there are significant drawbacks in their biological applications. The most significant ones are the autofluorescence of living tissue in the visible range (Figure 1.14), limited penetration depth of the UV and visible light, absorption and scattering due to some biological components like hemoglobin and water in the visible range and excitation in the UV. [18, 24]In recent years, the proper wavelength window for biological applications (such as biolabeling, deep tissue imaging, and photodynamic therapy systems) has been proposed as the near IR range (700-900 nm). [25]

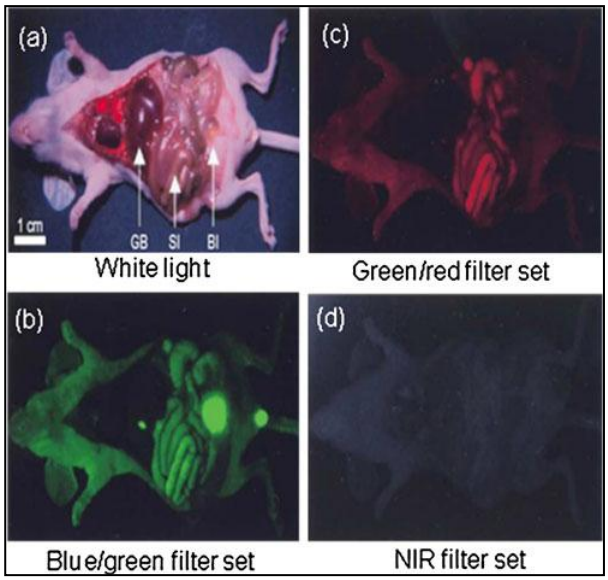

Figure 1.14 Image of a sacrificed athymic *nu/nu* mouse (a) under white light, and autofluorescence detected at excitation/emission sets of **(b)** blue/green (460–500 nm/505–560 nm), **(c)** green/red (525–555 nm/590–650 nm) and **(d)** NIR (725–775 nm/790–830 nm). [26]

Cytotoxicity is another crucially important aspect of quantum dots when considered for bio-applications. In the literature there are many NIR quantum dots such as CdSeTe, CdSeTe/Cd, and PbS. Yet, they have highly toxic heavy metals such as cadmium, lead etc..[27] To decrease the toxicity of Cd-based quantum dots, they are usually with biocompatible polymers like polyethylene glycol, but this solution has its own problems such as limited internalization of QDs. So, heavy metal-free quantum dots with NIR emission are the most desired nanoparticles recently for biomedical applications. Ag_2S quantum dots that are both heavy metal free and fluorescent in the NIR has emerged as the most promising QDs in the recent years [28, 29,30]

Colloidal stability, high QY and nontoxicity in HeLa and NIH-3T3 cells up to 600 μg/mL particle doses were obtained with 2MPA coated Ag_2S quantum dots (Figure 1.15). [18]

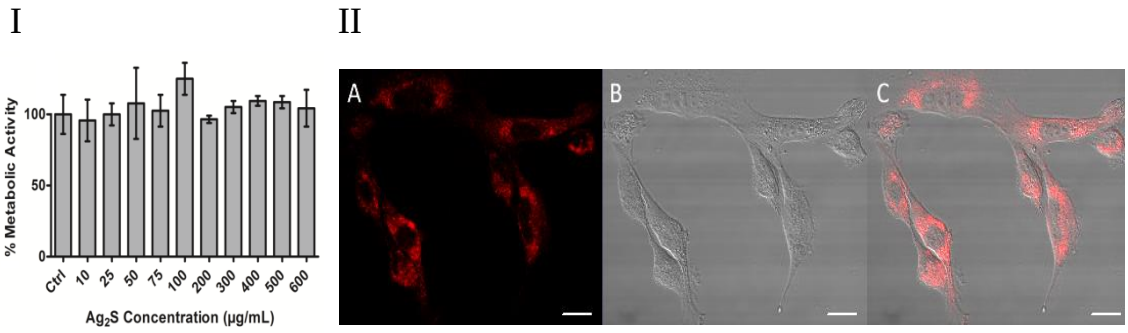

Figure 1.15 (1) Viability of NIH/3T3 mouse fibroblast cells after 24 h exposure to 2MPA coated Ag_2S quantum dots. (II) Cellular uptake and localization of Ag_2**S** QDs by NIH/3T3 mouse fibroblast cells (200 µg mL^{-1} QDs, 24 h incubation). (A) Fluorescence, (B) transmission and (C) merged.[18]

Several groups have studied the biodistribution and tumor imaging properties of Ag_2S NIR QDs that are luminescent n the NIRI or NIRII regions (Figure 1.16).

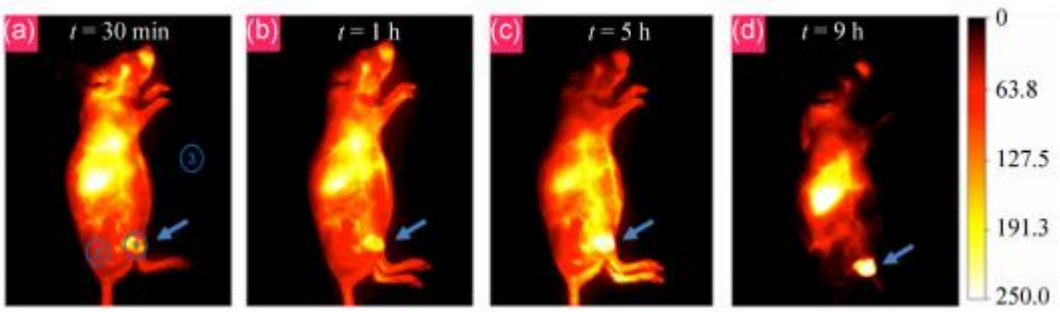

Figure 1.16 **(a)–(d) Time course of NIR-II fluorescence images of the mouse injected with DOX@PEG–Ag_2S.** [31]

1.6 Gene Therapy

Gene therapy is a technique based on successful delivery of DNA into the cell nucleus. At first, in 1979 gene therapy was succeeded by calcium phosphate technology. Desired gene in the form of oligonucleotide or plasmid was sent into the cells that lack the gene, have mutated gene or need more gene.

Plasmid DNAs are small DNA molecules that are separated from chromosomal DNA physically and they exist in the cell in a circular shape. They consist of double stranded DNA. They are mostly found in bacteria but also found in archea and eukaryotic organisms, too. Their sizes range between a few thousand base pairs (bp) to 100 kilo (bp) which is about 4-20% of the genomic DNA. Like chromosomal DNA, plasmid DNA is also reproduced at each cell division process and split up into divided cells. Some plasmids encode enzymes that inactivate the antibiotics. So, bacteria can reproduce in the environment with antibiotics. In gene therapy techniques, the interested DNA plasmid is targeted into different cells to cause a gene expression. Plasmids are negatively charged due to the nucleic acids, so they cannot pass through the negatively charged cell membrane easily. Therefore, some techniques are investigated to increase the cell internalization. Some physical techniques such as sonoporation [32], heat shock and electroporation are used for extending pores on the surface of the cells and by this way allow the passage of plasmid DNA through the pores. However, these techniques don't provide high transfection efficiency and are inappropriate for the *in vivo* applications. In addition, protection of the gene is also crucial in the *in vivo* applications. Plasmid DNAs are usually digested by nuclease enzyme of the liver. Therefore, for the protection of the plasmid DNA and effective internalization by the cells, carrier vectors are required.

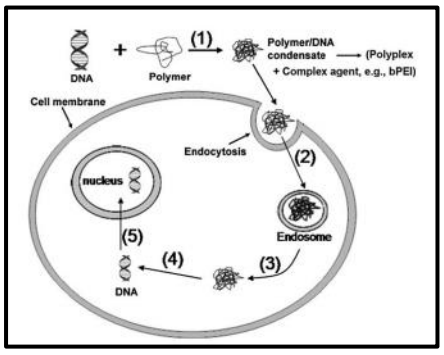

Figure 1.17 Schematic of non-viral gene transfection. [33]

Cancer is one of the most deadly diseases at the present time. The disease is seen as abnormal growth of the cells and their invasion to other parts of the body. In this disease, genes that are responsible for cell differentiation and cell growth are generally mutated and they cannot encode the respective proteins. If the tumor is localized at the defined area of the body; chemotherapy, radiotherapy and surgical operation can be applied. When cancer cells spread into the body and have metastasis, these therapy techniques remain incapable. Chemotherapeutic methods have low drug specificity and block also the fast division of some healthy cells, yet have serious side-effects. Chemotherapy may also cause development of drug-resistance. Because of these problems, new anticancer strategies that does not cause more resistant phenotypes should be investigated. Due to the human genome project, molecular level information of cancer disease is now much clearer. Comparing to classical procedures, gene therapy is much more effective and specific. By using this therapy, damaged genes can be replaced with the new ones and undesirable genes can be repressed.

In gene therapy both viral and non-viral systems are used as the carrier vector. In viral methods retroviruses, adenoviruses and adeno-assosive viruses are used. Although viral systems provide high transfection efficiency, it has high risk and causes immunologic problems.[34] Therefore, non-viral vectors are preferred in the recent years (Figure 1.9). Non-viral vectors, usually polymers, are more biocompatible and more reliable. Also, these vectors have ease of handling and their DNA loading capacity is high. These non-viral vectors can be functionalized for the target cells.[35] Mostly cationic polymers such as polyethyleneimine, poly(dimethylaminoethyl methacrylate) or liposomes are used as non-viral vectors, but there are also examples to dendrimers and peptides. Nanoparticles with cationic coatings can be utilized for gene transfection as well. Oligonucleotides, si-RNA, peptides, aptamers and antibodies can be bond to the surface of the cationic nanoparticles. Nanoparticles such as QDs, provide multimodality, such as targeted gene delivery and real time optical imaging which is very crucial to track the nanoparticles *in vivo* and track the outcome of the therapy. [35b]

1.6.1 p53 Gene and Cancer

There are two fundamental mechanisms that have responsibilities in cancer disease. These are oncogenes and tumor suppressor genes. Oncogenes are mutated version of proto-oncogenes that are normally responsible for cell growth, cell differentiation and regulation of mitogenic signals. On the other hand tumor suppressor genes regulate cell cycle and protect them from mutations. They recognize the DNA damages in the first phase of cell division and state them at G1/S phase. When DNA is damaged, DNA repair protein is activated by tumor suppressor genes but on the level of change beyond repair, these genes lead the cells to death.[52] One of the most known and important tumor suppressor genes is p53 gene encoding p53 protein. P53 protein participates in cell protection mechanisms such as DNA repair, apoptosis and cell cycle regulation.[53] Many cancers such as breast and prostate, are caused by the absence of p53 gene. More than 50% cancer patients have mutated p53 gene. Because of these reasons p53 is one of the most significant genes in cancer therapy.

1.7 Polyethyleneimine (PEI)

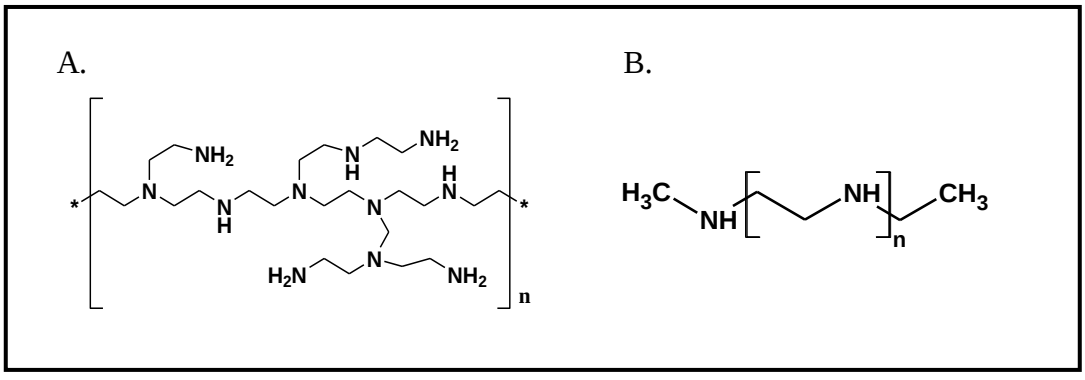

Figure 1.18 Chemical structures of branch (A) and linear (B) PEI polymers

DNA is a negatively charged polynucleotide that carries genomic code. Therefore, positively charged materials such as polymers, copolymers, liposomes and

inorganic materials can be used for DNA binding. Branched PEI (25 kDa) is so far the best non-viral vehicle with the highest transfection efficiency (Figure 1.18 A). Due to its high positive charge, PEI can easily bind to DNA.[37] After PEI-DNA complex formation, the polyplex still possesses a positive charge that allows favorable internalization of the polyplex into the target cells. Polyplexes are taken by the cells via endocytosis. The material is firstly localized in the endosome then goes into the cytoplasm of the cell. DNA release from the polyplex happens due to proton sponge effect. Released DNA goes into the cell nucleus and transcription process starts (Figure 1.19).

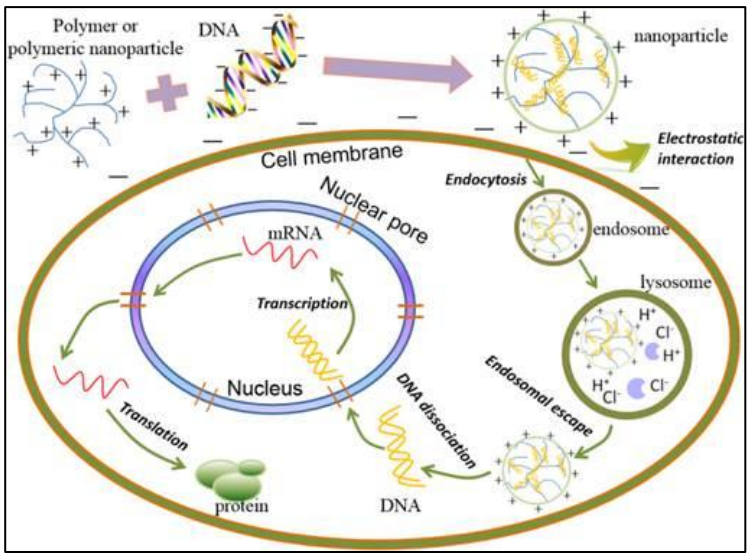

Figure 1.19 Formation of polyplexes and gene delivery process. [38]

Comparing to other cationic materials, PEI has more resistance to nuclease enzyme degradation. (40). Due to primary (25%), secondary (%50) and tertiary (25%) amine groups, PEI can be dissolved in water, easily. When the solvent is acidic, amines of PEI are protonated and they form highly branched webby structure. PEI can be linear or branch (Figure 1.18). Due to high transfection efficiency, branch PEI with 25kDa molecular weight is mostly preferred in gene therapy. The higher molecular weight

PEIs provide higher transfection efficiency of DNA and RNA. However, PEIs with higher molecular weight than 25kDa have serious toxicity issues. When the molecular weight of PEI decreases, transfection efficiency also decreases but viability increases and 25kDa PEI provides acceptable biocompatibility and transfection efficiency. [35b]Alternatively, linear PEI is also studied. Linear PEI is more biocompatible but also less effective in the transfection experiment.

In the selection of cationic polymers for polyplex formation there are couple of important points to be considered: Toxicity of the cationic polymer, formation of stable complexes, high specific internalization of polyplexes by the cells, effective release of the gene from the vector. In addition to these, surface charge and size of the polyplex are crucial as well since it impacts the blood circulation time and biodistribution. To reduce toxicity of the polymeric vectors such as PEI, more biocompatible polymers like PEG are attached to polymers. Another method to reduce the toxicity is to reduce the molecular weight of the polymer. [39] In order to leverage the reduced transfection efficiency due to the reduced molecular weight, Dr. Yağcı Acar and her coworkers, attached short PEI chains (1200 Da) to the surface of superparamagnetic nanoparticles to deliver siRNA (WO2006055447-A2).

1.7.1 PEI coated QDs

Nanoparticles are considered as good candidates for drug and gene because they have high surface to volume ratio, they can be internalized easily by endocytosis, they can be targeted by tagging with a specific ligand and their organic shell can be tailored in different chemical nature to bind drug or gene. QDs are one of the most attractive nanoparticles that can offer both means of diagnosis and therapy, which is highly desired in medicine. QDs with tunable strong emission and long luminescence lifetimes can be exploited as great real time optical imaging probes. When coated with a cationic polymer may bind and deliver genes to the target as well. Therefore, there is an effort in development of cationic QDs, such as PEI coated QDs. Such QDs were synthesized

in different ways like ligand exchange, electrostatic coating, covalent coating and direct coating.

- **Ligand exchange**

Original hydrophobic ligands (such as oleic acid and trioctylphosphine oxide (TOPO)) coating the crystal surface, are replaced with PEI in an organic solvent. However, this method caused a dramatic decrease in the original quantum yield of the QD (to 40%). [40]

- **Electrostatic coating**

QDs with anionic coatings can electrostatically interact with the cationic PEI. In the literature, mercaptoacetic acid (MAA) coated NIR luminescent CdTe QDs are electrostatically bond to linear and branch PEI chains.[41] In addition, MAA coated CdS QDs are bond to PEI polymers with 1.7kDa, 3kDa and 15kDa molecular weight and obtained better quantum yields upon PEI deposition. [41]

- **Covalent binding**

PEI can be covalently conjugated to QDs having coatings with carboxylic acid groups via amidation. In the literature, PEI was bond to mercaptoacetic acid coated CdS by amidation.[42] Utilizing the same chemistry folic acid for targeting folate receptors was conjugated to PEI, as well. Such chemistry usually causes a red shift in the emission peak of the QD.

- **Direct coating**

QDs can be synthesized directly in aqueous solution of PEI. In the literature, CdS/ZnS core shell QDs synthesized in the presence of branch PEI (10kDa) [43]There are also examples to CdS QDs synthesized in the presence of PEG5000-PEI (both linear and branch). [44]

1.7.2. PEI coated Ag_2S QDs

In an effort to develop cation and biocompatible QDs that are fluorescent in the medical window, Ag_2S coated with branch PEI (25 kDa) was produced by Fatma Demir et al [45] Yet, it was found that bPEI (25kDa) do not provide luminescent. Ag_2S QDs unless it is mixed with a small, strongly binding thiolated molecule, 2-mercaptopropionic acid. Such particles with the mixed coating effectively provide optical images *in vitro* and deliver GFP to cells.

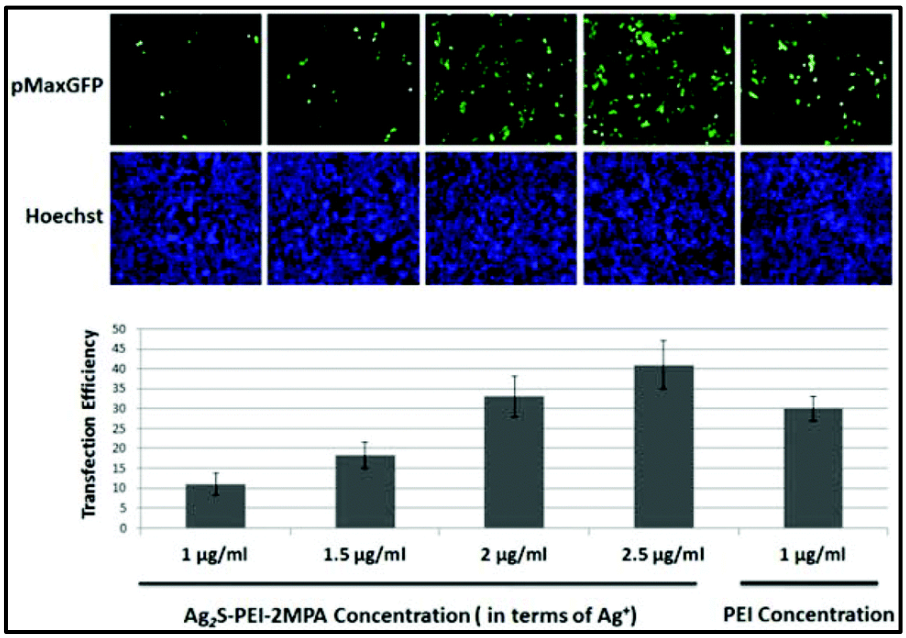

Figure 1.20 Transfection of HeLa cells. (A) Cells were transfected with the pMax-GFP plasmid using $_{Ag2S}$-PEI/2MPA NIR QDs or control PEI (1 µg ml^{-1}). Transfection efficiency was assessed using a fluorescence microscope. Hoechst staining was used to show the nuclei of all cells in the field. (B) Quantitative analysis of GFP positive cells n (A) (mean ± SD of independent experiments, n = 3).

1.8. Objective of this Thesis

There is a tremendous urge to develop multifunctional nanoparticles in medicine, especially nanoparticles that offer both therapeutic and diagnostic functions, simultaneously. Such particles are called *theranostic nanoparticles* and quantum dots, which are possibly the most studied nanoparticles in the last decade or so, are one of the most appropriate candidates. Nanoparticles with large surface to volume ratio and with carefully selected organic coatings can bind drugs, genes, proteins, etc and can be tagged for the targeted delivery of the cargo to the site of interest. If these nanoparticles are quantum dots, when excited, they would provide a long lasting strong photoluminescence, which can be utilized as optical imaging agents for diagnostic or tracking purposes. Compared to MRI, resolution in optical imaging is much better, but there is an important limitation: QDs with strong luminescence in the 700-900 nm range is required for low autofluorescence, deeper penetration and safer imaging. Second limitation is the biocompatibility of the inorganic core and the organic shell of QDs. The most widely studied Cd-chalcogenides that are luminescent in the visible range are hence inappropriate for *in vivo* applications, but Ag_2S QDs are very promising due to much better cytocompatibility and photoluminescence in the near-infrared region.

In recent years, gene therapy has become very popular and created a great hope in the treatment of many diseases. This approach requires internalization of nucleic acids into target cells for therapy. Many transfection vectors have been evaluated and among the non-viral ones, a polycation, branched-PEI emerged as the most effective transfection agent. PEI has molecular weight and structure dependent toxicity. Branched ones are more toxic than the linear ones and as the molecular weight increases the toxicity increase, but also the transfection efficiency. Branched PEI at 25kDa molecular weight is accepted as the golden standard with a good balance of toxicity and transfection efficiency.

In this thesis work, the main objective is to develop biocompatible, cationic, NIR emitting theranostic quantum dots suitable as gene transfection vectors and optical

imaging agents. For this purpose linear PEI with more favorable cytocompatibility compared to the branched one was planned to be used as the cationic organic shell for highly cytocompatible and NIR emitting Ag_2S QD core. Based on the prior work performed in our laboratory with the branched PEI, it was known that stability of the Ag_2S QDs with PEI coating is molecular weight dependent and Ag_2S QDs with branched PEI does not luminesce. Therefore, the major questions planned to be answered in this thesis are:

- Can linear PEI with no primary amine effectively bind to Ag_2S core?
- Can low molecular weight linear PEI effectively bind to Ag_2S core?
- How would the optical, physical, chemical and biological properties of Ag_2S QDs would change if a mixed coating composed of linear PEI and a small molecule is used?
- How would the properties of Ag_2S QDs would change by the molecular weight of the linear PEI, nature of the small molecule and the coating composition?
- Are such QDs potential theranostic nanoparticles?

To answer these questions and achieve the objective of this study, aqueous synthesis of Ag_2S NIR QDs with linear PEI at 25 and 2.5 kDa molecular weights and their mixture with 2-mercaptopropionic acid (2MPA) and L-Cyseine (Cys) at different ratios were performed. 2-MPA were chosen due to its superior stability and surface binding to other small thio-acid. L-Cyseine was chosen since it is a natural aminoacid which could provide better cytocompatibility and also contribute to cationic nature of the organic coating with its side chain primary amine.

Influence of reaction pH, molecular weight of linear PEI, nature of the small thiolated molecule, coating composition and medium pH on stability, emission window, luminescence intensity, size, charge and also on cytotoxicity and cell internalization was planned to be studied to determine the most suitable quantum dots for theranostic applications where optical imaging will be combined with gene therapy.

Chapter 2

EXPERIMENTAL

2.1 Materials

All the chemicals used were of analytical grade or of the highest purity commercially available. Silver nitrate ($AgNO_3$), 2-mercaptopropionic acid (2MPA) and L-Cyseine were purchased from Sigma-Aldrich. Sodium sulfide (Na_2S) was purchased from Alfa-Aesar. Linear polyethyleneimines (25kDa and 2.5kDa) were purchased from Polysciences, Inc. Thioacetamide (TAA) was purchased from Merck. Dimethyl sulfoxide (DMSO) was purchased from VWR. Ethanol (EtOH) was purchased from Merck. Phosphate buffered saline (PBS) tablets were purchased from Sigma and fetal bovine serum (FBS) was purchased from Capricorn. MTT (3-(4,5-dimethylthiazol-2-yl)-2,5-diphenyltetrazolium bromide) was purchased from AppliChem. Dulbeccos Modified Eagles Medium (DMEM; 4500 mg/L glucose, 4 mM L-glutamine, 110 mg/ L sodium pyruvate) and Trypsin–EDTA were purchased from Hyclone (USA). 96-well plates were purchased from Santa Cruz Biotechnology, Inc. (USA).LDS 798 near-IR laser dye (Quantum yield reported as 14% in DMSO by the producer) was purchased from Exciton Inc. Acetic acid and sodium hydroxide were purchased from Merck. Paraformaldehyde (4%) was purchased from Chemcruz. 4,6-Diamidino-2-phenylindole dihydrochloride (DAPI) was purchased from Sigma Aldrich. Milli-Q water (18 mOhm) was used as a solvent. HeLa (Human cervical carcinoma), HCT 116 WT (Human colon cancer) and HCT 116 P53(-) cells were received from Gözüaçık Laboratory (Sabancı University, Turkey).

2.2 Synthesis of 2MPA/L-PEI Coated Ag_2S NIR QDs

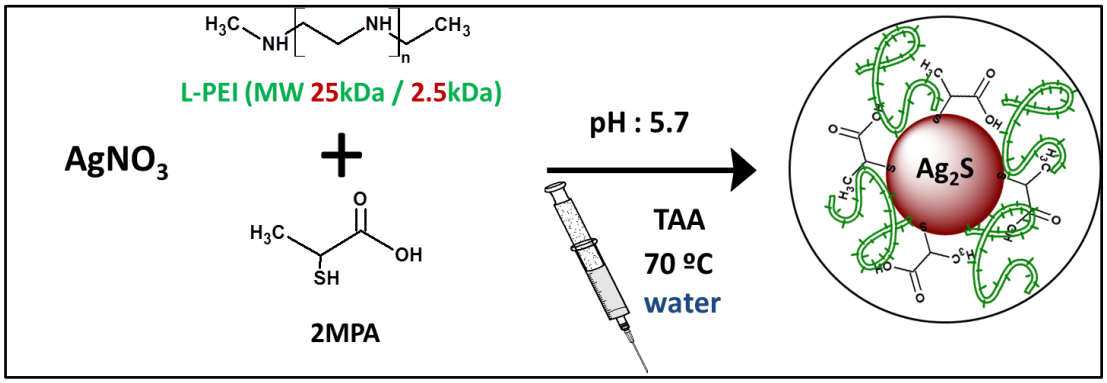

Figure 2.1. Schematic representation of the 2MPA/L-PEI coated Ag_2S NIR QD synthesis.

A typical preparation method of 2MPA/L-PEI coated Ag_2S NIR QDs is as follows (Figure 2.1): 75 mL deionized water in a three-neck round-bottom flask was purged with Argon for 15 minutes. Silver nitrate (0.25 mmol $AgNO_3$) was added into the flask. First, L-PEI is added to the silver nitrate solution. In order to dissolve L-PEI in water, pH was adjusted to 8.5 with sodium hydroxide (NaOH). Then, the appropriate amount of 2-mercaptopropionic acid (2MPA) was added into the solution. After addition of 2MPA, pH was adjusted to 5.7 with acetic acid (CH_3COOH). Thioacetic acid (0.0625 mmol TAA) was dissolved in 25 mL deoxygenated water in a separate round bottomed flask. TAA solution was sonicated under Argon for 15 minutes and transferred into the reaction solution via a syringe. Reactions were carried out for 3-5 hours under Argon and vigorous mechanical stirring at 70 ºC. During the synthesis, aliquots were taken at different time points to follow the particle growth. Results colloidal suspension of Ag2S QDs were washed with MilliQ water in Amicon-Ultra centrifugal filters (3kDa and 30kDa cut off) depending on MW of L-PEI (2.5k and 25kDa) and stored at 4 °C in the dark.

Coating materials/Ag/S mole ratio was set to 20/4/1. Mole of the secondary nitrogens in L-PEI and the mole of the thiol group in 2MPA were used in such formulations. When 20/80 2MPA/L-PEI is used, this means mole ratio of the SH groups of 2MPA to N of PEI is equal to 20/80. Influence of 2MPA/L-PEI mole ratio, pH and MW of L-PEI (2.5k and 25kDa) on particle properties were studied.

2.3 Synthesis of L-Cyseine/L-PEI Coated Ag_2S NIR QDs

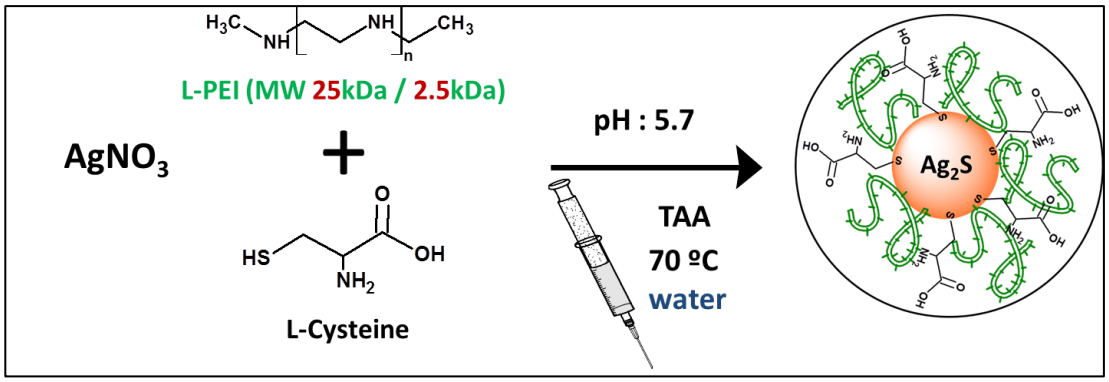

Figure 2.2 Scheme of L-Cyseine/L-PEI coated Ag_2S NIR QD synthesis.

A typical preparation method for L-Cyseine/L-PEI coated Ag_2S NIR QDs is very similar to the synthesis of 2MPA/L-PEI coated Ag_2S NIR QDs as detailed in Section 2.2 of this thesis. Reactions were carried out for 2-3 hours under Argon and vigorous mechanical stirring at 70 ºC. Coating materials/Ag/S mole ratio was set to 20/4/1 again. Mole of the secondary nitrogens in L-PEI and the mole of the thiol group in Cyseine was used in such formulations. When 20/80 Cyseine/L-PEI is used, this means mole ratio of the SH groups of Cyseine to N of PEI is equal to 20/80. Influence of Cyseine/L-PEI mole ratio, pH and MW of L-PEI (2.5k and 25kDa) on particle properties were studied.

2.4 Cell Culture

Human cervical carcinoma (HeLa) cells were cultured in complete DMEM medium consisting of 10% fetal bovine serum, 1% penicillin-streptomycin antibiotic solution and 4 mM L-glutamine. Human colon carcinoma (HCT 116 WT) and Human colon carcinoma p53 gene (-) (HCT 116 p53(-)) cells were incubated in complete McCoy's 5A Medium containing 10% fetal bovine serum, 1% penicillin-streptomycin antibiotic solution, 1.5 mM L-glutamine and 2200 mg/L sodium bicarbonate. All cell lines were incubated at 37°C under 5% CO_2. Cell passage with fresh medium is performed once in two days. For cell detachment process, Trypsin-EDTA was used and paraformaldehyde was used to fix the cells on the 6 well plates for microscopic images. DAPI was used for labeling the cell nuclei.

2.5 Determination of Cell viability via MTT Cytotoxicity Test

Human cervical carcinoma (HeLa) and Human colon carcinoma WT and p53(-) (HCT 116) cells were cultured at a $1x10^4$ cells/well in 96-well plates in complete DMEM and McCoy's 5A Medium, as described above. After 24 hours, nanoparticles were added in to each well with fresh medium up to 200 µL at doses between 0.8-10 µg Ag/mL for 24 hours incubation and 25-50 µg Ag/mL for 4 hours incubation time. In the control group, the medium was replaced with only fresh medium. For cell viability test, 5 mg/mL MTT solution in 1M PBS was prepared. After 24 hour incubation with nanoparticles, the medium (consisting of the un-internalized nanoparticles and dead cells, if any) in the wells were replaced with 150 µL specific medium for the cell type and 50 µL of MTT solution. Mitochondrial activity of viable cells reduces MTT to formazan product (Figure 2.39. After 4 h incubation time with MTT reagent, medium

was discarded and in order to dissolve purple formazan product, 200 µL DMSO:EtOH (1:1) was added

to each well. Quantity of formazan was determined by the absorbance at 600 nm (ELx800 Biotek Elisa reader) indicating the number of viable cells. To correct any errors that would come from the absorbance of cells, absorbance value at 630 nm coming from background signals was subtracted from the absorbance value at 600 nm. Percent viability was calculated as the average of five replicates with respect to absorbance average of control with no nanoparticle exposures. Statistical analysis was performed by one-way ANOVA with Tukey's multiple comparison test of the Graph Pad Prism 5 software from GraphPad Software, Inc., USA.

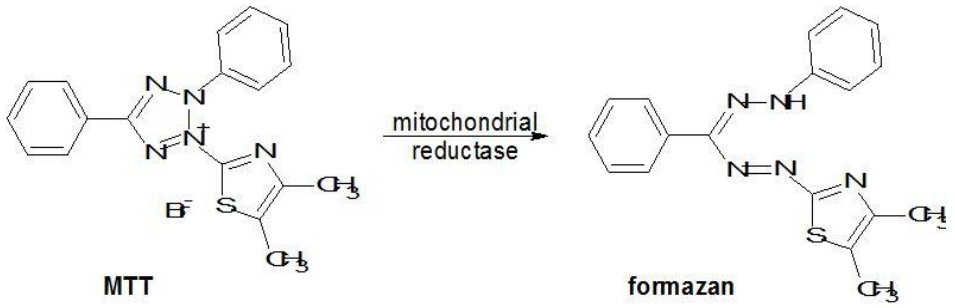

Figure 2.3 Chemical structures of MTT dye and formazan. [46]

2.6 Cell Uptake

Amount of the Ag_2S QDs internalized by cells was measured by the amount of silver ion in the cell lysates via Genesis ICP-OES. For this purpose, cells were incubated with QDs as explained in the previous section, in 96 well plates. After 4 hours incubation, to remove un-internalized nanoparticles, the medium was replaced with 200 µL DI water. Then the contents of each well were transferred carefully into a 10ml volumetric flask containing 200 µL nitric acid and 200 µL sulfuric acid. Remaining volume was filled with DI water. As a control wells with cells but no QD incubation and QDs at the applied doses were used and prepared for ICP as described above. Cell uptake was calculated as silver amount of five replicate wells of each dose

with respect to control wells. ICP measurement of each sample was repeated three times. A standard calibration curve for Ag was generated before the analysis of cell lysates (Figure 2.4). Statistical analysis was performed by one-way ANOVA with Tukey's multiple comparison test of the Graph Pad Prism 5 software from GraphPad Software, Inc., USA.

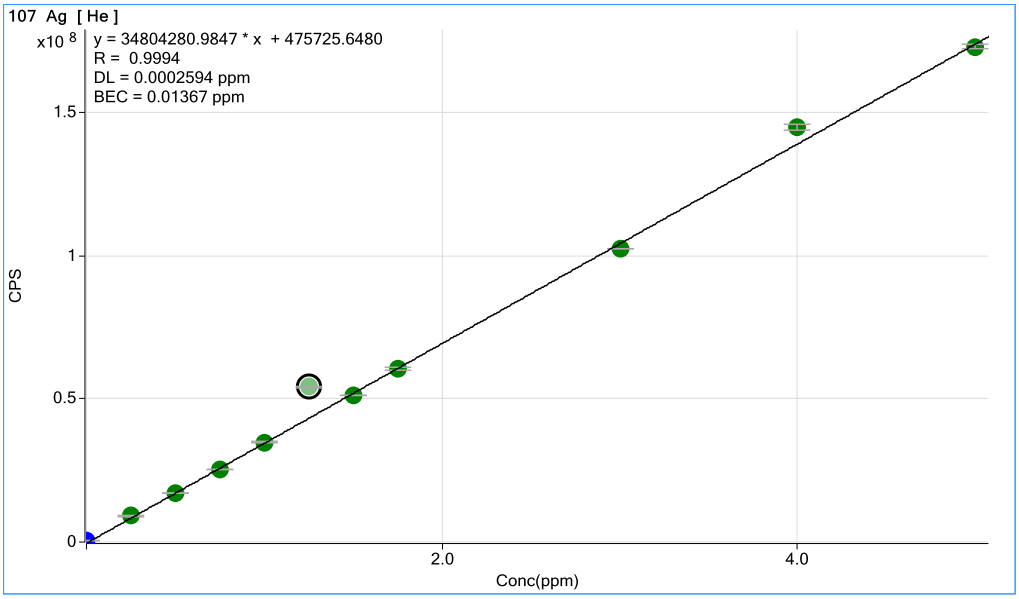

Figure 2.4 Calibration curve of Ag ion via ICP-MS.

2.7 Cell Imaging

Human cervical carcinoma (HeLa) cell lines were cultured at $5x10^4$ cells/well in 6-well plates in complete DMEM culture medium overnight, then the medium was replaced with fresh DMEM and QDs at 25 and 50 µg Ag/mL doses. After 4 hours incubation time, the medium was discarded and the cells were washed with PBS (1M) for three times. Then, 1 mL paraformaldehyde was added to each well and stored in dark to fix cells for 20 minutes. Then paraformaldehyde was removed and each well was washed with PBS (1M) for three times. Following this protocol, DAPI dye was

added into each well at 1 µL dye /mL PBS (1M) concentration and the plate was stored in dark for 30 minutes to stain cell nuclei with DAPI dye. Then DAPI dye and PBS (1M) were discarded and each well was washed with 1 M PBS for three times. 1 mL PBS was left in each well. The fixed cell samples were examined under the Inverted Life Science Microscope (Olympus-Xcellence RT Life Science Microscopy). Two different filters that were specific for DAPI dye region (λ_{exc}: 352-402 nm and emission: 417-477 nm) and NIR region (λ_{exc}: 550 nm and emission: 650 nm long pass) were used for microscopic images of cellular nucleus and NIR emitting QDs. As a control, same experimental process was performed with control cells with no nanoparticles.

2.8 Characterization

Functional group analysis was done by recording IR spectrum on a Thermo Scientific Nicolet iS10 instrument (ATR-FTIR) in the wavenumber range of 400-4000 cm^{-1}. Absorbance spectra for Ag_2S-PEG QDs were recorded on a Shimadzu 3101 PC UV-vis-NIR spectrometer in the 300–800 nm range. Particle sizes were calculated from the absorbance onset using Brus equation (Eqn. 1). [47]

Eqn 1.
$$\Delta E = \frac{\hbar^2 \pi^2}{8R^2}\left[\frac{1}{m_e} + \frac{1}{m_h}\right] - 1.8\frac{e^2}{\varepsilon_{Ag_2S} 4\pi\varepsilon_0 R}$$

ΔE is the band gap energy difference between the bulk semiconductor and the quantum dot and R is the radius of the quantum dot, effective electron and hole masses for Ag_2S are m_e ($0.286m_0$) and m_h (1.096) [48] and dielectric constant (ε_{Ag2S}) of bulk Ag_2S is 5.95 [48].

Hydrodynamic size and zeta potential measurements were performed by Malvern zetasizer nano ZS.

Ag^+ ion amount of the quantum dot solutions was determined by Spectro Genesis FEE Inductively Coupled Plasma Optical Emission Spectrometer (ICP OES). The results were calculated based on reference curve that was prepared by standard solutions. For the ICP analysis procedure, QD solutions were prepared with nitric acid, sulfuric acid and diluted with DI water.

TEM analysis was performed at UNAM, Ankara. A dilute solution of QDs were dropped on a carbon coated Cu-grid and evaporated. For the high resolution images, FEI Tecnai G2 F30 TEM operated at 200kV was used.

For Photoluminescence spectroscopy, a home-made instrument with gold reflector, 0.5 m Czerny-Turner monochromator and silicon detector that is sensitive over the wavelength range of 400-1100 nm and Si detector with femto-watt sensitivity (Thorlabs PDF10A, 1.4×10^{-15} W $Hz^{-1/2}$) were used. A continuous-wave, frequency doubled Nd:vanadate laser operating at 532 nm was used for excitation. 590 nm long pass filter was used at the emission site. Slid width was arranged to 0.2 nm for the measurements.

Eqn 2. $$\Phi_{yield} = \frac{m_{sample}}{m_{standart}} \times 100$$

Quantum yield (QY) was calculated based on the detailed procedure in the literature.[49] As a reference dye, LDS 798 NIR dye (QY = 14%, reported by the producer) was used. For this calculation, four different concentrations of dye and sample solutions were prepared in water. The absorbance values were kept below 0.1 at 532 nm. The area under the emission peak of each sample versus absorbance values at excitation wavelength (532 nm) were plotted and the QY was calculated from the slopes of these lines created for the sample and the reference dye using Eqn 2.

Chapter 3

DEVELOPMENT OF 2MPA/L-PEI STABILIZED Ag_2S QUANTUM DOTS

3.1 Research Objectives

Research presented in this thesis aims to invent new generation quantum dots as transfection agents for cancer therapy. The heavy metal free, biocompatible, highly fluorescent and stable Ag_2S NIR quantum dots were planned to be exploited for this purpose. Since these Ag_2S NIR quantum dots were designed to be used as transfection vector, Polyethyleneimine (PEI) was chosen as the coating material. PEI is a cationic polymer that can strongly bind to oligonucleotides and due to its proton sponge effect, this cargo can be released from the polymer into cytoplasm when internalized by the cells. Instead of branched PEI, that was mostly preferred in the literature, linear PEI (L-PEI) was chosen here because of the superior biocompatibility of the L-PEI compared to the branched one However, L-PEI coated Ag_2S NIR QDs didn't show any luminescence. Yet, combination of the L-PEI and 2-mercapto propionic acid (2MPA) provided stable and luminescent Ag2S NIR QDs. Chapter 3, mainly includes the synthesis and characterization of Ag_2S NIR QDs that are co-encapsulated with L-PEI and 2MPA. Variables of the reaction was altered to understand their influence in the final particle properties and to achieve the target NIR QD which is colloidally stable,

highly luminescent between 700-900 nm for diagnosis purpose, cationic for oligonucleotide delivery, biocompatible and possess a high transfection efficiency for therapeutic purpose. Since it is well known that the molecular weight of PEI influences the toxicity and the transfection efficiency both 2.5kDa and 25kDa L-PEI were investigated in this project. Also, PEI/2MPA ratio and the pH of the reaction medium were changed. Particle properties such as particle sizes, luminescence wavelength, quantum yield, colloidal stability and toxicity were determined as a function of these variables. Also, gene binding ability and potential as optical imaging agents were evaluated.

3.2 Results and Discussion

3.2.1 Quantum Dot Synthesis and Characterization

All QDs were synthesized by using the best coating/Ag/S ratio as 20/4/1 that was known from our previous studies for Ag_2S quantum dots. All reactions were performed at pH 5.7, where the solution became clear and L-PEI was completely solved. 2MPA/L-PEI ratios of 20/80 and 40/60 were studied.

Table 3.1 Formulation and Properties of 2MPA/L-PEI coated NIR Ag_2S Quantum Dots

Rxn Code	PEI MW (kDa)	2MPA/PEI (mol ratio)	pH	Emission λ_{max} (nm) (pH 5)	D[b] (nm)	Band Gap (eV)	QY[a] (%)
DAA-34	25	0/100	5.7	-	2.6	1.6	-
DAA-35	25	20/80	5.7	872	2.2	1.9	-
DAA-36	25	40/60	5.7	897	2.3	1.8	-
DAA-37	2.5	0/100	5.7	-	2.6	1.5	-
DAA-38	2.5	20/80	5.7	791	2.5	1.7	310
DAA-39	2.5	40/60	5.7	810	2.3	1.8	-
DAA-40	-	100/0	5.7	828	2.5	1.6	-

[a]Quantum yield calculated with respect to LDS 798 near-IR dye [b] Particle sizes calculated by Brus equation.[47]

Even though linear PEI (2.5kDa and 25kDa) coated Ag_2S quantum dots had colloidal stability, they didn't have any luminescence property. All QDs that were coated with only 2MPA or 2MPA/ L-PEI mixture have luminescence in the NIR region (between 790-900 nm) when excited at 512 nm. All crystal sizes were calculated from Brus equation using the absorbance onset determined from the absorbance spectra (Figure 3.1). Band gap energies corresponding to calculated sizes are between 1.5-1.9 eV. NIR QD coated with 2MPA had an emission maxima at 828 nm with a crystal size of 2.5 nm (Table 3.1). Ag_2S QDs synthesized with only L-PEI were about 2.6 nm but not luminescent. Ag_2S QDs with the mixed coatings were mostly smaller than the both based on the Brus eqn. based crystal size. When emission maxima of the Ag_2S QDs with the mixed coatings were compared with the Ag_2S/2MPA, those with 2.5kDa L-PEI/2MPA were emitting at shorter wavelengths (791-810 nm) and those with 25kDa L-PEI were emitting at longer wavelengths (872-897 nm). Increasing 2MPA amount in the coating mixture caused a red shift in the emission maxima, 25 nm for 2.5kDa L-PEI and 19 nm for 25kDa L-PEI.

3.2.1.1 Influence of Reaction Time on Particle Size and Emission Properties of Ag_2S QDs

Mixing L-PEI and 2MPA as a Ag_2S coating provided a synergistic effect. Ag_2S/L-PEI QDs were not luminescent and Ag_2S/2MPA QDs were highly luminescent (Figure 3.1). Yet, Ag_2S coated with 2MPA/L-PEI luminesce better than the later (Figure 3.2). Based on the absorption data, all Ag2S QDs with the mixed coating have absorbance onset at shorter wavelengths than PEI coated ones and hence indicate smaller crystal sizes. When the emission peak of Ag_2S QDs synthesized in 3 hours were compared, composition of the mixed coating influenced the peak position and the intensity mostly for the compositions containing 25kDa L-PEI, but was insignificant for the compositions containing 2.5 kDa L-PEI. Higher 2MPA amount (40 mol %) caused a red shift about 100nm and increased the intensity almost 4 times over the one

containing 20 mol % 2MPA in the coating composition (Figure 3.1a). On the other hand, maximum emission peak positions of 20/80 2MPA/L-PEI (2.5kDa) QD and 40/60 2MPA/L-PEI (2.5kDa) QD were around 820 nm with a slightly better luminescence.

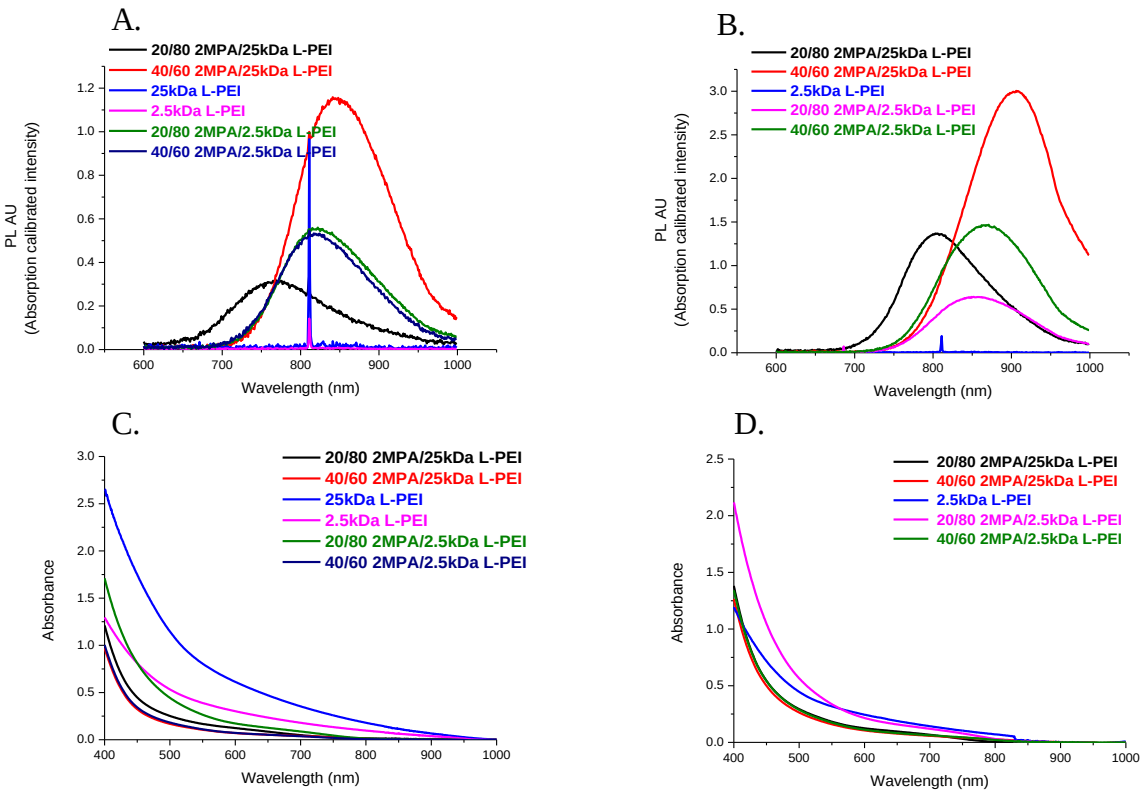

intensity of 40/60 2MPA/L-PEI (25kDa) (Figure 3.1 (A)).

Figure 3.1 Photoluminescence and absorbance intensity results of 2MPA/l-PEI (MW: 2.5kDa and 25kDa) coated NIR Ag_2S Quantum Dots in 3h (A and C) and 5h (B and D) reaction time points.

When the crystal growth was allowed for 5 hours, larger crystals with red shifted absorbance onset and emission maxima (40-50 nm) were obtained (Figure 3.1 (B and D). One of the major impact of extended reaction time was seen in the three times enhancement of the emission intensity of Ag_2S coated with 40/60 2MPA/L-PEI (2.5kDa) compared to the QD synthesized at this composition and conditions in 3 h. In

case of mixed coatings with 25kDa L-PEI, intensity increase in the emission peak was increased 4 times with 20/80 and almost 3 times with 40/60 2MPA/L-PEI (25kDa). Overall, based on this data, it can be concluded that the emission peak position can be tuned further by the reaction time, 40/60 2MPA/L-PEI provide more luminescent QDs, 25kDa L-PEI is more influenced from the reaction variables and the best luminescing Ag2S QDs are produced by 40/60 2MPA/L-PEI (25 kDa) coating.

For comparison with the available data in the literature, quantum yield of the freshly preapared 20/80 2MPA/L-PEI (25kDa) QD was calculated as 310 % with respect to LDS 798 near-IR dye which is way above the highest recorded QY of 150% for 2MPA/B-PEI (25 kDa) until today.

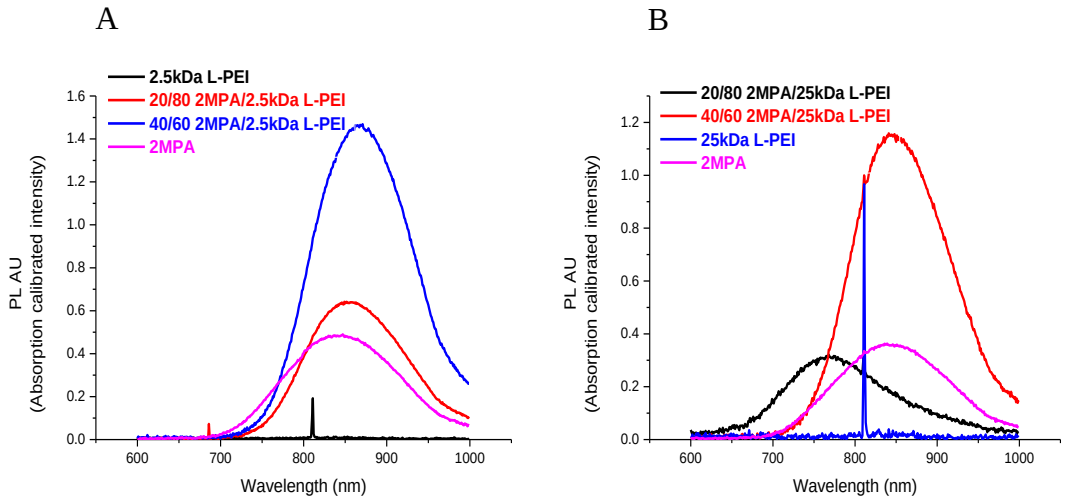

Figure 3.2 Photoluminescence intensity results of 2MPA, L-PEI and 2MPA/L-PEI (MW 2.5kDa) (5h) and 2MPA/L-PEI (MW 25kDa) (5h) coated NIR Ag_2S Quantum Dots.

Synergistic effect of the mixed coating is well presented in Figure 3.2 where the emission spectra of Ag_2S/2MPA, Ag_2S/L-PEI and Ag_2S/2MPA/L-PEI are shown. Except 20/80 2MPA/L-PEI (25kDa) case, all QDs with the mixed coating luminesce much better than the Ag_2S/2MPA. Ag_2S with 40/60 2MPA/L-PEI luminesce about 3

times more strongly than the Ag_2S/2MPA. One interesting observation is that, the emission maxima did not shift to lower wavelengths when 2MPA amount was decreased except 20/80 2MPA/L-PEI 25 (kDa).

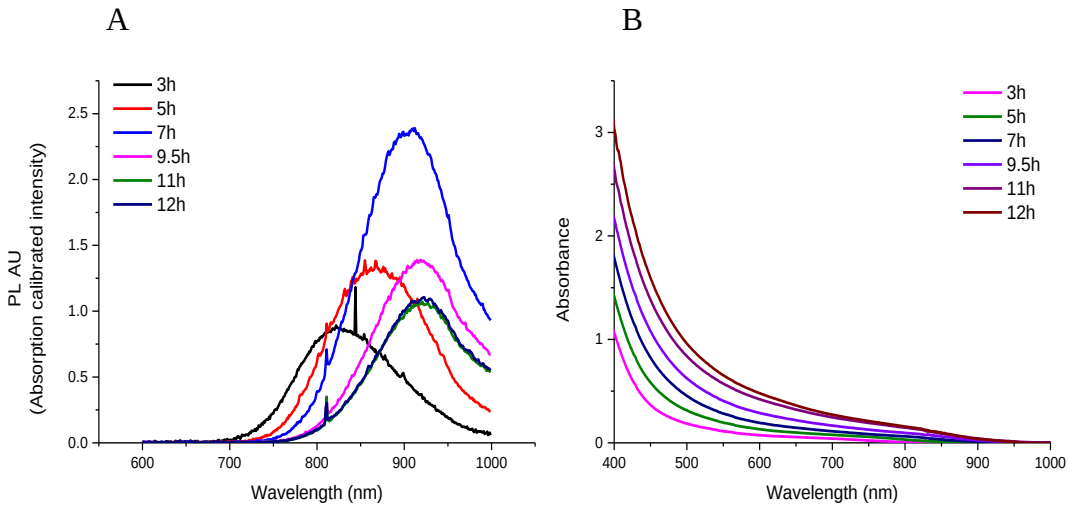

Figure 3.3 Photoluminescence spectra (A) and absorbance (B) intensity results of 40/60 2MPA/25kDa L-PEI NIR Ag_2S Quantum Dots at different time points during the synthesis.

Effect of reaction time on particle size and particle quality was examined further with 40/60 2MPA/L-PEI (25kDa) coating composition. Emission and absorbance spectra of these QDs were recorded at different time points for 12 hours (Figure 3.3). Time dependent growth of QDs is indicated by the red shift of the emission peak and the absorbance onset. The major change in both is more significant within the first 9.5 h and the most intense emission peak was achieved in 7h around 900 nm.

3.2.1.2 Influence of the pH on Optical properties of Ag_2S NIR QDs

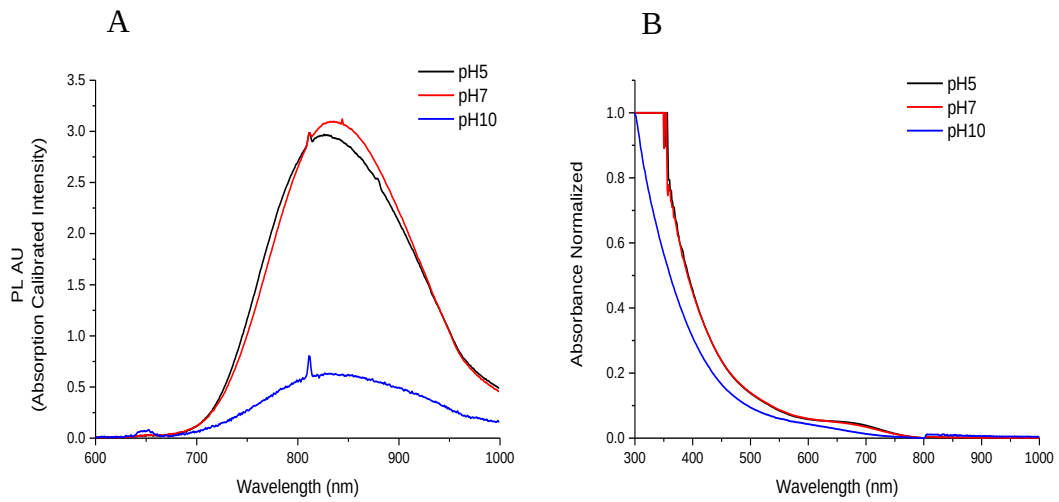

Figure 3.4 Absorbance calibrated photoluminescence (A) and absorbance spectra (B) of 2MPA coated NIR Ag_2S quantum dots at different pH values after the synthesis.

Due limitation in the solubility of L-PEI and the L-PEI/2MPA/$AgNO_3$ mixture, the optimum pH for the particle synthesis was determined as 5.7. All QDs were synthesized at pH 5.7 but after purification their optical properties were tested at different pH values, namely pH 5,7,10. For this study, the particles that are summarized in Table 3.1 were used. In case of 2MPA coating alone, no significant shift in the peak position was observed with the pH but overall, QDs showed strong emission in neutral and acidic pH (Figure 3.4). QDs coated only with L-PEI had no significant emission at any pH values (Figure 3.5).

In case of Ag_2S QDs with mixed coatings, the effect was different. For both 20/80 2MPA/L-PEI (25kDa) and 40/60 2MPA/L-PEI (25kDa) coated QDs, the best luminescence intensities were recorded at pH 5 and the worst at pH 10 with no significant shift in the peak maxima. Absorbance of the QDs had red shift at pH 10 as well (Figure 3.5). The most dramatic emission enhancement in acidic pH was observed

with 40/60 2MPA/L-PEI (25kDa) QD, since the pH sensitive coating component is the 2MPA but not PEI as shown in Figure 3.4 and Figure 3.5a. Yet, part of the weaker emission intensity of the QDs as pH 7 may be partially due to the poor solubility of L-PEI at pH7. On the other hand, such strong pH dependence can be very handy in optical imaging where internalized QDs would luminesce stronger than the ones in the blood stream.

QDs coated with the 2MPA/L-PEI (2.5 kDa) had similar results (Figure 3.6). pH didn't change the PL peak positions but changed the emission intensities. 20/80 2MPA/L-PEI (2.5kDa) QD obtained the highest PL intensity at pH 5 and 7 (Figure 3.6 (b)). The highest PL intensity of 40/60 2MPA/L-PEI (2.5kDa) QD was seen at pH 5 (Figure 3.6 (c)). Differently PL intensity of 40/60 2MPA/L-PEI (2.5kDa) QD at pH10 was founded higher than PL intensity at pH7 (Figure 3.6 (c)). However the highest PL intensities of 2MPA/L-PEI (2.5kDa) QDs having different coating ratio were obtained at pH5.

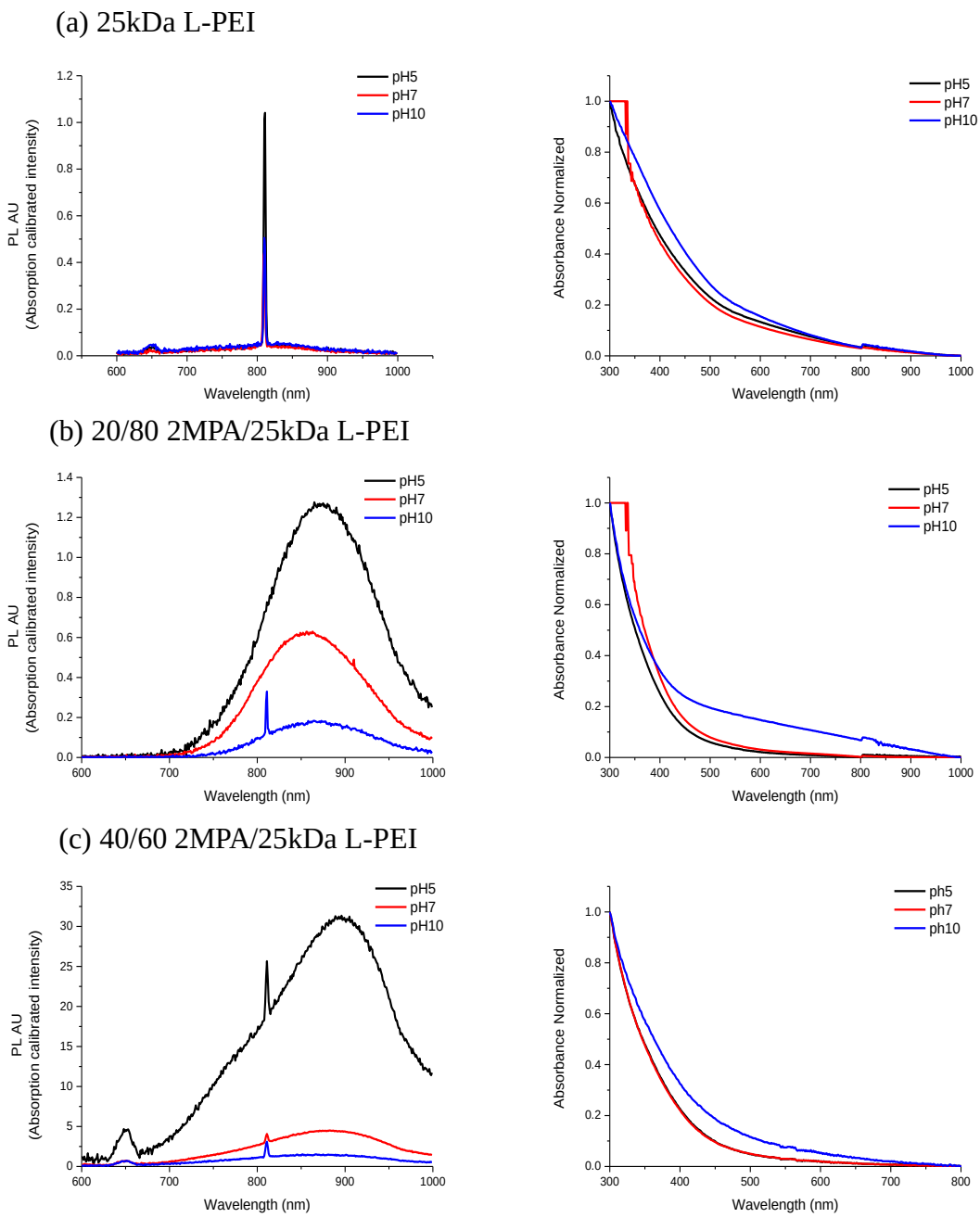

Figure 3.5 Absorption calibrated photoluminescence (left hand side) and normalized absorbance (right hand side) spectra of 2MPA/25kDa L-PEI Ag_2S NIR QDs at different pH values.

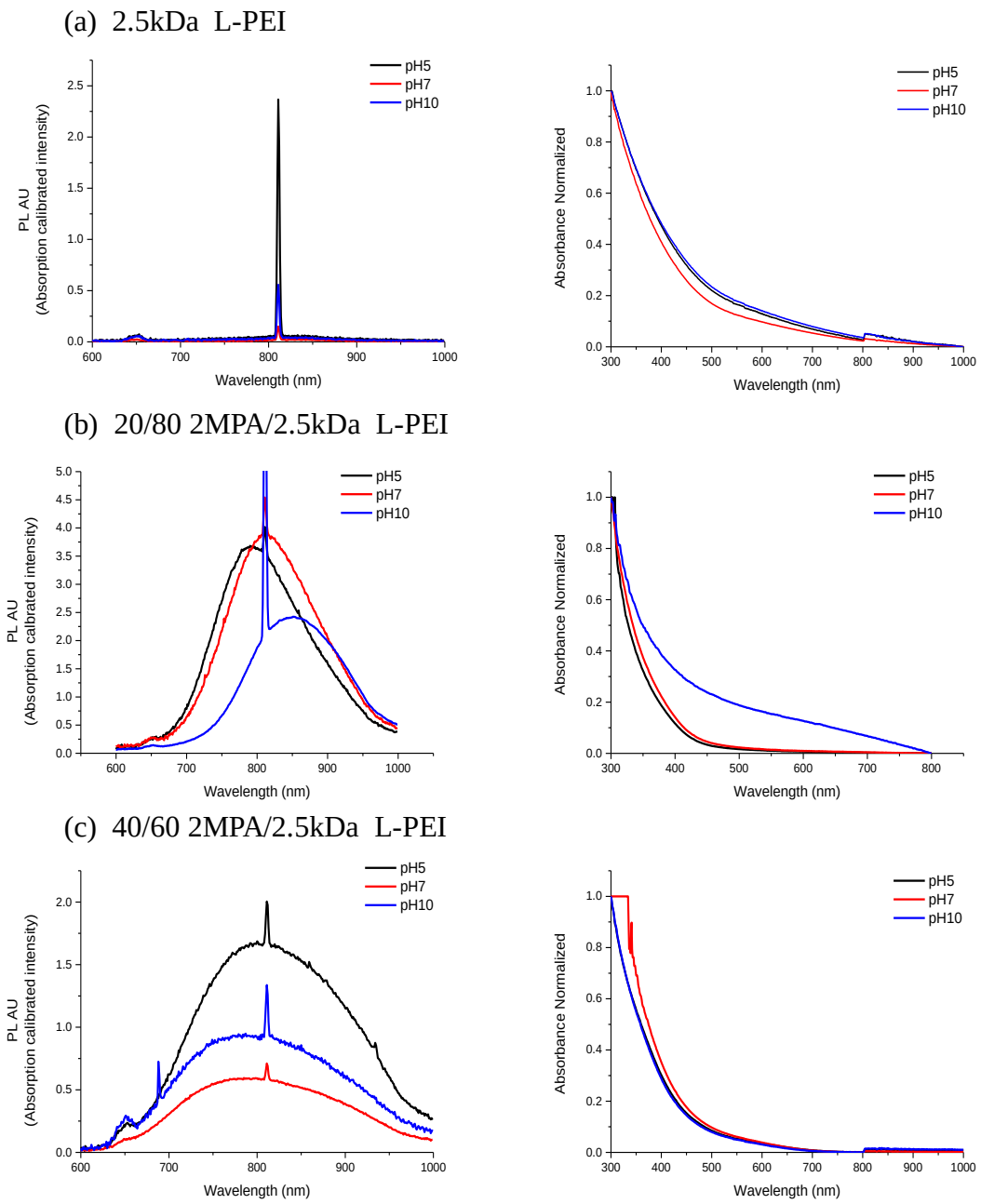

Figure 3.6 Absorption calibrated photoluminescence (left hand side) and normalized absorbance (right hand side) spectra of 2MPA/2.5kDa L-PEI Ag_2S NIR QDs at different pH values.

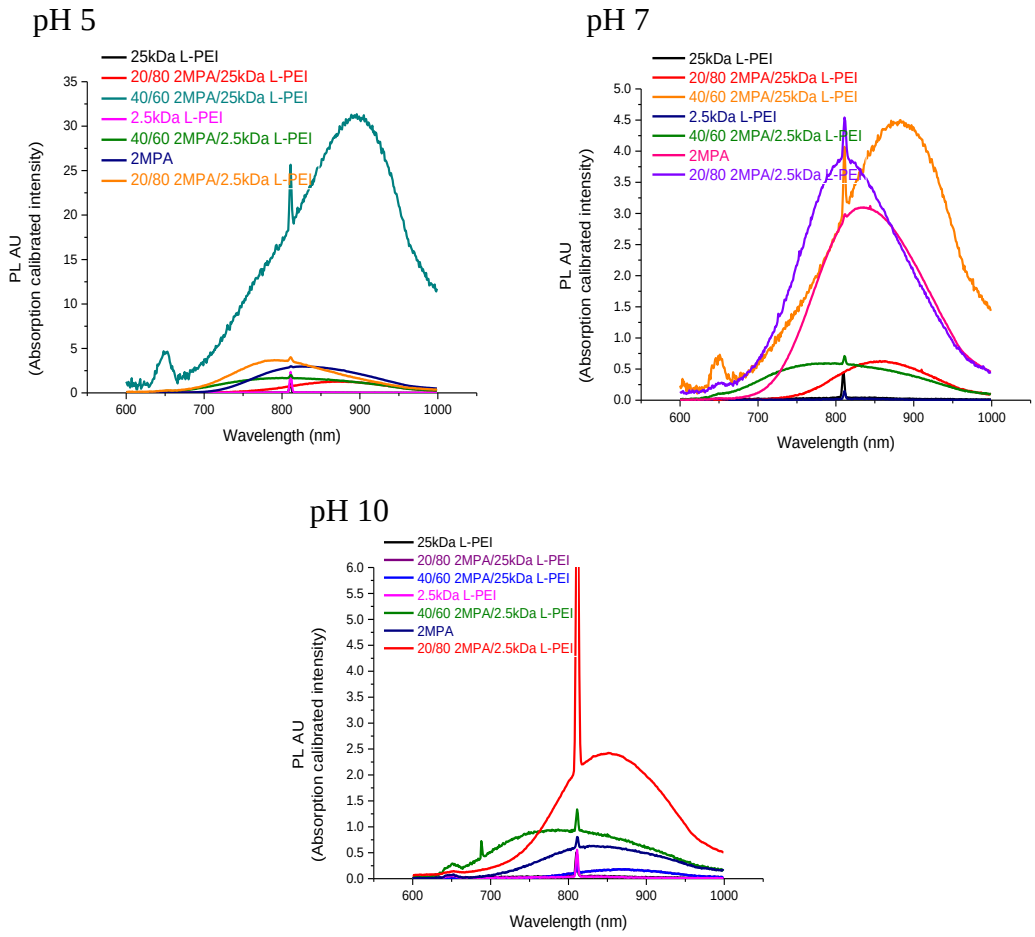

Figure 3.7 Photoluminescence spectra of 2MPA/L-PEI (MW: 2.5kDa and 25kDa) coated NIR Ag_2S quantum dots at different pH points (pH 5, 7 and 10) after synthesis.

When the emission spectra of QDs with different coatings at different pH values were investigated, the strongest luminescence peaks were detected at pH 5. Strongest luminescence was obtained from Ag_2S QD coated with 40/60 2MPA/L-PEI 25kDa at 895 nm. Other QDs had nearly same PL intensities with different peak positions (Figure 3.7). At pH 7 the most luminescent QDs were 40/60 2MPA/ L-PEI 25kDa (882 nm) and 20/80 2MPA/ L-PEI 2.5kDa (810 nm) coated ones and they luminesce also stronger than 2MPA coated ones. At pH 10, each particle lost

significant amount of intensity but 20/80 2MPA/L-PEI 2.5kDa coated QDs showed the strongest emission. At all pH values, the QD that had the most luminescence was found as 20/80 2MPA/l-PEI 2.5kDa QD.

Overall, the influence of pH was more dramatic in the luminescence intensity and especially for the 2MPA/ L-PEI 25kDa coatings. This may be due to longer chain length of the polymer and the unbound nitrogen atom amount and number of free electron pairs. The main reason behind enhanced luminescence intensity is proposed as the protonation of the amine groups. At acidic pH, protonated PEI causes electrostatic repulsion that inhibits particle aggregation and also eliminates the free electron pair which may trap the photogenerated holes in the valence band, reducing emissive electron-hole coupling process. Therefore, elimination of these processes by protonation of PEI should increase the luminescence intensity.

3.2.1.3 Quantum Yield of 20/80 2MPA/ L-PEI 2.5kDa QD

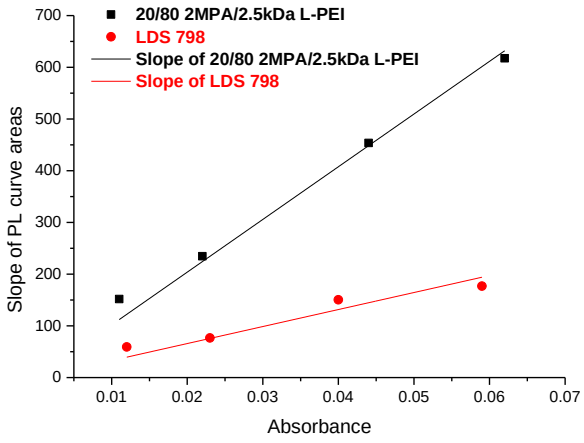

Figure 3.8 Graph of Slope of PL curve areas versus Absorbance of 20/80 2MPA/2.5kDa L-PEI QD and LDS 798 NIR dye.

Highly luminescent colloidal Ag_2S QDs were obtained with 2MPA/L-PEI mixed coatings. In order to calculate the quantum yield, Ag_2S QDs coated with 20/80 2MPA/ L-PEI 2.5kDa which showed the strongest emission at all pH values was synthesized again. Four different concentration of these QDs with absorbance values below 0.1 (0.01, 0.02, 0.04 and 0.06) at the excitation wavelength (532 nm) and LDS 798 NIR dye were prepared and the QY was calculated as detailed in chapter 2**.** At pH5, calculated QY is 310 % which is exceptionally high. However, emission intensity of the QDs decreased with time (Figure 3.9). However, even after 8 months, these particles still have strong enough emission for biomedical imaging.

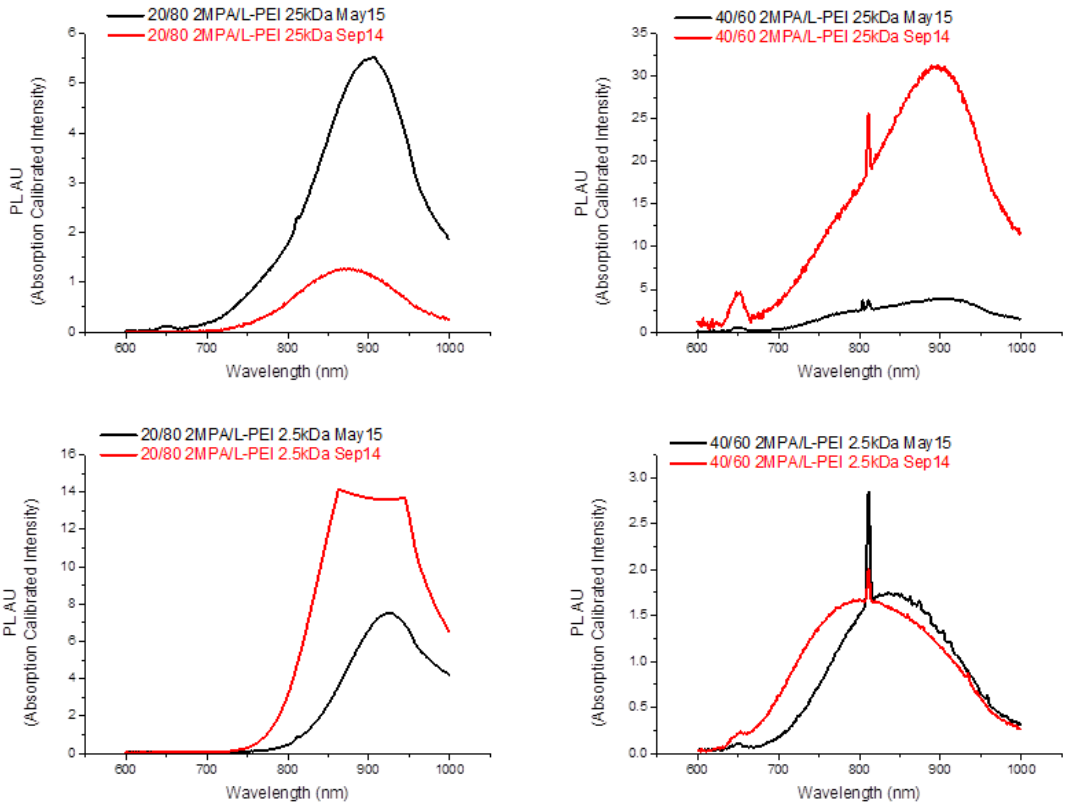

Figure 3.9 Photoluminescence spectra of 2MPA/L-PEI (MW: 2.5kDa and 25kDa) on May 2015 and September 2014.

3.2.1.4 Size Analysis of 2MPA/L-PEI Coated Ag_2S NIR QDs

Table 3.2 Hydrodynamic size and Zeta potential of 2MPA/L-PEI (MW: 2.5kDa and 25kDa) coated Ag_2S NIR QDs in different mediums.

			DIW pH 7.4		DMEM pH 7.4		DIW pH 5	
Rxn ID	**L-PEI (kDa)**	**2MPA/L-PEI**	**D[a] (nm)**	**Zeta Pot.[b] (mV)**	**D[a] (nm)**	**Zeta Pot.[b] (mV)**	**D[a] (nm)**	**Zeta Pot.[b] (mV)**
DAA-34	25	0/100	3.45±0.8	18.8 ±5.9	6.7 ± 1.5	-8.1	54.0 ± 21.8	28.2 ± 10.7
DAA-35	25	20/80		6.6 ± 5.5	7.2 ± 1.6	-13.2	25.4 ± 13.9	3.9 ± 7.6
DAA-36	25	40/60	42.8 ± 18.1		5.5 ± 1.5	-9.7	17.6 ± 6.5	42.6 ± 9.0
DAA-37	2.5	0/100	3.19 ± 0.6	3.5 ± 5.3	6.1 ± 1.5	-8.5	7.9 ± 2.6	1.3 ± 2.9
DAA-38	2.5	20/80	5.7 ±1.7	4.0 ± 3.6	836.6 ± 478.4	-12.8	3.5 ± 1.0	0.98 ± 4.5
DAA-39	2.5	40/60	3.4 ± 0.7	4.2 ± 4.0	5.5 ± 1.4	-8.73	3.4 ± 0.8	2.7 ± 5.3

[a,b] Average hydrodynamic number average and zeta potential of QDs were measured by DLS instrument.

Hydrodynamic size and zeta potential of 2MPA/L-PEI (2.5kDa and 25kDa) coated Ag_2S NIR QDs in water (pH 5 and 7.4) and DMEM were tabulated in Table 3.2. Instead of 40/60 2MPA/ L-PEI 25kDa QD, size data of all other QDs were found as less than 10 nm in water (pH 7.4). Ag_2S NIR QDs coated with 25kDa L-PEI has a very positive surface charge of +18 mV at pH 7.4 and +28 mV at pH 5 but with 2.5 kDa L-PEI had a zeta potential of 1-3 eV, almost zero. This indicates that with the higher molecular weight, more and more free amine groups on the polymeric shell is available, and with the low molecular weight, a significant portion of the amines are surface bound. Also, more positive values at lower pH is supposed to be due to the protonation of the amine groups. Actually, these reflect themselves on hydrodynamic size, as well. QDs with the mixed coating have larger hydrodynamic size in general if the L-PEI is 25kDa. Also, hydrodynamic size does not got affected from the pH (Table 3.2) significantly if low molecular weight L-PEI is used, supporting this assumption. Because protonated amine amount on L-PEI (25kDa) is more than L-PEI (2.5kDa). Similarly, except for the 40/60 2MPA/L-PEI (25kDa) coated one, all QDs with the mixed coating has a very low positive zeta potential (less than 10 mV). In general, both hydrodynamic size and zeta potential increased a little bit at pH 5. At pH 5, 2MPA/L-PEI (25kDa) QDs had bigger hydrodynamic number sizes and more positive zeta potentials than 2MPA/L-PEI (2.5kDa) QDs had. In DMEM medium, except 20/80 2MPA/L-PEI (2.5kDa) coated QD, hydrodynamic sizes of all part with larger size compared to pH 7.4 buffer, in general. Indeed, the surface charge of the particles became negative in the DMEM, indicating surface adsorption of some medium components. Since DMEM has many inorganic salts, amino acids and vitamins in its composition, it is highly possible that some of these materials interact with the QD surface altering charge and stability. Such a change in the surface charge indicated that DMEM is not a suitable medium for loading genes onto these QDs.

Particle size calculated from the Brus equation indicates the crystal core size and the size measured by DLS indicates the hydrodynamic size which includes the crystal core and the organic shell. TEM images also gives information about the morphology and the crystal size. Spherical shaped nanoparticles with particle sizes between 2 to 6nm were observed in the TEM images of 40/60 2MPA/L-PEI 25kDa coated QDs (Figure 3.10). Other QDs are expected to have similar morphology and dispersity since full width at half maximum values of the particles are similar.

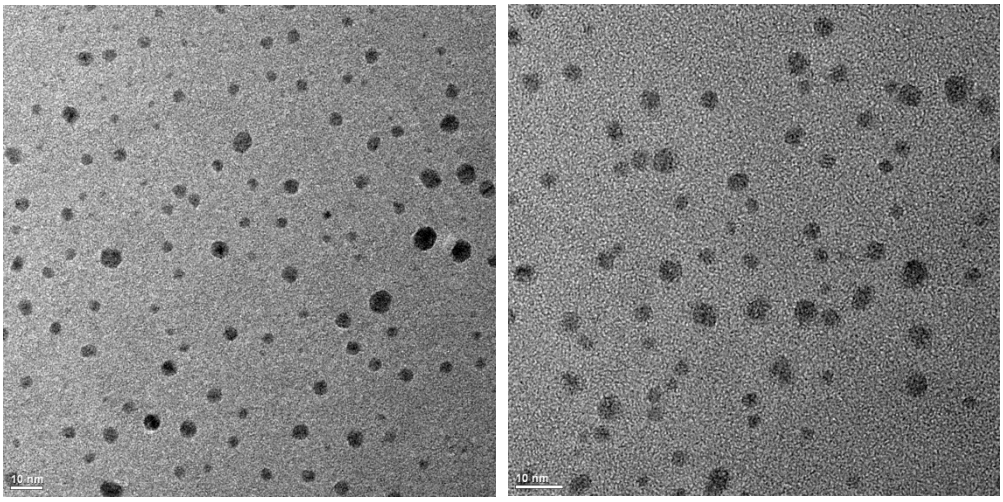

Figure 3.10 TEM images of 40/60 2MPA/L-PEI 25kDa coated QDs.

3.2.1.5 Coating Composition

The coating composition is stated as the mole ratio of the amine groups coming from the PEI and the thiol of the 2MPA used in the synthesis. However, this does not necessarily reflect the actual coating composition in the final QD synthesized. Elemental analysis of the cleaned QDs provided the actual N/S ratio in the organic coating, giving information about the actual 2MPA/L-PEI ratio.

Table 3.3 N/S ratio of L-PEI/2MPA (MW: 2.5kDa and 25kDa) coated NIR Ag_2S quantum dots.

Rxn ID	L-PEI (kDa)	L-PEI/2MPA	N (wt %)	Experimental* N/S (g/g)	S mol %
DAA-35	25	80/20	9.6	1.00	30
DAA-36	25	60/40	8.1	0.69	39
DAA-38	2.5	80/20	8.7	1.23	26
DAA-39	2.5	60/40	7.4	0.61	42

*Elemental analysis result.

Elemental analysis determines the N and S weight % of the "burned" component of the QDs (Table 3.3). Theoretically, QDs having same L-PEI/2MPA ratio should have same amount of nitrogen atom mole. When N/S w/w ratios were examined, it was found that 60/40 L-PEI (2.5kDa and 25kDa) /2MPA coated Ag_2S QDs had nearly same ratio, 0.61 and 0.69, respectively. When nitrogen mole content increased from 60 to 80 mole %, N/S ratio was increased to 1 and 1.23, for 25kDa and 2.5 kDa PEI, respectively. When these values were converted into N and S mol%, it was found that 30 and 39 mol % 2MPA is present in the final coating when 20 and 40 mol % 2MPA was used in the synthesis in case of high molecular weight PEI mixtures. When low molecular weight PEI was used, 26 and 42 mol % 2MPA was incorporated to the coating with 20 and 40 mol% initial 2MPA. Since, 2MPA has thiol groups which has higher affinity to particle surface, higher amounts of 2MPA than the formulation was found in the final composition.

3.2.1.6 *In Vitro* Toxicity Evaluation of 2MPA/ L-PEI Coated Ag_2S QDs

Table 3.4 Silver and nanoparticle concentration of 2MPA/ L-PEI Ag_2S QD solutions.

Rxn Code	PEI MW (kDa)	2MPA/PEI (mol ratio)	Ag[a] (µg/mL)	Particle[b] (µg/mL)
DAA-34	25	0/100	10	42.4
DAA-35	25	20/80	10	37.6
DAA-36	25	40/60	10	43.4
DAA-37	2.5	0/100	10	105.8
DAA-38	2.5	20/80	10	45.2
DAA-39	2.5	40/60	10	62

[a] ICP-OES, [b]Weight of solid content after evaporation of water.

Cell viability studies of 2MPA/ L-PEI (2.5kDa and 25kDa) Ag_2S QDs were performed by MTT test. Doses of the QDs were prepared based on Ag ion content of the particles which was detected by ICP-MS. Ag concentration in the range of 0.75-10 µg/mL was used for the cell viability studies. Since each formulation had different particle concentration and crystal size, particle concentration was reported at fixed Ag concentration of 10 µg/mL Ag in Table 3.4. It seems like there is more organic content in formulations with higher PEI content.

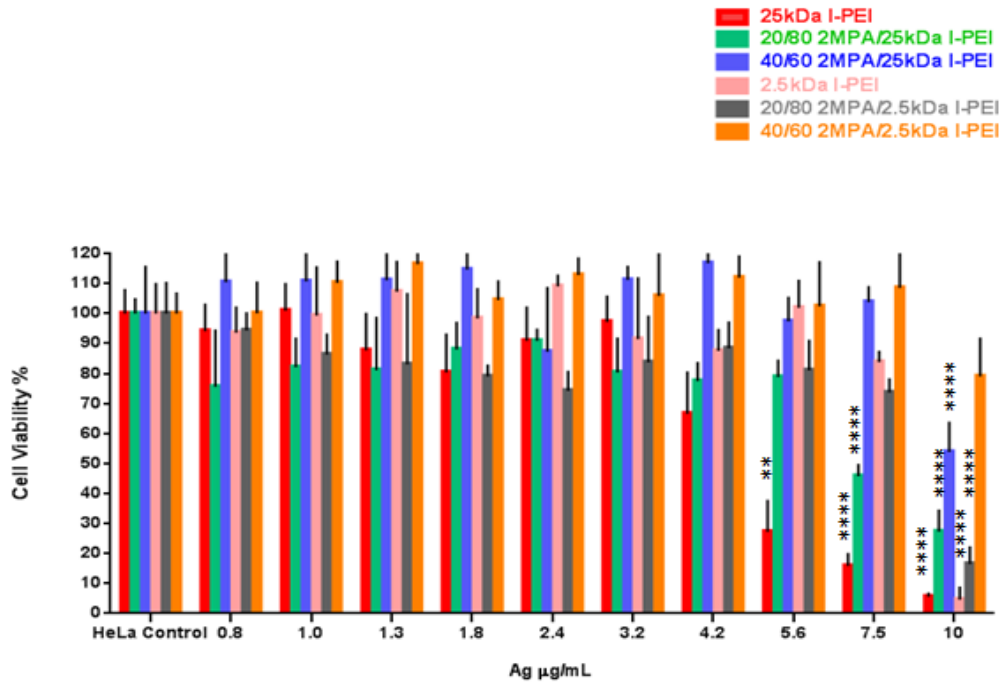

Figure 3.11 Viability of HeLa cells in the presence of 2MPA/L-PEI Ag_2S QDs (pH 7.4) after 24 hours incubation as determined by MTT assay (one-way ANOVA with Tukey's multiple comparison at $p < 0.05$(*), $p < 0.01$ (**), $p < 0.001$ (***) and $p < 0.0001$(****).

In the cell viability studies one of the most studied cells, human cervical cancer (HeLa) cell line was used. pH of the particles were set to 7.4 before incubation. According to the results shown in Figure 3.11, the most toxic QD is the L-PEI (25kDa) coated Ag_2S and at 5.6 µg/mL Ag dose cell viability decreased below 30%. As expected, QD coated with 2.5kDa L-PEI is much less toxic and the significant toxicity was seen at 10 µg/mL Ag dose. This is in agreement with the molecular weight dependent toxicity data reported in the literature. When QDs with the mixed coatings were investigated, it was seen that increasing L-PEI in the compositions increased the toxicity. However, mixed coating compositions bring about a synergy in the toxicity and reduced toxicity compared to pure PEI coatings.

Overall, QDs with mixed coating having 2.5kDa L-PEI were more biocompatible and actually up till 5.5 µg/mL Ag dose they are all cytocompatible. One of the important discoveries of this study is that 40/60 2MPA / L-PEI (25kDa) Ag_2S QDs are not toxic even at 10 µg/mL Ag dose. Since this QD has 25kDa L-PEI, non-toxic nature is very valuable since the transfection efficiency usually increases with the molecular weight. (Figure 3.11)

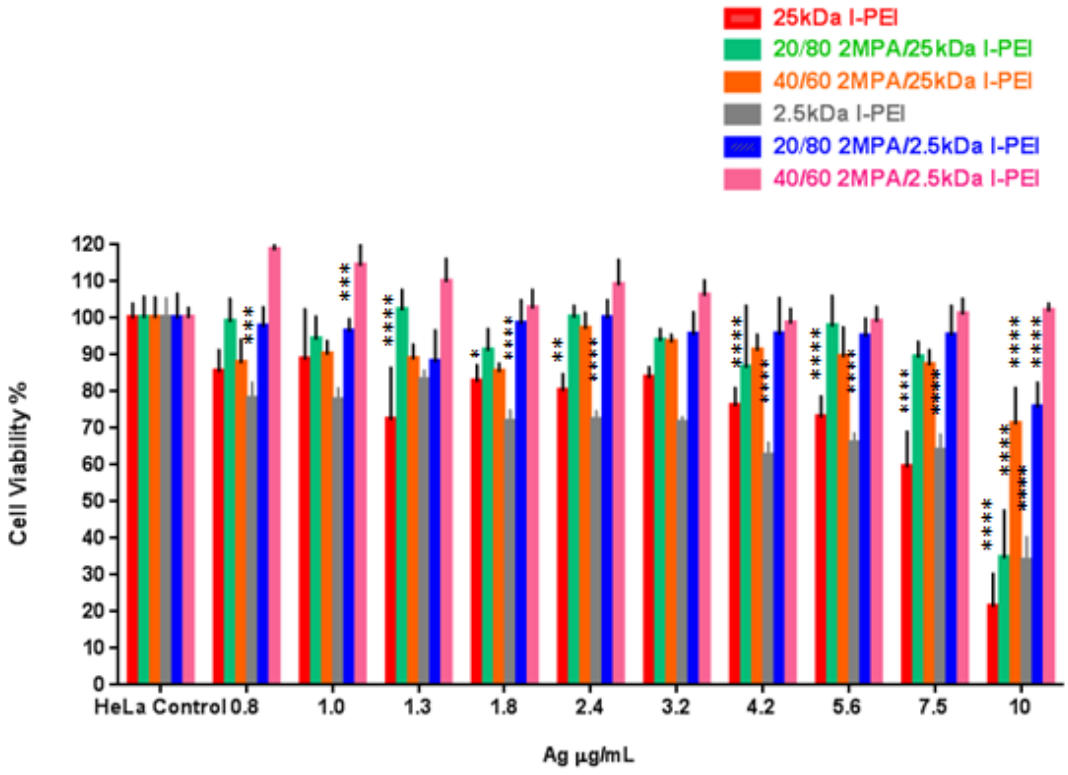

Figure 3.12 Viability of HeLa cells in the presence of 2MPA/L-PEI Ag_2S QDs (pH 5) after 24 hours incubation as determined by MTT assay (one-way ANOVA with Tukey's multiple comparison at $p < 0.05$(*), $p < 0.01$ (**), $p < 0.001$ (***) and $p < 0.0001$(****).

To examine the effect of acidic pH also on the cell viability, MTT assay was also performed at pH 5 (Figure 3.12). For exact comparison, again HeLa cell line and same doses were used. When Figure 3.12 was investigated, it was seen that QDs, specifically the L-PEI coated ones, showed slightly higher toxicity at low doses when their pH was adjusted to 5 with much less difference between the 2.5 and 25 kDa PEI. In this study, toxicity of 2.5kDa L-PEI coated QDs started at 0.8 μg/mL Ag dose and 25kDa L-PEI coated QDs started at 1.3 μg/mL Ag dose. It was expected that acidic pH would produce more positive surface which may increase cell internalization and toxicity, yet on the other hand the most dramatic charge and size change based on acidic pH was observed only in case of 25kDa L-PEI coated QDs (Table 3.2). Also, since the incubation medium is DMEM and all particles possess a negative charge in this medium, no dramatic difference may be normal. Amongst the QDs with the mixed coating, the most toxic one was 20/80 2MPA /L-PEI (25kDa) QD again. The most biocompatible QD at acidic pH was found as 40/60 2MPA/L-PEI (2.5kDa). The pH study also showed that when mole amount and molecular weight of L-PEI increased, toxicity also increased. Because of this reason 20/80 2MPA/L-PEI (2.5kDa) QD emerged as the most biocompatible QD.

2MPA/L-PEI Ag_2S QDs are expected to be effective gene delivery vehicles. p53 tumor suppressor gene is one of the targets for such a study. Because of this reason, p53 positive (HCT 116 WT) and negative human colon cancer cell lines were also used in the toxicity studies of 2MPA/L-PEI (2.5kDa ve 25kDa) Ag_2S QDs. In the HCT 116 WT (Figure 3.13) significant toxicity was seen even at 1 μg/mL Ag concentration. On the other hand, viability above 100% at high doses were seen. 2.5kDa L-PEI coated QD had 150% viability at 0.8 μg/mL Ag concentration and 20/80 2MPA/L-PEI (25kDa) Ag_2S QD had between 130% and 150% viability values at each dose from 2.4 to 7.5 μg/mL Ag. 20/80 2MPA/L-PEI (2.5kDa) Ag_2S QD had also more than 100% viability at each dose between 2.4 to 7.5μg/mL Ag. Similar results were also seen in our previous experiments with other Ag2S QDs. MTT viability test is not directly related to viable cell number. MTT viability test is directly related to activity of the enzyme that reduces

MTT dye into formazan dye. These QDs could cause stress for cell line after internalization and the activity of the mitochondrial enzyme could increase because of the stress. All results that were above 100% viability dramatically decreased at 10µg/mL Ag dose. Dose dependent toxicity of L-PEI (2.5 and 25kDa) coated QDs was seen and these QDs were found as the most toxic QDs for this cell line, too (Figure 3.13). All QDs with mixed coatings are dramatically more cytocompatible and caused ca 80% viability at 7.5µg/mL Ag dose. The most biocompatible QD in HCT 116 WT cell line were found as 40/60 2MPA/L-PEI (2.5 and 25kDa) Ag_2S QDs with no significantly toxicity even at 10µg/mL (Figure 3.13).

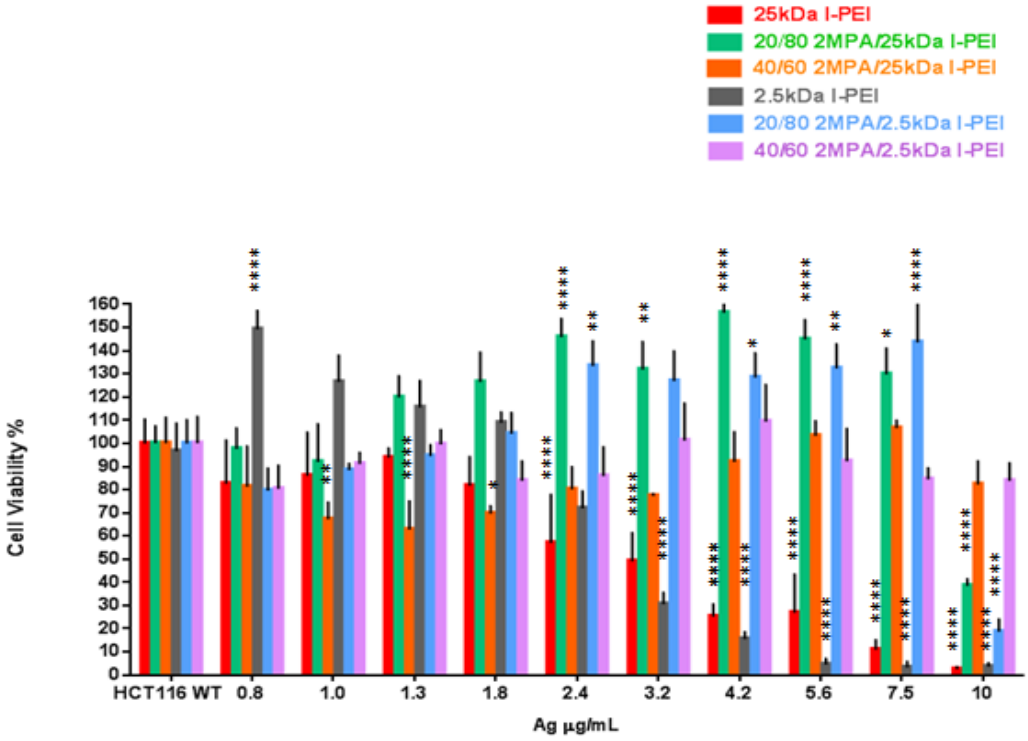

Figure 3.13 Viability of HCT116WT cells in the presence of 2MPA/L-PEI Ag_2S QDs (pH 7.4) after 24 hours incubation as determined by MTT assay (one-way ANOVA with Tukey's multiple comparison at $p < 0.05$(*), $p < 0.01$ (**), $p < 0.001$ (***) and $p < 0.0001$(****).

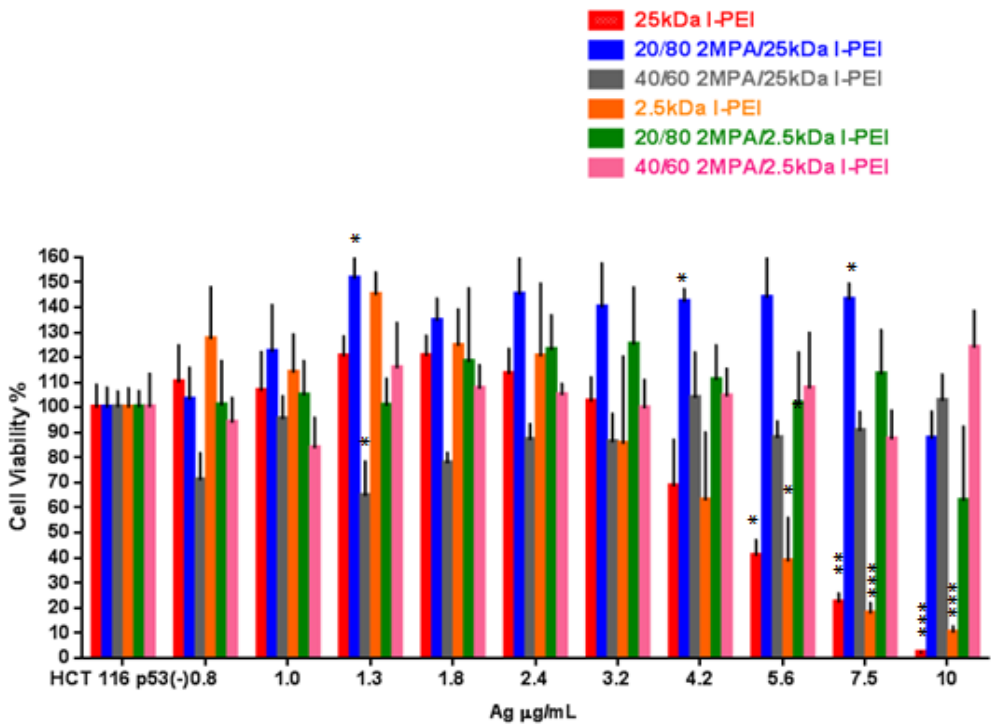

Figure 3.14 Viability of HCT116 p53(-) cells in the presence of 2MPA/L-PEI Ag_2S QDs at pH 5 after 24 hours incubation time and measured by MTT assay (one-way ANOVA with Tukey's multiple comparison at $p < 0.05$(*), $p < 0.01$ (**), $p < 0.001$ (***) and $p < 0.0001$(****).

Cytocompatibility of these QDs in HCT166 p53(-) cells which lack the p53tumor suppressor gene was also determined by MTT assay (Figure 3.14). The most toxic QDs are again the ones with only PEI coating with no dramatic difference between the molecular weights. Toxicity with only PEI coated QDs were seen first at 5.6µg/mL Ag dose. Again QDs with the mixed coating were much more cytocompatible and none of them showed any significant toxicity even at 10µg/mL Ag dose. 40/60 2MPA/L-PEI (2.5 kDa) Ag_2S QDs was detected as the least toxic QD. These results were found consistent. HCT 116 p53(-) cells were expected to be more resistant than the WT, because these cells didn't have tumor suppressor p53 gene that also induces apoptosis, and MTT results supports this.

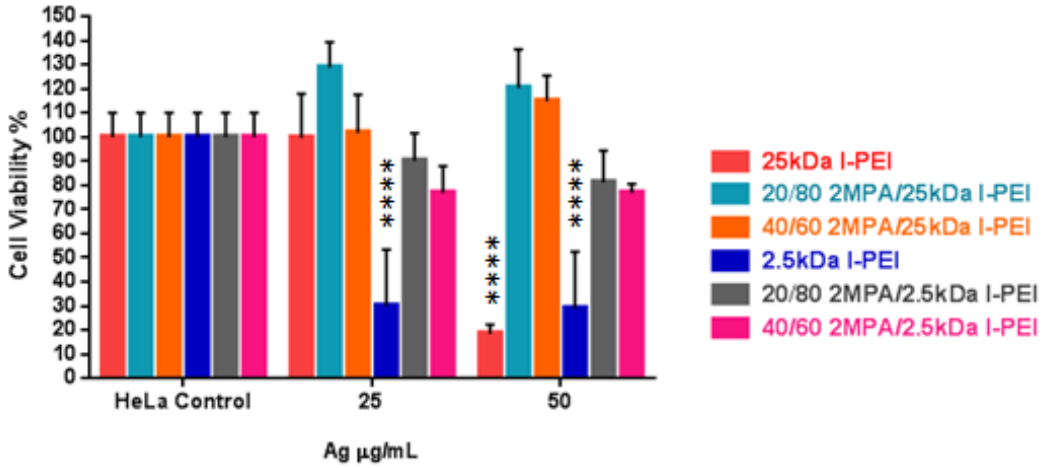

Figure 3.15 Cell viability of HeLa cells in the presence of 2MPA/L-PEI Ag_2S QDs at pH 5 after 4 hours incubation time and measured by MTT assay (one-way ANOVA with Tukey's multiple comparison at $p < 0.05$(*), $p < 0.01$ (**), $p < 0.001$ (***) and $p < 0.0001$(****).

It is important to relate the cell viability to the cellular internalization of QDs. Many times, the lower cytotoxicity is due to lower uptake of the particles by the cells. ICP-MS technique was utilized to measure the amount of internalized QDs by the cells. Due to the detection limits of the instrument, high doses of QDs (25 and 50µg/mL Ag) were incubated with cells for 4 hour. Then both toxicity by MTT and uptake by ICP-MS was determined. Under these conditions, only PEI coated QDs showed significant toxicity and indeed, 2.5kDA PEI coated Ag2S QD caused about 30% viability at both doses but 25kDa PEI coated Ag2S showed dramatic toxicity only at 50 µg/mL Ag dose (Figure 3.15). This is somewhat different than what was observed at low doses (Figure 3.11). But actually, at 10ug Ag/mL, after 24h incubation both nanoparticles showed similar toxicity to HeLa cells. This can be correlated well with much higher internalization of 2.5kDa L-PEI Ag2S QDs compared to 25kDa L-PEI Ag2S QDs

(Figure 3.16). However, the origin of such difference in cell internalization is not clear since in DMEM both QDs have similar zeta potential and hydrodynamic size (Table 3.2) The only major difference is that at pH 7.4 Ag2S QDs coated with 25kDa PEI has mcuh higher positive zeta potential, meaning more cationic surface which could have actually increase the cellular internalization. Therefore, the origin of such behaviour needs further investigation such as determination of protein corona.

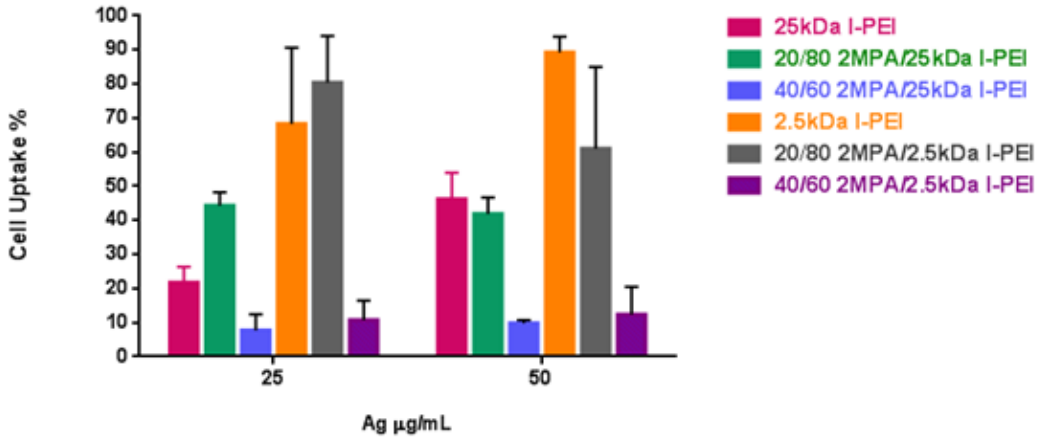

Figure 3.16 Quantification of internalized 2MPA/L-PEI Ag_2S QDs (pH 7.4) by HeLA cells in 4 hours incubation time.

In the same study, QDs having a mixed coating didn't show any significant toxicity; therefore these cell uptake data should be quite reliable. The most dose dependent uptake was determined for Ag2S QDs coated with 25kDa L-PEI. For the rest, considering the error bars, there is no significant dose dependence. An interesting finding is that QDs with 40/60 2MPA/L-PEI (2.5kDa and 25kDa) coating were internalized in the least amount by HeLa cells: less than 20% at each dose. Cells internalized about 40% of the material if 20/80 2MPA/L-PEI (25kDa) coating was used

(Figure 3.15) regardless of the dose used. But the internalization increased with 2.5 kDa L-PEI mixed coatings. Overall, low molecular weight PEI caused higher internalization and the mixed coatings with 80% PEI with the 2.5kDa L-PEI were internalized more, yet allowed more than 80% viability. High uptake and low toxicity is very crucial for drug and gene delivery studies. QDs with 60% L-PEI regardless of the molecular weight were internalized in smaller amounts and did not cause significant toxicity.

3.2.1.7 Evaluation of 2MPA/ L-PEI Ag_2S QDs as Optical Probes

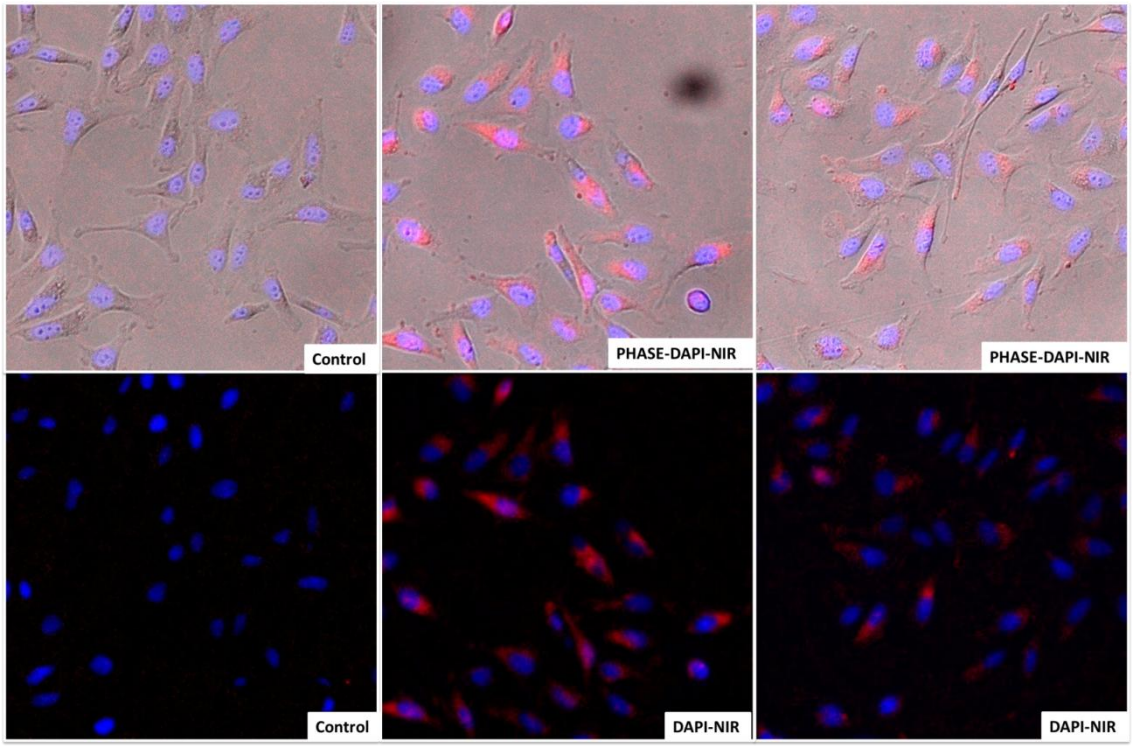

Figure 3.17 Inverted fluorescence microscopy images of HeLa cells incubated with 40/60 2MPA/L-PEI (25kDa) Ag_2S QD at 50µg/mL Ag dose for 4 hours. NIR filter (excitation wavelength = 550 nm, 640 nm long pass emission filter)

In order to visually confirm the internalization of 2MPA/L-PEI Ag_2S QDs by the cells and evaluate their use as optical diagnostic probes, cell incubated with QDs were imaged under inverted fluorescence microscope (Figure 3.17). High dose and short incubation times were used (50µg/mL Ag dose). DAPI dye and DAPI filter was utilized to stain the cell nucleus. Even though, the sensitivity of the detectors used in the microscope falls around 30 % right after 800 nm, 40/60 2MPA/L-PEI Ag_2S QD with emission peak maximum at 897 nm, showed a very strong signal with a NIR filter (excitation wavelength = 550nm, 640 nm long pass emission filter). In Figure 3.17, the red color represents the emission originating from 40/60 2MPA/L-PEI Ag_2S QD using the NIR filter and the blue color represents cell nucleus that is imaged by DAPI filter. When the images of QD internalized cells were compared with the control cell images, highly strong optical signal was observed. The QD signal was distributed in the cytoplasm of the cells.

In order to support optical probe feature of the 2MPA/L-PEI Ag_2S QDs, another biological model, c.elegans, was also used. C.elegans have many advantages to be chosen as a model for biological studies. First of all, they are transparent and they can be easily analyzed. They are resistant to extreme conditions and have 35 % homolog human genes. C.elegans were incubated in QD (20/80 2MPA/L-PEI (25kDa) Ag_2S) solution at 320µg/mL Ag dose for 2 hours. Then the images were taken by inverted fluorescence microscope. QD internalized c.elegans showed very strong NIR signal that was homogeneously distributed (Figure 3.17). The optical signal was only absent in the eggs of the c.elegans because of the anatomically very hard protective coating of the eggs.

These confirm the suitability of these new QDs as optical probes in optical imaging studies.

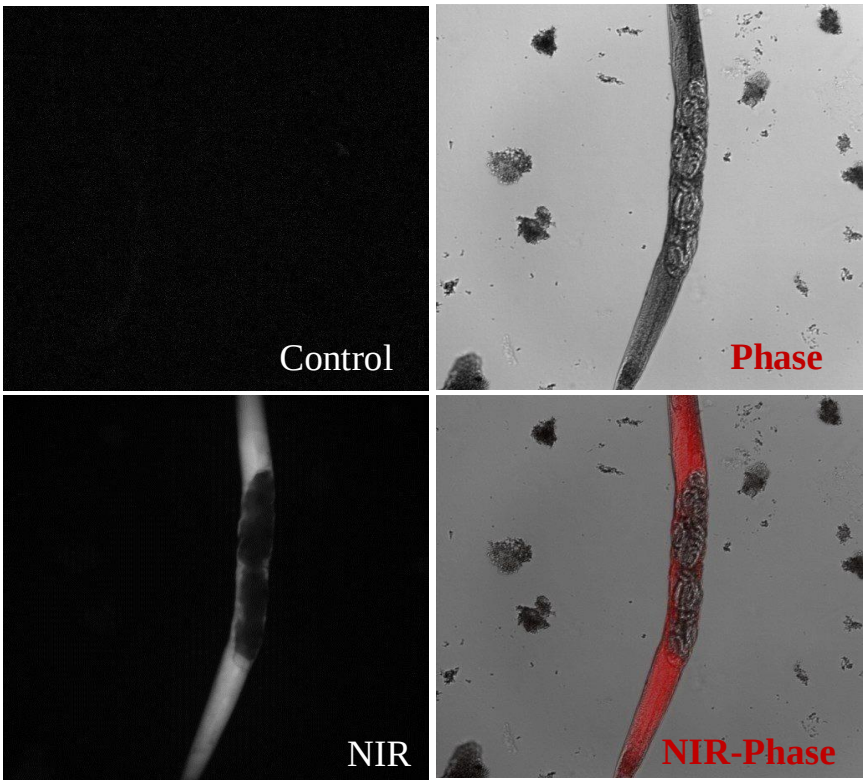

Figure 3.18 Inverted fluorescence microscopy images of 20/80 2MPA/L-PEI (25kDa) Ag_2S QD internalized c. elegans. Incubation dose : 320µg/mL Ag, İncubation time: 2h. Excitation at 550nm and NIR filter was used in the emission.

3.3 Conclusion

Colloidal L-PEI and 2MPA/L-PEI coated Ag_2S QDs were synthesized in aqueous solution. L-PEI produced colloidally stable but non-luminescent particles, regardless of the molecular weight (2.5 and 25 kDa). 2MPA/L-PEI mixed coatings produced colloidally stable, small, cationic Ag_2S QDs that are highly luminescent in the NIR region. The crystal size and the emission wavelength of the QDs can be tuned by the 2MPA/L-PEI ratio. The emission peak maxima of the QDs are between 791-897 nm which is quite suitable for medical imaging. Mixed coating provided a synergy in the optical properties. In general, all QDs with the mixed coating showed a stronger

luminescence than the 2MPA coated QDs. Yet, emission properties were influenced by the pH of the environment: QDs showed higher luminescence intensity at pH 5, which may be partly due to disaggregation of particles upon protonation. These are all favorable properties for biological studies utilizing these QDs.

Cytocompatibility of all QDs were determined in three different cell lines: One of the most widely used cells, HeLa, and also HTC 116 both wild type and p53 negative. In general, Ag_2S QDs coated only with L-PEI were the most toxic ones. Those with the mixed coatings were more cytocompatible based on the MTT assay, indicating a synergy in the toxicity as well. Toxicity started at around 7.5 and 10 μg Ag/mL dose, respectively in HeLa and HCT116 WT cells. HCT116 p53(-) cells were more robust and no toxicity was observed with mixed coatings even at 10μg Ag/mL. Toxicity of the Ag_2S QDs with the mixed coating is higher if the When L-PEI amount in the composition increased, formulation has 80% PEI compared to those with 60%. Molecular weight of the L-PEI did not show a uniform trend in the toxicity if a mixed coating is used, which is actually an advantages outcome of the study. Internalization of the nanoparticles by the HeLa cells were determined at high dose and short incubation time which indicated that only L-PEI coated Ag_2S QDs are internalized more than the ones with 60% L-PEI in the coating formulation, 2.5 kDa L-PEI coated ones are internalized most, and 80% L-PEI containing ones have a dose independent uptake around 40% with 25KDa L_PEI and 70-80% with 2.5kDa PEI. Most importantly, under these circumstances none of the QDs with the mixed coating caused any significant toxicity to HeLa cells whereas the only L-PEI coated caused a significant drop in the cell viability.

QDs with the mixed coating were also evaluated as optical probes using HeLa cells and c. elegans. In both studies, using a NIR filter set in the fluorescent microscope and a visible light excitation source, very strong optical images were obtained.

Overall, 2MPA/L-PEI coating provided biocompatible NIR emitting Ag2S QDs with strong optical signals both *in vitro* and *in vivo*. Hence, they have great potential as multifunctional nanoparticles.

Chapter 4

DEVELOPMENT OF Cyseine/L-PEI STABILIZED Ag_2S QUANTUM DOTS

4.1 Research Objectives

In an effort to develop cationic and biocompatible Ag_2S QDs, as shown in Chapter 3, L-PEI can be successfully used as the organic cationic coating, but in order to have strongly luminescent NIR Ag_2S QDs, a mixed coating composed of L-PEI with a small thiolated molecule, 2MPA, is necessary. Indeed, both optical properties and the Cytocompatibility of cationic Ag_2S QDs improved with the incorporation of 2MPA into the coating.

Research presented in this chapter focuses on development of Ag_2S NIR QDs with Cyseine/L-PEI mixed coatings. Cyseine is an amino acid having a thiol side chain and biosynthesized in the humans. It was considered as a good alternative to 2MPA in the co-stabilization of Ag_2S QDs with L-PEI, since it is a biocompatible amino acid, has a thiol group for surface binding and also a free amine group in addition to a free carboxylic acid. In the literature many examples of Cyseine coated QDs can be found. As an example, Cyseine coated CdSe/CdS QDs reported to have narrower size distribution and higher QY than mercaptoacetic acids coated CdSe/CdS QDs. In this chapter, effects of Cyseine (Cys) in the mixed coating on Ag_2S properties, specifically stability, QY, emission wavelength and toxicity will be discussed.

4.2.1 Quantum Dot Synthesis and Characterization

Table 4.1 Formulation and Properties of Cyseine/L-PEI coated NIR Ag_2S Quantum Dots

Rxn Code	PEI MW (kDa)	Cys/PEI (mol ratio)	pH	Emission λ_{max} (nm) (pH 5)	D[a] (nm)	Band Gap (eV)
DAA-41	25	40/60	5.7	830	2.5	1.7
DAA-42	25	50/50	5.7	828	2.5	1.6
DAA-43	25	20/80	5.7	727	2.3	1.8
DAA-44	2.5	40/60	5.7	810	2.5	1.6
DAA-45	2.5	20/80	5.7	783	2.3	1.8
DAA-46	2.5	50/50	5.7	897	2.6	1.6
DAA-47	-	100/0	5.7	910	2.5	1.6

[a] Particle sizes calculated by Brus equation [47]

All particles were prepared at fixed coating/Ag/S mole ratio of 20/4/1 at 70 ºC and pH 5.7 where L-PEI was dissolved completely. Cys/L-PEI ratios of 100/0, 20/80, 40/60 and 50/50 were studied (Table 4.1). Two different molecular weights of L-PEI that are 2.5 kDa and 25 kDa were studied. All QDs with the Cys/ L-PEI mixed coatings were colloidally stable and luminesce in the NIR region when excited at 532 nm. Crystal sizes of these QDs were calculated from Brus equation using the absorbance onset determined from the absorbance spectra as explained in Chapter 2. Band gap energies of the QDs related to their crystal sizes were calculated between 1.6 eV and 1.8 eV. The emission maxima of only Cys coated Ag_2S QD was found as 910 nm. Cys/L-PEI mixed coated Ag_2S QDs had emission maxima wavelengths between 727-897 nm. The emission maxima of Ag_2S QDs with the mixed coating having 25kDa L-PEI were between 727-830 nm. When 2.5 kDa L-PEI was used, this range red shifted to 783-897 nm. In general, as the PEI content increased the emission maxima shifted to lower wavelengths indicating smaller crystal sizes (Table 4.1). This is similar to trend seen in 2MPA/L-PEI coated Ag_2S QDs (Figure 3.1). However, in case of 2MPA containing mixed coatings, 25 kDa L-PEI caused larger particle sizes and hence emission at longer

wavelengths. This may suggest that in case of Cyseine/L-PEI, longer polymer chains passified the crystal surface more effectively than shorter chains, but it is vice versa in case of 2MPA/L-PEI coatings. In addition the effect of the coating composition in the emission maxima position is more dramatic in case of Cys containing coatings compared to 2MPA containing ones. For example as Cyseine increased from 20 to 40%, emission maxima showed about 113 nm red shift with 25kda PEI and 27 nm with 2.5kDa L-PEI (Table 4.1). These values were 25 nm and 21 nm in case of 2MPA/L-PEI coated Ag_2S QDs. This indicates a difference in the surface passivation of Cyseine versus 2MPA and difference in the interaction between L-PEI and 2MPA versus L-PEI and Cyseine. Yet, since small molecules can adsorb on the crystal surface more quickly with faster diffusion and thiolated molecules bind more strongly to the crystal surface (thiols are soft bases and Ag^+ is a soft acid, whereas amines and carboxylic acids are hard bases), decreasing crystal sizes were expected with increasing amount of 2MPA or Cyseine. Observation of just the opposite suggests that, when higher content of a macromolecule is used, Ag ions are mostly coordinated with the relatively slowly diffusing macromolecules, and as the concentration and/or the molecular weight of the macromolecule increases, number of Ag ions per chain decreases. Each Ag-polymer complex may be considered as a nanoreactor and each nanoreactor has less Ag as the molecular weight and/or the amount of macromolecule increases, hence produces smaller crystals. Emission maxima of 20 and 40 % Cyseine containing and 2MPA containing Ag_2S QDs with mixed coatings are similar when 2.5kDA PEI was used (Table 3.1 and 4.1), but significantly shifted to lower wavelengths with Cyseine compared to 2MPA if 25kDa L-PEI was used. This may indicate better surface passivation of Cyseine versus 2MPA and/or larger amount of Ag-Cyseine complex formation compared to Ag-2MPA.

4.2.1.1 Influence of Reaction Time on Particle Size and Emission Properties of Ag_2S QDs

Particle growth and the optical properties Ag_2S QDs with 40/60 and 50/50 Cys/ L-PEI 25kDa were tracked by analyzing the aliquots taken from the reaction mixture during crystal growth. When photoluminescence spectra of these aliquots were examined (Figure 4.1), the maximum luminescence intensity was detected at the 3rd hour of the reaction when 40/60 Cys/25kDa L-PEI was used. However, most intense luminescence was obtained in the 1h aliquot of the Ag_2S QD synthesis with 50/50 Cys/25kDa L-PEI coating. Yet, between 5 min to 3-4h there was no significant difference in the emission peak position, which may indicate that as time passes, just the quality of the particle improved not the stable size of the crystal at this temperature. Such difference in the optimum reaction time may have various origins. Increasing Cys in these compositions increases the Ag-Cys complex which would have faster diffusion to crystal surface compared to Ag-PEI complexes and since thiols bind more strongly, less desorption takes place on the nanocrystal surface.

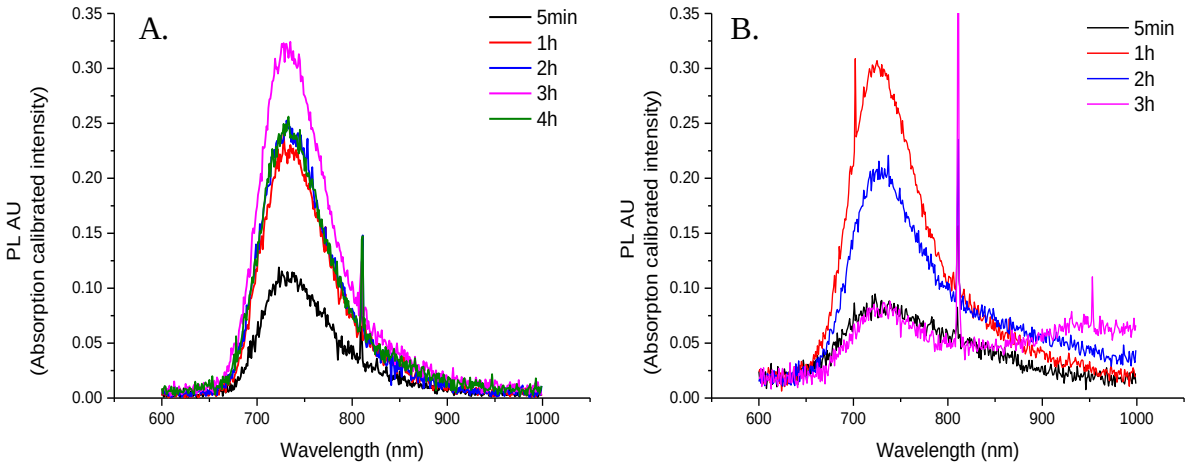

Figure 4.1 Photoluminescence spectra of (A) 40/60 and (B) 50/50 Cys/25kDa L-PEI coated Ag_2S NIR Quantum Dots at different time points during the synthesis.

4.2.1.2 Influence of the pH on Optical properties of Ag_2S NIR QDs

All QDs were synthesized at pH 5.7 because of the limitation in the solubility of L-PEI, but the influence of the pH (pH 5, 7, 10) of the medium after synthesis on the particle properties were determined. 100% L-PEI coated Ag_2S quantum dots didn't show any photoluminescence (PL) after synthesis at any of these pH values. A significant change in the photoluminescence of 100% Cys coated Ag_2S quantum dots at different ph values: the strongest emission was seen in acidic (pH 4.5) and then neutral (pH 7.5) conditions. The weakest PL emission intensity was observed under basic (pH 10.5) condition. Photoluminescence peak position of Cys coated Ag_2S quantum dots in acidic medium was 25 nm longer than the peak position in basic medium (Figure 4.2).

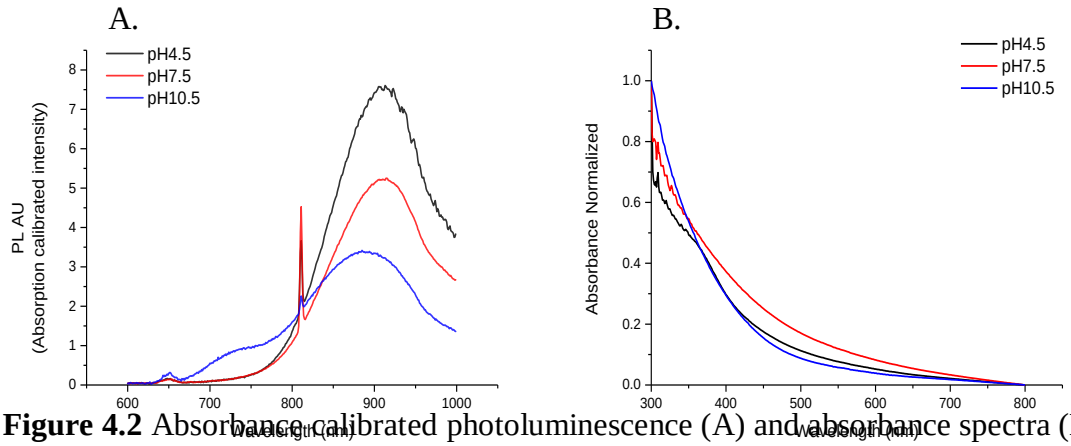

Figure 4.2 Absorbance calibrated photoluminescence (A) and absorbance spectra (B) of Cys coated Ag_2S NIR quantum dots at different pH values after the synthesis.

Photoluminescence of Ag_2S QDs with the Cys/L-PEI coatings showed a pH dependent emission maximum and emission intensity as well (Figure 4.3 and Figure 4.4). Similar to the 2MPA/L-PEI coated QDs, the weakest emission was detected under basic conditions (pH 10.5) and in general the strongest emission was seen under acidic conditions. Absorbance of QDs with 40/60 and 50/50 Cys/L-PEI (25kDa) coatings is significantly higher under neutral condition which may be partially due to aggregation (Figure 4.3). PL emission maxima of 40/60 and 50/50 Cys/L-PEI (25kDa) coated QDs at neutral pH were broad and located between the peak positions at acidic and basic

conditions. This may also indicate pH dependent aggregation. Emission maxima of each QD was detected at lower wavelengths with decreasing pH. The emission maxima of 40/60 Cys/L-PEI (25kDa) coated QD was at 750 nm at pH 10.5 and 828 nm at pH 4.5 (Figure 4.3a). Emission maxima of 50/50 Cys/L-PEI (25kDa) coated QD was at 740 nm at pH 10.5 and 827 nm at pH 4.5 (Figure 4.3b). 20/80 Cys/L-PEI (25kDa) coated QD didn't have any luminescence at basic pH but it had highly strong PL emission at acidic condition (pH 4.5) (Figure 4.3c). This composition was unstable at neutral pH.

LPEI has only secondary amines with a pKa of 7.9. Isoelectric point of Cyseine is at pH 5.05 and pKa of the acid, amine and thiol groups are 1.92, 10.7 and 8.30, respectively. Therefore at pH 4-5, lysosomal pH, except the carboxylic acid all functional groups should be protonated, yet if an excessive protonation of the surface bound thiol would have taken place than a decrease in the luminescence intensity and particle dissolution would be observed. At pH 7, lower amount of PEI amines will be protonated and at basic pH no amine protonation would take place.

Disaggregation of loose aggregates with protonation of amine groups and removal of free electron pair of nitrogens, which may act as hole-scavengers, would be expected under acidic conditions, hence stronger emission intensity was expected and actually observed. In this case surface charge, interaction between coating materials and intermolecular interaction of these QDs should have caused the differences in emission wavelengths corresponding to the change in pH. Similar results were obtained with Cys/L-PEI (2.5kDa) coated Ag_2S QDs with slightly smaller shifts in the emission maxima (Figure 4.4). When both molecular weights are taken into account, the most dramatic effect of acidification on luminescence intensity was seen in case of 20/80 Cys/L-PEI Ag_2S QDs. This is interesting since Cys coated QDs showed sensitivity to pH but not PEI coated one. Yet, when these two were used together, difference behavior may be expected. Since QDs with larger PEI content benefit most from the acidic pH, in terms of PL intensity, it may be suggested that elimination of free electrons, disaggregation of particles, and more rigid structure of the polymer are the key factors enhancing the luminescence.

(a) 40/60 Cys/25kDa L-PEI

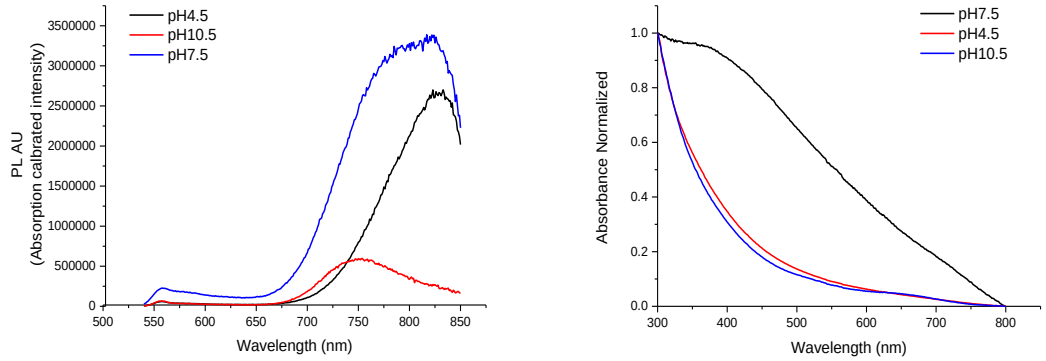

(b) 50/50 Cys/25kDa L-PEI

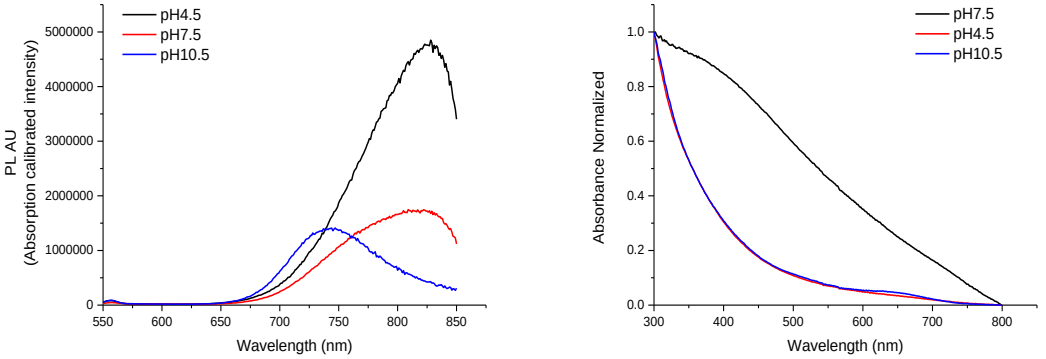

(c) 20/80 Cys/25kDa L-PEI

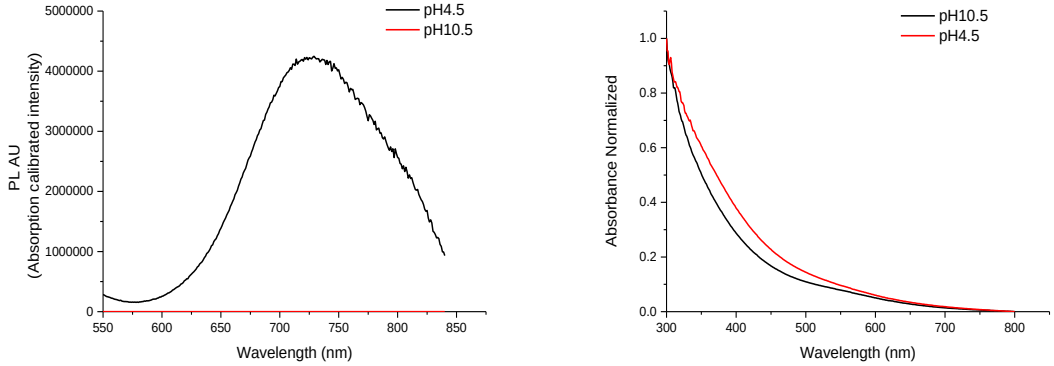

Figure 4.3 Absorption calibrated photoluminescence (left hand side) and normalized absorbance (right hand side) spectra of Cys/25kDa L-PEI Ag_2S NIR QDs at different pH values.

(a) 40/60 Cys/2.5kDa L-PEI

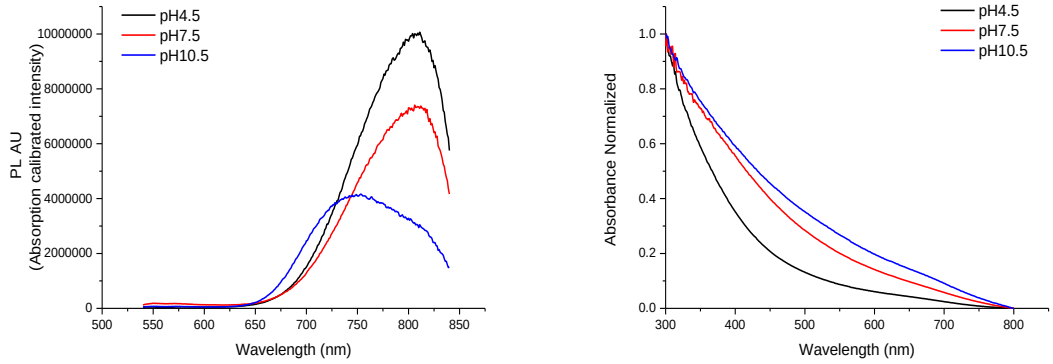

(b) 20/80 Cys/2.5kDa L-PEI

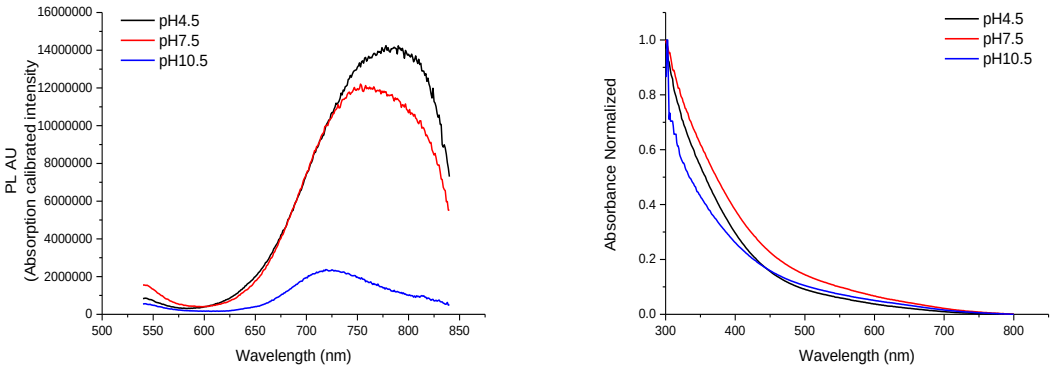

(c) 50/50 Cys/2.5kDa L-PEI

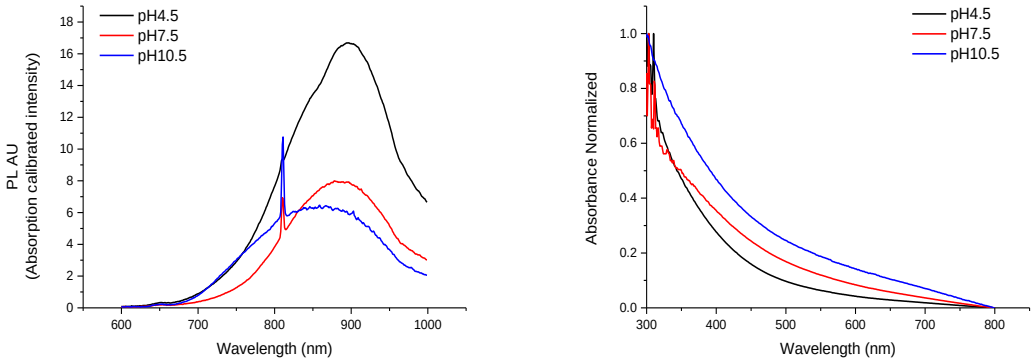

Figure 4.4 Absorption calibrated photoluminescence (left hand side) and normalized absorbance (right hand side) spectra of Cys/2.5kDa L-PEI Ag_2S NIR QDs at different pH values.

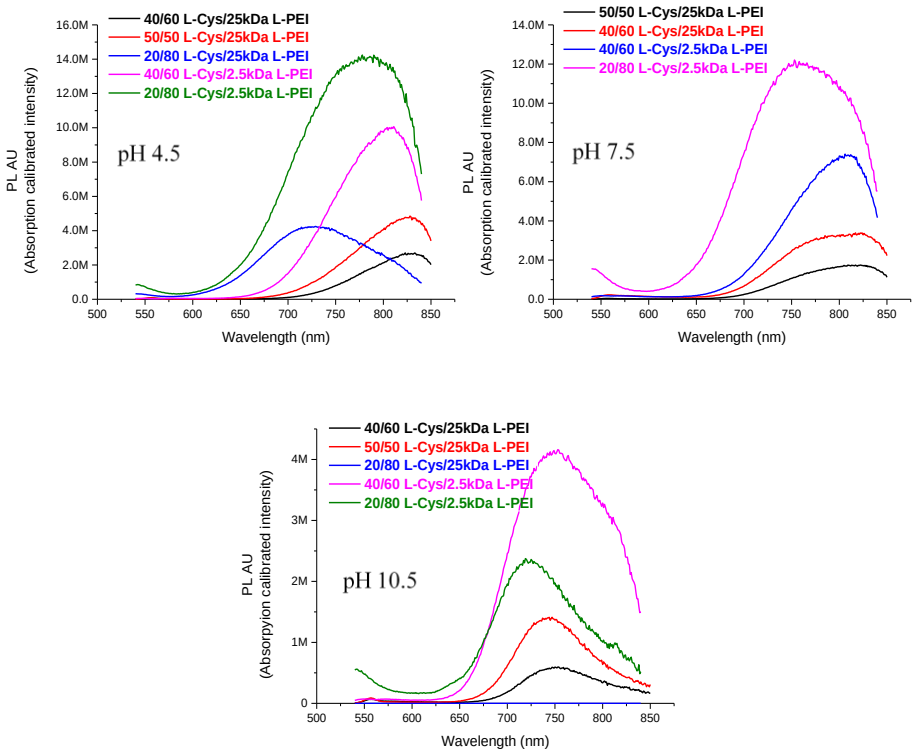

Figure 4.5 Photoluminescence spectra of Cys/L-PEI (MW: 2.5kDa and 25kDa) coated Ag_2S NIR quantum dots at different pH values (pH 4.5, 7.5and 10.5) after synthesis.

In order to see the effect of different composition and molecular weight of L-PEI better, PL spectra of the QDs with different compositions at the same pH values are plotted in Figure 4.5. 20/80 Cys/L-PEI (2.5kDa) Ag_2S QD showed the strongest photoluminescence emission at acidic and neutral conditions. Based on the emission intensity the second best particle is the 40/60 Cys/L-PEI (2.5kDa) Ag_2S QD. In general, QDs with Cys/2.5 kDa L-PEI luminesce much more strongly than those with 25kDa L-PEI. Only at basic pH, the emission intensity increased with the increasing content of the Cyseine, which supports the hypothesis that protonation of the amine groups of L-PEI is the key factor in the enhancement of the luminescence intensity.

In addition, similar to the mixed coatings with 2MPA, Cys/L-PEI mixed coating also provided stronger luminescence compared to Cys coated Ag_2S QDs (Figure 4.6). PL of 100% Cys and 50/50 Cys/2.5kDa L-PEI coated Ag_2S QDs were recorded with Si detector because the emission maxima of these particles are above 850 nm where PMT is inadequate (Figure 4.6).

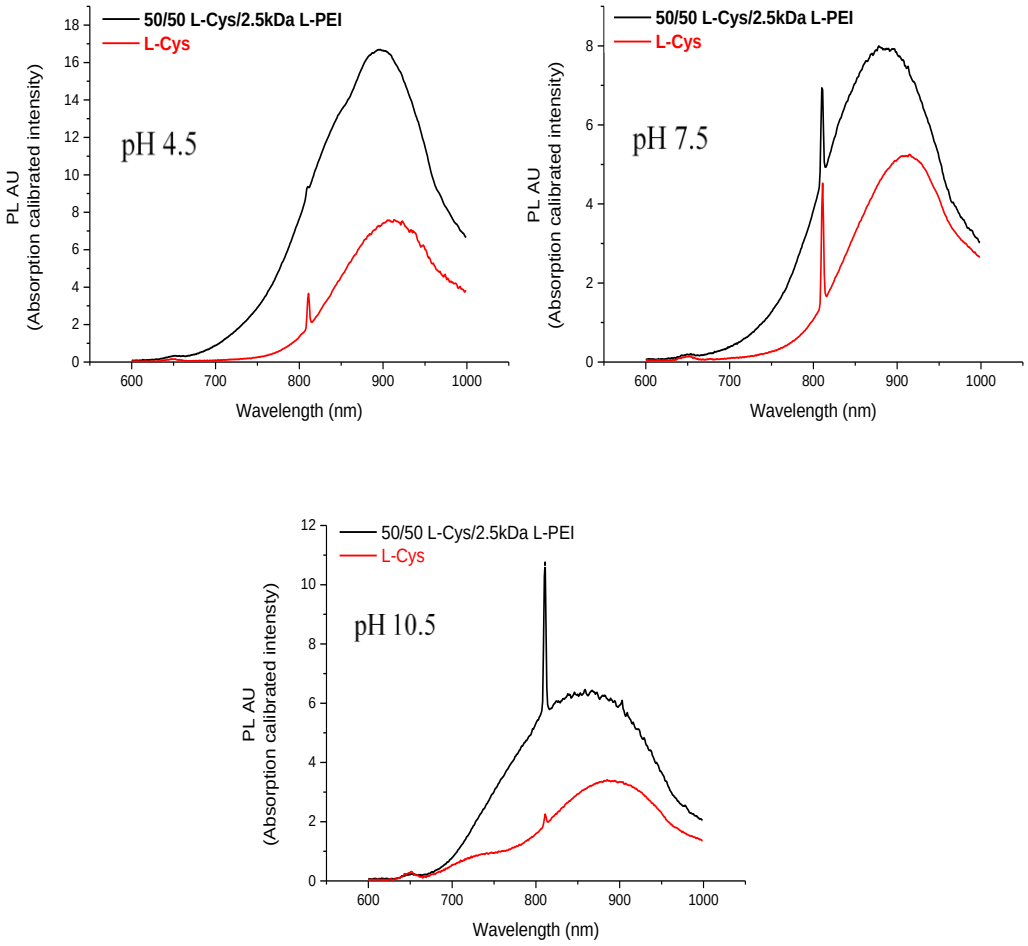

Figure 4.6 Photoluminescence spectra of Cys and Cys/L-PEI (MW: 2.5kDa and 25kDa) coated Ag_2S NIR quantum dots at different pH values (pH 4.5, 7.5 and 10.5) after synthesis.

4.2.1.3 Size and Surface Charge of Cys/L-PEI Coated Ag_2S NIR QDs

Table 4.2 Hydrodynamic size and Zeta potential of Cys/L-PEI (MW: 2.5kDa and 25kDa) coated Ag_2S NIR QDs in distilled water.

[a] Crystal size calculated by Brus equation (Table 4.1), [b]Average number average size distribution measured by DLS, [c] zeta potential of QDs.

				DIW pH 5	
Rxn ID	**L-PEI (kDa)**	**Cys/L-PEI (mole ratio)**	**D[a] (nm)**	**D[b] (nm)**	**Zeta Pot.[c] (mV)**
DAA-41	25	40/60	2.5	44.8±13.1	38.9±13.6
DAA-42	25	50/50	2.5	53.9±17.5	41.5±9.9
DAA-43	25	20/80	2.3	40.8±13.1	37.9±7.9
DAA-44	2.5	40/60	2.5	11.5±4.1	25.5±7.9
DAA-45	2.5	20/80	2.3	50.5±18.4	33.1±7.9
DAA-46	2.5	50/50	2.6	22.6±7.5	46.1±7.5
DAA-47	-	100/0	2.5	127.6±94.22	-23.8±3.8

Hydrodynamic size and zeta potential of Cys/L-PEI (2.5kDa and 25kDa) coated Ag_2S NIR QDs in water (pH 4.5) were tabulated in Table 4.2.

Except 100% Cys coated one, all Ag_2S QDs are ultra-small in size (10-54 nm) and have a strong positive zeta potential (25-46 mV) at (pH 4.5). The largest particle (54 nm) is the QD with 20/80 Cys/L-PEI (25kDa) coating. The smallest particle (11 nm) 40/60 Cys/2.5kDa L-PEI coated QDs. However, size distribution is quite broad. In general, Ag_2S QDs with the Cys/25kDa L-PEI coatings are larger and have more positive zeta potential. This may be due to availability of free polymer segments when larger polymer chains are used. With the low L-PEI, majority of the N-groups may be

attached on the surface creating a thin or more tightly bound organic shell. Such differences in the hydrodynamic size should be related to the organic shell thickness and swelling as well as aggregation since the crystal sizes are similar (Table 4.2). Although the zeta potentials were measured around the isoelectric point of the Cyseine, Cys/Ag_2S QDs have a strong negative surface charge. Since at this pH, amines would be protonated and the carboxylic acids should be deprotonated, may be amine groups are also adsorbed on the crystal surface, leaving the carboxylates dominate the surface charge. Besides, Cys/Ag_2S QDs suffer from stability, but mixed coatings provided excellent colloidal stability.

When compared with Ag_2S QDs coated with 2MPA/L-PEI hydrodynamic size of Cys/L-PEI coted QDs are larger in general but have more positive zeta potentials. This may be due to the extra amine group of Cys. These results can provide advantages over 2MPA/LPEI coated QDs in gene binding and release.

4.2.1.4 Coating Composition

The coating composition used in the synthesis was based on the moles of N coming from the L-PEI and moles of SH coming from the Cys. The actual composition of the final QD was determined by the elemental analysis. Elemental analysis states the N and S weight % of QDs (Table 4.3). Theoretically, QDs consisting of same L-PEI/ Cys ratio should have same N/S (w/w) ratio, considering the N coming from the Cyseine as well or not. However, when experimental N/ S w/w ratios were compared for 50/50 L-PEI (2.5kDa and 25kDa)/Cys coated Ag_2S QDs, a ratio of 1.3 in case of 25kFa and 0.9 in case of 2.5kDa PEI was calculated. From the weight % of N and S, number of moles were calculated. Experimental S mole % was calculated based on the moles of S from Cys and N from only PEI, since this was how the initial formulation was set. Results indicate that, even at identical N/S formulation in the synthesis, when low molecular weight PEI was used, more Cys was incorporated, reaching actually the theoretical value (49 mol %), whereas only 34% Cys was found in the final coating if

25kDa PEI was used. In case of 20/80 L-PEI/Cys formulations, the difference is less dramatic between the Cys content of the final coatings: 16% if 25kDa and 12 % if 2.5 kDa PEI was used. Basically, about 60-80% of the Cys bound to the surface, except the 50/50 mixture with 2.5kda L-PEI. These results also showed that both the molecular weight of PEI and the initial composition affected the actual coating compositions, but with 50% Cys in the formulation, roughly 35-50 % Cys and 20% Cys in the feed, roughly 12-16 mol% Cys was found in the final coating. Higher binding affinity of Cys to particle surface, steric hindrance by the long polymeric chains, thickness of the polymeric shell on the crystal surface, difference in the diffusion and interaction of the Cys and PEI may be some of the causes of such behavior, yet since there is not a clear trend, it is difficult to suggest the real effect of the molecular weight.

Table 4.3 Coating composition of Ag_2S NIR QDs with mixed coating of L-PEI/ Cys.

Rxn ID	L-PEI (kDa)	L-PEI/ Cys (mol/mol)[a]	Total* (w %)[b]	N * (w %)	S * (w %)	Experimental* N/S (g/g)[c]	Exp. Cys (mol %)[d]
DAA-42	25	50/50	45.0	7.2	5.5	1.3	34
DAA-43	25	80/20	45.8	7.4	2.7	2.7	16
DAA-45	2.5	80/20	40.4	4.0	1.1	3.6	12
DAA-46	2.5	50/50	45.4	7.3	8.5	0.9	49

*Elemental analysis. [a]Moles of N coming from PEI/ moles of SH coming from Cys, [b]Total organics that were determined by elemental analysis, [c] Experimental N= N from PEI + N from Cys, [d] Experimental Cys (mol%)=(moles of N measured by elemental analysis/(total moles of N + S)††Total moles of N+S= Moles of N (from PEI and Cys moles of N from Cys + moles of SH from Cys.

4.2.1.5 Photoluminescence Stability of Cys/L-PEI Ag_2S QDs

Optical stability of Cys/L-PEI (MW: 2.5kDa and 25kDa) coated Ag_2S QDs were tracked by the Pl and absorbance spectra taken at different time points during their storage of 3 months. Emission intensity of QDs decreased with time (Figure 4.7, 4.8 and 4.9). However, after 3 months, these particles still have strong enough emission for biomedical imaging as will be shown in later sections. Pretty good biomedical images were gotten by the QDs after 3 months by using HeLa cell line as a model. For a strong performance, these QDs were recommended to be used within 3 months

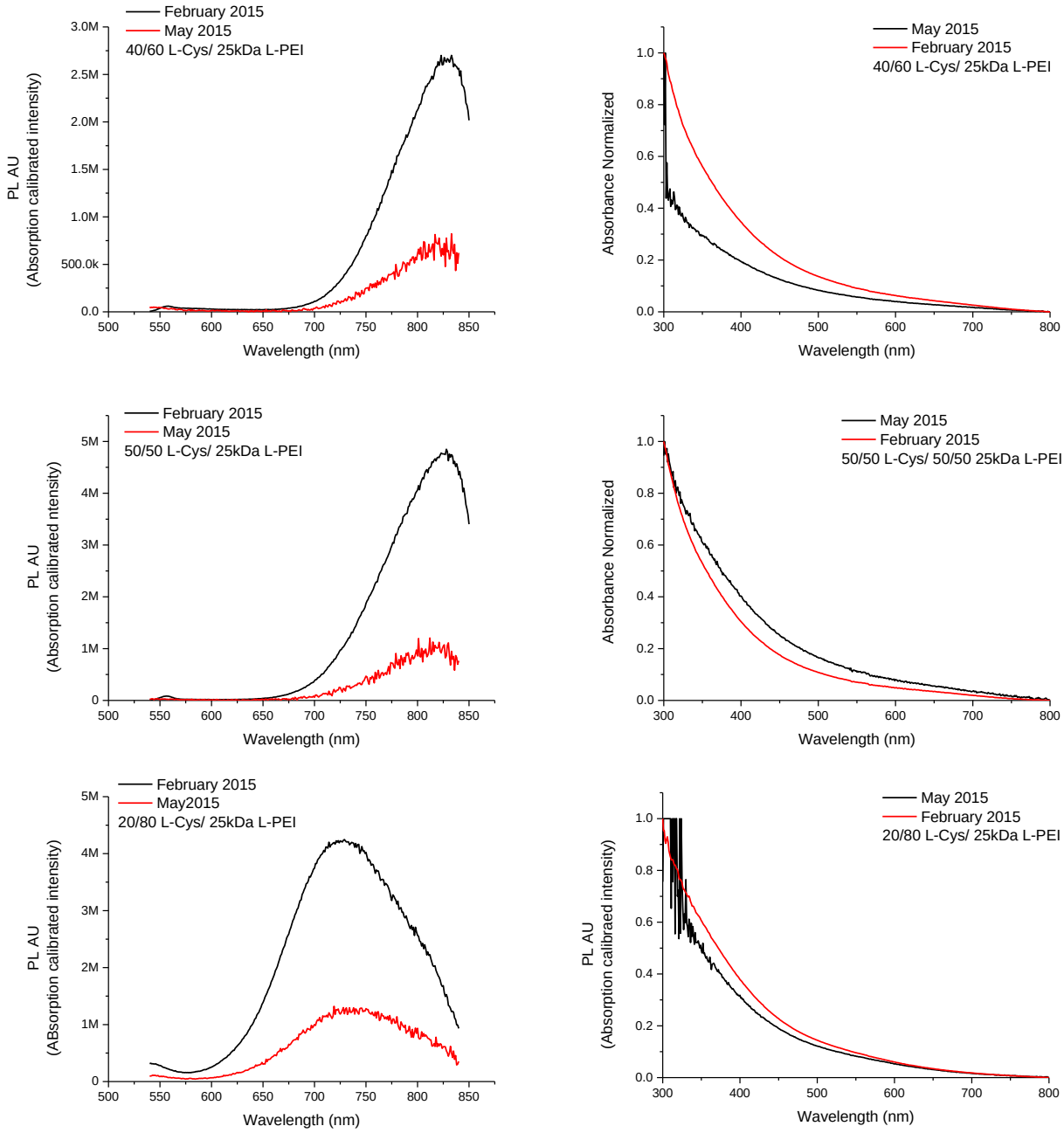

Figure 4.7 Photoluminescence and normalized absorbance spectra of Cys/L-PEI (MW: 25kDa) coated Ag_2S QDs on February 2015 (shortly after synthesis) and on May 2015.

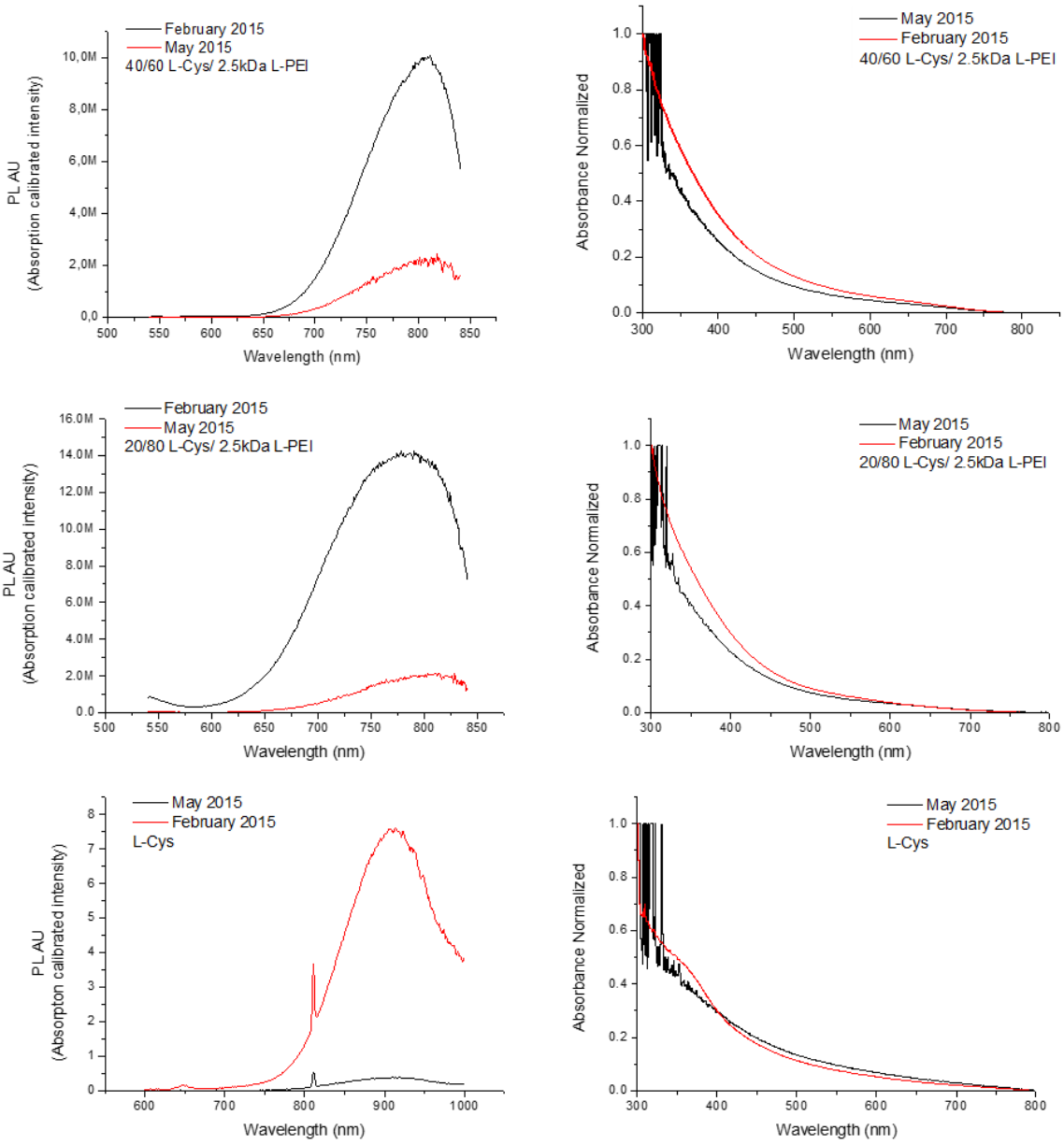

Figure 4.8 Photoluminescence and normalized absorbance spectra of Cys/L-PEI (MW: 2.5kDa) Ag_2S QDs on February 2015 and on May 2015.

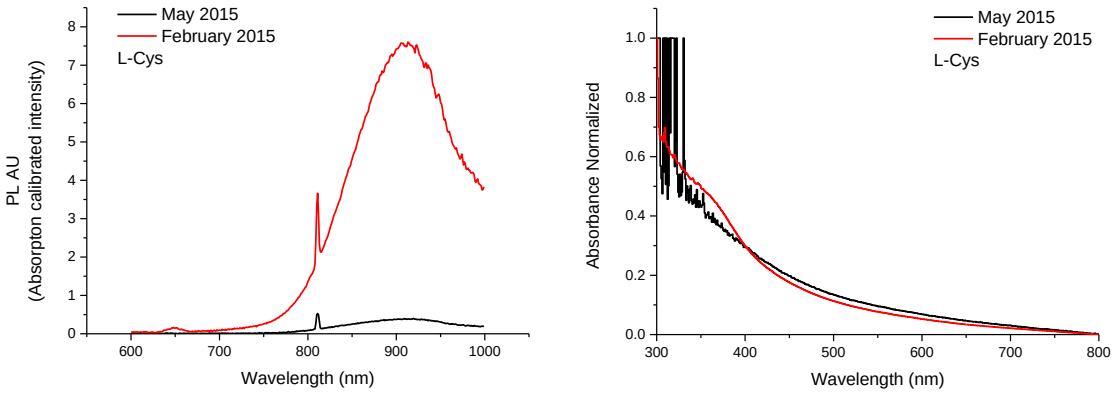

Figure 4.9 Photoluminescence and normalized absorbance spectra of Cys Ag_2S QD on February 2015 and on May 2015.

4.2.1.6 *In Vitro* Toxicity Evaluation of Cys/ L-PEI Coated Ag_2S QDs

Cell viability of Cys/ L-PEI (2.5kDa and 25kDa) coated Ag_2S QDs were determined by MTT assay as explained in Chapter 2 and 3. QDs doses were based on the Ag concentration and set between 0.75-10 µg Ag/mL. Particle concentrations corresponding to 10 µg/mL Ag were listed in Table 4.4. The table showed that there is more organic content in the compositions of the QDs.

Table 4.4 Silver and nanoparticle concentration of Cys/ L-PEI Coated Ag_2S QD solutions.

Rxn Code	PEI MW (kDa)	Cys/PEI (mol ratio)	Ag[a] (µg/mL)	Particle[b] (µg/mL)
DAA-42	25	50/50	10	171.7
DAA-43	25	20/80	10	207,1
DAA-45	2.5	20/80	10	561,6
DAA-46	2.5	50/50	10	602,6

[a] ICP-OES, [b]Weight of solid content after evaporation of water.

Human cervical cancer (HeLa), HCT 116 WT and HCT 116 p53 (-) cell lines were used in the toxicity study. The pH of the particles were set to 5 based on the stability and better luminesence at this pH. Figure 4.10 indicates that in HeLa cells, all particles caused 80% or better viability uptill 2.4 µg/mL Ag dose. Especially, at 5.6 2.4 µg/mL Ag and above, the QD with 20/80 Cys/L-PEI 25kDa is the most toxic one with a dose dependent toxicity. Rest of the particles have similiar toxicity and the viability fell below 50 % rapidaly at 10 µg /mL dose. Since doses below 4 µg/mL Ag is usually enough for the transfection studies, these particles are quite promising.

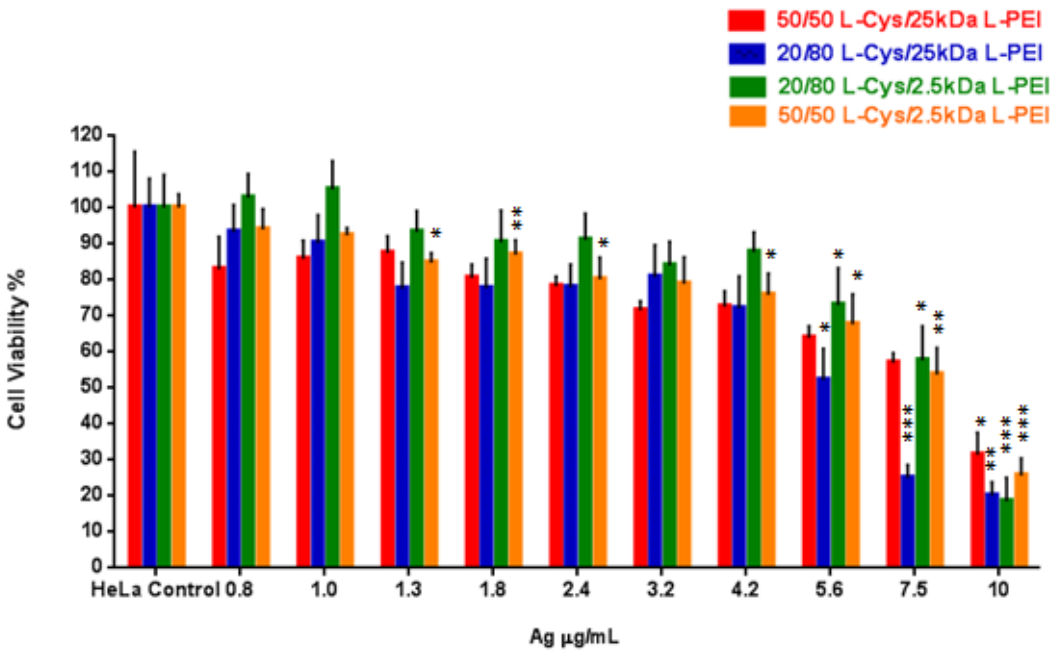

Figure 4.10 Viability of HeLa cells in the presence of Cys/L-PEI Ag_2S QDs (pH 5) after 24 hours incubation as determined by MTT assay (one-way ANOVA with Tukey's multiple comparison at $p < 0.05$(*), $p < 0.01$ (**), $p < 0.001$ (***) and $p < 0.0001$(****).

Particles found to be very toxic to HCT 116 WT (Figure 4.11) cells. The most toxic QD was found as the 20/80 Cys/L-PEI 25kDa QD again but at 0.8 µg/mL Ag dose this time. It seems like only 1 µg/mL Ag dose could be utilized in any transfection studies with these QDs and this cell line.

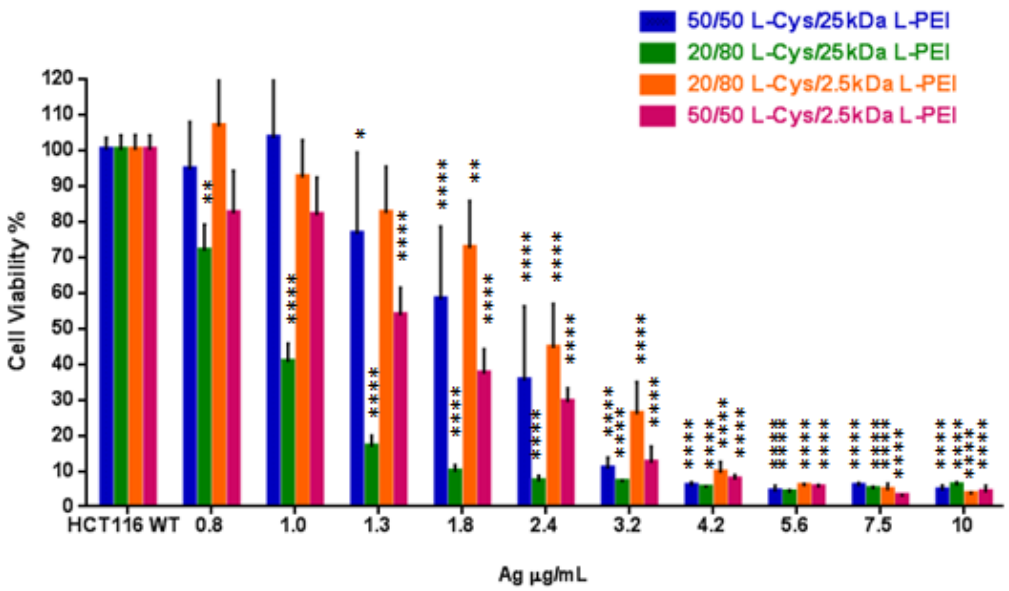

Figure 4.11 Viability of HCT 116 WT cells in the presence of Cys/L-PEI Ag_2S QDs (pH 5) after 24 hours incubation as determined by MTT assay (one-way ANOVA with Tukey's multiple comparison at $p < 0.05$(*), $p < 0.01$ (**), $p < 0.001$ (***) and $p < 0.0001$(****).

Interestingly, 20/80 Cys/L-PEI 25kDa QD that was found as the most toxic QD in HCT 116 WT cell line, didn't show any toxicity untill at 5.6 µg/mL Ag dose in HCT 116 p53 (-) cell line (Figure 4.12). Toxicity of the other three QDs were similar to each other and significantly higher (at and below 80% viability at a1.3 µg/mL Ag dose) than 20/80 Cys/L-PEI 25kDa QD after 1 µg/mL Ag dose. Overall, HCT 116 p53 (-) cell line is slightly more resistance than HCT 116 WT, possibly due to the absence of the tumor suppressor p53 gene that also induces apoptosis. For possible gene transfection to HTC 116 p53(-) cells, either QD at and below 1 µg/mL Ag dose can be used but higher doses are required than only 20/80 Cys/L-PEI 25kDa QD will be suitable.

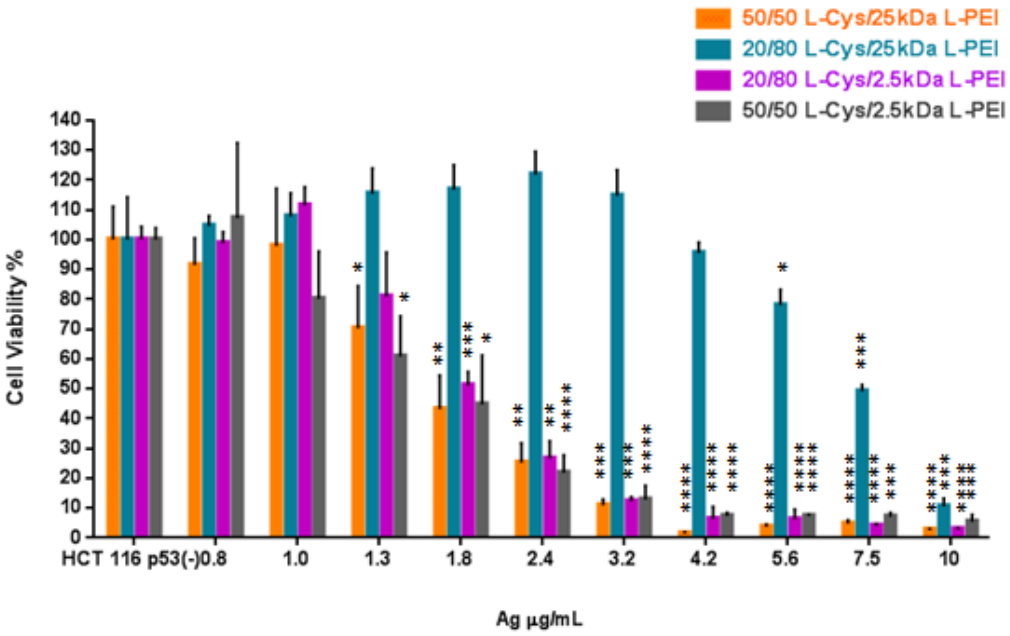

Figure 4.12 Viability of HCT 116 p53 (-) cells in the presence of Cys/L-PEI Ag_2S QDs (pH 5) after 24 hours incubation as determined by MTT assay (one-way ANOVA with Tukey's multiple comparison at $p < 0.05$(*), $p < 0.01$ (**), $p < 0.001$ (***) and $p < 0.0001$(****).

Cell viability and cellular internalization of QDs should be correlated to interpret the toxicity data better. Since no significant difference in the cell internalization data of 2MPA/LPEI coated Ag_2S QDs at different 25 and 50 µg/mL Ag doses, cell uptake and toxicity of Cys/L-PEI QDs were determined at only 25 µg/mL Ag dose after 4 hours incubation with HeLa cells. Under these conditions no significantly toxicity was observed (Figure 4.13), so cell uptake results would be confidential.

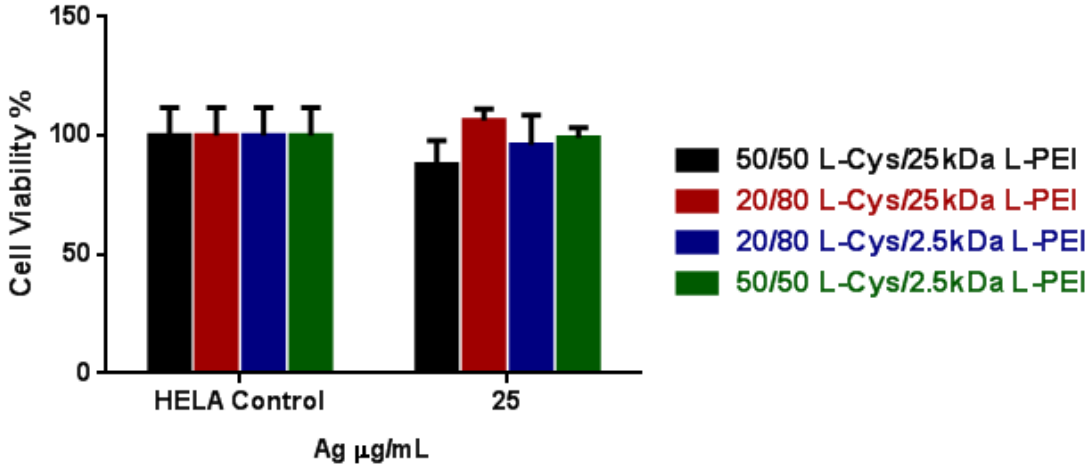

Figure 4.13 Viability of HeLa cells in the presence of Cys/L-PEI Ag_2S QDs (pH 5) after 4 hours incubation as determined by MTT assay (one-way ANOVA with Tukey's multiple comparison at $p < 0.05$(*), $p < 0.01$ (**), $p < 0.001$ (***) and $p < 0.0001$(****).

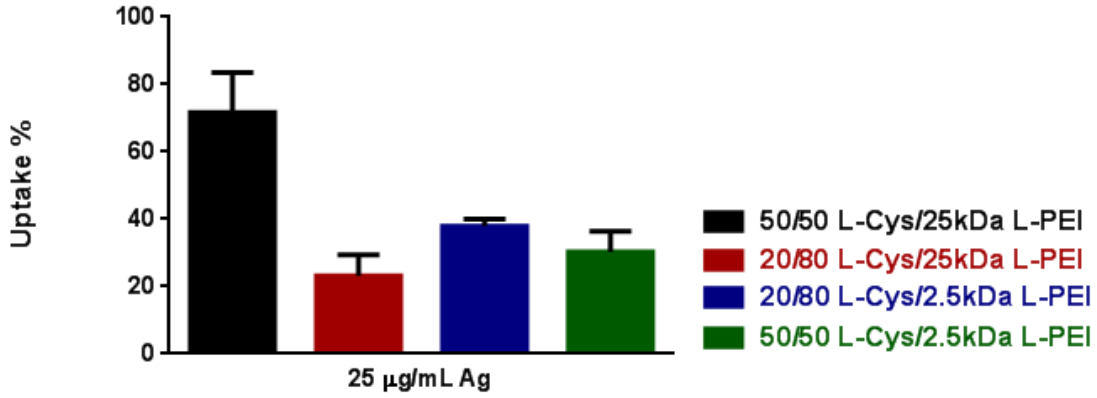

Figure 4.14 Quantification of internalized Cys/L-PEI Ag_2S QDs (pH 5) by HeLa cells in 4 hours incubation time.

About 70 % of the 50/50 Cys/L-PEI 25kDa were internalized by the HeLa cells and it is most heavily internalized one (Figure 4.14). Considering its non-toxic nature in HeLa cells, this QD can be consider quite compatible with HeLa cells. The QDs have nearly same hydrodynamic size and zeta potential so the cell internalization should not be size or charge dependent. For the rest, considering the error bars, there is no significant difference and their cell uptake results were found between 20 % and 38 %.

4.2.1.7 Evaluation of Cys/ L-PEI Ag_2S QDs as Optical Probes

In order to visually confirm the internalization of Cys/L-PEI Ag_2S QDs by the cells and evaluate their use as optical diagnostic probes, HeLa cells incubated with QDs were imaged under inverted fluorescence microscope (Figure 4.15). Due to the limitation of ICP-MS that was needed to detect Ag ion for uptake analysis, high doses and short incubation times were used (25 and 50 μg/mL Ag dose).

DAPI dye and DAPI filter was utilized to stain and image the cell nucleus. Even though, the sensitivity of the detectors used in the microscope falls around 30 % right after 800 nm, 50/50 Cys/ 2.5kDa L-PEI Ag_2S QD with emission peak maximum at 897 nm after 3 months demonstrated a very intense signal with the NIR filter (excitation wavelength = 550nm, 640 nm long pass emission filter). In Figure 4.15, the red color represents the emission signal from 50/50 Cys/ 2.5kDa L-PEI Ag_2S QD by NIR filter and the blue color represents cell nucleus that is stained by DAPI dye and imagined by DAPI filter (λ_{exc}: 352-402 nm and emission: 417-477 nm). When the internalized cells were compared with the control group, very strong distinguishable NIR signal was detected in the cytoplasm, proving the use of these QDs as optical probes.

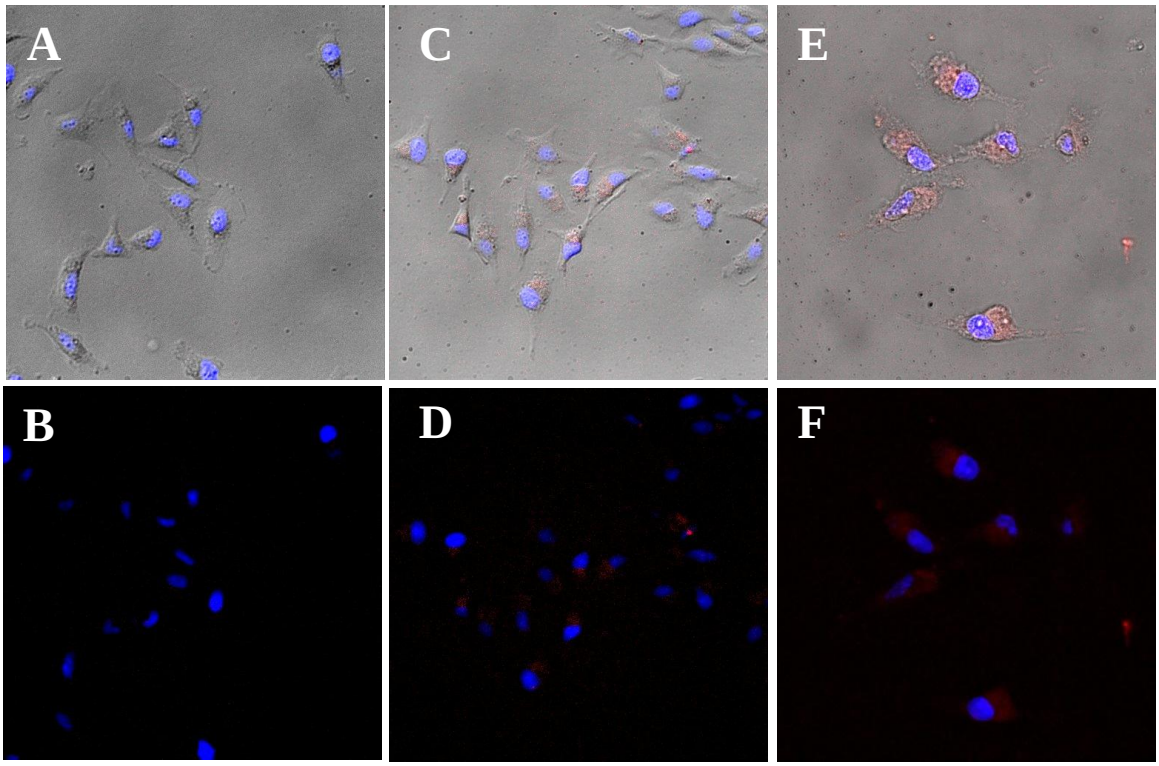

Figure 4.15 Inverted fluorescence microscopy images of HeLa control cells (A and B) and HeLa cells incubated with 50/50 Cys/L-PEI (2.5kDa) Ag_2S QD at 25µg/mL Ag dose (C and D) and 50µg/mL Ag dose (E and F) for 4 hours. Red color represents NIR filter (λ_{exc}: 550 nm and emission: 650 nm long pass) and blue color represents DAPI filter (λ_{exc}: 352-402 nm and emission: 417-477 nm).

4.3 Conclusion

Colloidal Cys and Cys /L-PEI coated Ag_2S QDs were synthesized in water. It was known that L-PEI (2.5 and 25kDa) produced colloidally stable but non-luminescent particles. Cys /L-PEI coated Ag_2S QDs provided a synergistic effect over only Cys coated Ag_2S QDs and PEI coated Ag_2S QDs. The crystal size and the emission wavelength of QDs can be tuned by the Cys /L-PEI ratio. Emission maxima and intensity influenced dramatically by the pH of the medium with an enhanced luminescence intensity at longer wavelengths at acidic pH (4.5-5). The emission peak maxima of these QDs are between 727-897 nm, suitable for medical imaging.

Cytocompatibility of all QDs was determined in three different cell lines: One of the most widely used cells, HeLa, and also HTC 116 both wild type and p53 negative. The most toxic QDs in HeLa cell line are 50/50 Cys/L-PEI 2.5kDa and 20/80 Cys/L-PEI 25kDa QDs, basically those with the higher Cys content in the final coating. Cys/L-PEI QDs were found highly toxic especially in HCT 116 WT and HCT116 p53(-) cells. Even at 0.8 and 1.3 μg Ag/mL doses significant toxicity was seen. Only 20/80 Cys/L-PEI 25kDa QD didn't show toxicity in HCT116 p53(-) cells until at 5.6 μg Ag/mL dose. Molecular weight of the L-PEI did not show a uniform trend in the toxicity of these QDs. Internalization of QDs by the HeLa cells indicated that about 70% of the dose was internalized in 4h if 50/50 Cys/L-PEI coated QDs were used but otherwise this value dropped down to 20% to 38%.

Based on the fluorescent microscopy studies, QDs are distributed uniformly into the cytoplasm of the HeLa cells and provide a very strong signal in the NIR.

Overall, Cys/L-PEI coated Ag_2S QDs can be used easily as diagnostic probes and delivery vehicles.

Chapter 5

CONCLUSION

Biocompatible heavy metal free, cationic Ag_2S QD as new theranostic nanoparticles were attempted in this thesis. QDs were coated with linear PEI to achieve cationic, gene binding organic coating. Since high molecular weight and/or branch PEI structures cause deadly toxicity, linear PEI at two different molecular weights (2.5 and 25kDa) were investigated as a coating for the NIR QDs. L-PEI coating at both molecular weights provided colloidally stable Ag_2S nanoparticles but, they didn't exhibit any luminescence. This problem was solved by the application of mixed coatings composed of small, more strongly and densely binding thiolated molecules, 2MPA and Cys, with less strongly binding L-PEI polymers. Both 2MPA and Cys have been used successfully to coat various QDs in the literature. However, linear PEI or their mixture have never been utilized before.

Such mixed coatings compositions provided a synergistic effect on the luminescence properties of Ag_2S QDs. They luminesce much more strongly than 2MPA or Cys coated Ag_2S QDs. The crystal size and hence, the emission wavelengths of the QDs were tuned by the 2MPA/L-PEI and Cys/L-PEI ratios. The emission peak maxima of these QDs are changed between 791-897 nm for 2MPA/L-PEI coated QDs, 727-897 nm for Cys/L-PEI coated QDs. Due to solubility limitation of L-PEI, all synthesis were performed at pH 5.7. However, luminescence properties were strongly dependent on the environmental pH. It was found that acidification increased the luminescence intensity of 2MPA/L-PEI and Cys/L-PEI coated QDs and also caused a red shift of the emission maxima of Cys/L-PEI coated QDs. All 2MPA/L-PEI coated QDs were found colloidally stable between pH 5-10 but, Cys/L-PEI coated QDs were not so stable at neutral pH.

Based on the emission maxima of the QDs and the crystal sizes, it seems like 2MPA/L-PEI mixtures produce slightly larger crystals but hydrodynamic size and the surface charge of the Cys/L-PEI QDs were larger. This may be due to more swollen organic shell and due to the extra amine groups brought by Cys.

Cytocompatibility of all QDs were determined in three different cell lines: One of the most widely used cells, HeLa, and also HTC 116, both wild type and p53 negative. In general, Ag_2S QDs coated only with L-PEI were the most toxic ones. 2MPA/L-PEI coated QDs were found more biocompatible based on the MTT assay, indicating a synergy in the toxicity as well. Toxic effect started around 7.5 and 10 μg Ag/mL dose, respectively, in HeLa and HCT116 WT cells. In general, Cys/L-PEI QDs were more toxic. The most toxic QDs to HeLa cells were 50/50 Cys/L-PEI 2.5kDa and 20/80 Cys/L-PEI 25kDa QDs, basically those with the higher Cys content in the final coating composition. Cys/L-PEI QDs were found highly toxic especially in HCT 116 WT and HCT116 p53(-) cells. Even at 0.8 and 1.3 μg Ag/mL doses significant toxicity was seen. Only the 20/80 Cys/L-PEI 25kDa QD didn't show toxicity in HCT116 p53(-) cells up to 5.6 μg Ag/mL dose.

Internalization of QDs by the HeLa cells was performed based on Ag ion concentration detected by ICP-MS. In 2MPA/L-PEI coated QDs, the highest uptake was recorded with the 20/80 2MPA/L-PEI compositions (2.5 and 25kDa): 75% and 45%, respectively. However, in case of Cys/L-PEI QDs, no clear trend was detected in the uptake.

Fluorescent microscopy studies were performed with both QD sets in HeLa cells. All indicated homogenized distributed in cytoplasm of the cell with strong NIR signal. Also, strong NIR signal was obtained from the images of C.elegans treated with 2MPA/L-PEI QDs. These successful results prove that these QDs can be used as strong diagnostic probes in biomedical imaging, successfully.

In conclusion, these QDs constitute a new set of theranostic nanoparticles utilizing polymers effective in gene delivery and small molecules effective in producing strongly luminescent quantum dots. These cationic heavy-metal free, NIR active QDs

have great potential to be used as new optical diagnostic agents capable of gene transfection.

BIBLIOGRAPHY

1. Smith, A. M.; Nie, S., Chemical analysis and cellular imaging with quantum dots. *Analyst* **2004,** *129* (8), 672-677.
2. Ekimov, A.; Onushchenko, A., Quantum size effect in the optical-spectra of semiconductor micro-crystals. *Soviet Physics Semiconductors-Ussr* **1982,** *16* (7), 775-778.
3. Roduner, E., Size matters: why nanomaterials are different. *Chemical Society Reviews* **2006,** *35* (7), 583-592.
4. Han, M.; Gao, X.; Su, J. Z.; Nie, S., Quantum-dot-tagged microbeads for multiplexed optical coding of biomolecules. *Nature biotechnology* **2001,** *19* (7), 631-635.
5. Filikhin, I.; Matinyan, S.; Vlahovic, B., Quantum mechanics of semiconductor quantum dots and rings. *arXiv preprint arXiv:1206.1354* **2012**.
6. Drbohlavova, J.; Adam, V.; Kizek, R.; Hubalek, J., Quantum dots—characterization, preparation and usage in biological systems. *International journal of molecular sciences* **2009,** *10* (2), 656-673.
7. Bailey, R. E.; Smith, A. M.; Nie, S., Quantum dots in biology and medicine. *Physica E: Low-dimensional Systems and Nanostructures* **2004,** *25* (1), 1-12.
8. Peng, X., Mechanisms for the Shape-Control and Shape-Evolution of Colloidal Semiconductor Nanocrystals. *Advanced Materials* **2003,** *15* (5), 459-463.
9. Thuy, U. T. D.; Toan, P. S.; Chi, T. T. K.; Khang, D. D.; Liem, N. Q., CdTe quantum dots for an application in the life sciences. *Advances in Natural Sciences: Nanoscience and Nanotechnology* **2010,** *1* (4), 045009.
10. Ioannou, D.; Griffin, D. K., Nanotechnology and molecular cytogenetics: the future has not yet arrived. *Nano reviews* **2010,** *1*.
11. Smith, A. M.; Duan, H.; Mohs, A. M.; Nie, S., Bioconjugated quantum dots for *in vivo* molecular and cellular imaging. *Advanced drug delivery reviews* **2008,** *60* (11), 1226-1240.
12. Murray, C.; Norris, D. J.; Bawendi, M. G., Synthesis and characterization of nearly monodisperse CdE (E= sulfur, selenium, tellurium) semiconductor nanocrystallites. *Journal of the American Chemical Society* **1993,** *115* (19), 8706-8715.
13. Chan, W. C.; Nie, S., Quantum dot bioconjugates for ultrasensitive nonisotopic detection. *Science* **1998,** *281* (5385), 2016-2018.
14. Acar, H. Y.; Kas, R.; Yurtsever, E.; Ozen, C.; Lieberwirth, I., Emergence of 2MPA as an effective coating for highly stable and luminescent quantum dots. *The Journal of Physical Chemistry C* **2009,** *113* (23), 10005-10012.

15. Shen, L., Biocompatible polymer/quantum dots hybrid materials: current status and future developments. *Journal of functional biomaterials* **2011,** *2* (4), 355-372.
16. Libert, S.; Gorshkov, V.; Privman, V.; Goia, D.; Matijević, E., Formation of monodispersed cadmium sulfide particles by aggregation of nanosize precursors. *Advances in colloid and interface science* **2003,** *100*, 169-183.
17. Priyam, A.; Chatterjee, A.; Das, S.; Saha, A., Synthesis and spectral studies of Cyseine-capped CdS nanoparticles. *Research on chemical intermediates* **2005,** *31* (7), 691-702.
18. Hocaoglu, I.; Çizmeciyan, M. N.; Erdem, R.; Ozen, C.; Kurt, A.; Sennaroglu, A.; Acar, H. Y., Development of highly luminescent and cytocompatible near-IR-emitting aqueous Ag 2 S quantum dots. *Journal of Materials Chemistry* **2012,** *22* (29), 14674-14681.
19. Sevinç, E.; Ertas, F. S.; Ulusoy, G.; Ozen, C.; Acar, H. Y., Meso-2, 3-dimercaptosuccinic acid: from heavy metal chelation to CdS quantum dots. *Journal of Materials Chemistry* **2012,** *22* (11), 5137-5144.
20. Gao, X.; Cui, Y.; Levenson, R. M.; Chung, L. W.; Nie, S., In vivo cancer targeting and imaging with semiconductor quantum dots. *Nature biotechnology* **2004,** *22* (8), 969-976.
21. Goldman, E. R.; Clapp, A. R.; Anderson, G. P.; Uyeda, H. T.; Mauro, J. M.; Medintz, I. L.; Mattoussi, H., Multiplexed toxin analysis using four colors of quantum dot fluororeagents. *Analytical Chemistry* **2004,** *76* (3), 684-688.
22. Gao, X.; Yang, L.; Petros, J. A.; Marshall, F. F.; Simons, J. W.; Nie, S., In vivo molecular and cellular imaging with quantum dots. *Current opinion in biotechnology* **2005,** *16* (1), 63-72.
23. Tan, A.; Yildirimer, L.; Rajadas, J.; De La Peña, H.; Pastorin, G.; Seifalian, A., Quantum dots and carbon nanotubes in oncology: a review on emerging theranostic applications in nanomedicine. *Nanomedicine* **2011,** *6* (6), 1101-1114.
24. Du, Y.; Xu, B.; Fu, T.; Cai, M.; Li, F.; Zhang, Y.; Wang, Q., Near-infrared photoluminescent Ag2S quantum dots from a single source precursor. *Journal of the American Chemical Society* **2010,** *132* (5), 1470-1471.
25. Li, K.; Ding, D.; Huo, D.; Pu, K. Y.; Thao, N. N. P.; Hu, Y.; Li, Z.; Liu, B., Conjugated Polymer Based Nanoparticles as Dual-Modal Probes for Targeted In Vivo Fluorescence and Magnetic Resonance Imaging. *Advanced Functional Materials* **2012,** *22* (15), 3107-3115.
26. Frangioni, J. V., In vivo near-infrared fluorescence imaging. *Current opinion in chemical biology* **2003,** *7* (5), 626-634.
27. (a) Lee, J.; Ji, K.; Kim, J.; Park, C.; Lim, K. H.; Yoon, T. H.; Choi, K., Acute toxicity of two CdSe/ZnSe quantum dots with different surface coating in Daphnia magna under various light conditions. *Environmental toxicology* **2010,** *25* (6), 593-600; (b) Geszke, M.; Murias, M.; Balan, L.; Medjahdi, G.; Korczynski, J.; Moritz, M.; Lulek, J.; Schneider, R., Folic acid-conjugated core/shell ZnS: Mn/ZnS quantum dots as targeted probes for two photon fluorescence imaging of cancer cells. *Acta biomaterialia* **2011,** *7* (3), 1327-1338.

28. Chen, H.; Li, B.; Zhang, M.; Sun, K.; Wang, Y.; Peng, K.; Ao, M.; Guo, Y.; Gu, Y., Characterization of tumor-targeting Ag 2 S quantum dots for cancer imaging and therapy *in vivo*. *Nanoscale* **2014,** *6* (21), 12580-12590.
29. Hocaoglu, I.; Demir, F.; Birer, O.; Kiraz, A.; Sevrin, C.; Grandfils, C.; Acar, H. Y., Emission tunable, cyto/hemocompatible, near-IR-emitting Ag 2 S quantum dots by aqueous decomposition of DMSA. *Nanoscale* **2014,** *6* (20), 11921-11931.
30. Zhang, X.; Gu, Y.; Chen, H., Synthesis of biocompatible near infrared fluorescence Ag 2 S quantum dot and its application in bioimaging. *Journal of Innovative Optical Health Sciences* **2014,** *7* (03), 1350059.
31. Hu, F.; Li, C.; Zhang, Y.; Wang, M.; Wu, D.; Wang, Q., Real-time *in vivo* visualization of tumor therapy by a near-infrared-II Ag2S quantum dot-based theranostic nanoplatform. *Nano Research* **2014,** *8* (5), 1637-1647.
32. Pan, H.; Zhou, Y.; Sieling, F.; Shi, J.; Cui, J.; Deng, C. In *Sonoporation of cells for drug and gene delivery*, Engineering in Medicine and Biology Society, 2004. IEMBS'04. 26th Annual International Conference of the IEEE, IEEE: 2004; pp 3531-3534.
33. Wan, F.; Tang, Z.; He, W.; Chu, B., A chemistry/physics pathway with nanofibrous scaffolds for gene delivery. *Physical Chemistry Chemical Physics* **2010,** *12* (39), 12379-12389.
34. El-Aneed, A., An overview of current delivery systems in cancer gene therapy. *Journal of Controlled Release* **2004,** *94* (1), 1-14.
35. (a) Liu, F.; Shollenberger, L. M.; Conwell, C. C.; Yuan, X.; Huang, L., Mechanism of naked DNA clearance after intravenous injection. *The journal of gene medicine* **2007,** *9* (7), 613-619; (b) Qi, L.; Gao, X., Emerging application of quantum dots for drug delivery and therapy. **2008**; (c) Deng, R.; Yue, Y.; Jin, F.; Chen, Y.; Kung, H.-F.; Lin, M. C.; Wu, C., Revisit the complexation of PEI and DNA—How to make low cytotoxic and highly efficient PEI gene transfection non-viral vectors with a controllable chain length and structure? *Journal of Controlled Release* **2009,** *140* (1), 40-46.
36. Dufes, C., Beyond delivery. *Gene therapy* **2006,** *13*, 739-740.
37. Hildebrandt, I.; Iyer, M.; Wagner, E.; Gambhir, S., Optical imaging of transferrin targeted PEI/DNA complexes in living subjects. *Gene therapy* **2003,** *10* (9), 758-764.
38. Jin, L.; Zeng, X.; Liu, M.; Deng, Y.; He, N., Current progress in gene delivery technology based on chemical methods and nano-carriers. *Theranostics* **2014,** *4* (3), 240.
39. (a) Goula, D.; Remy, J.; Erbacher, P.; Wasowicz, M.; Levi, G.; Abdallah, B.; Demeneix, B., Size, diffusibility and transfection performance of linear PEI/DNA complexes in the mouse central nervous system. *Gene therapy* **1998,** *5* (5), 712-717; (b) Wightman, L.; Kircheis, R.; Rössler, V.; Carotta, S.; Ruzicka, R.; Kursa, M.; Wagner, E., Different behavior of branched and linear polyethylenimine for gene delivery *in vitro* and *in vivo*. *The journal of gene medicine* **2001,** *3* (4), 362-372.

40. Duan, H.; Nie, S., Cell-penetrating quantum dots based on multivalent and endosome-disrupting surface coatings. *Journal of the American Chemical Society* **2007,** *129* (11), 3333-3338.
41. Zintchenko, A.; Susha, A. S.; Concia, M.; Feldmann, J.; Wagner, E.; Rogach, A. L.; Ogris, M., Drug nanocarriers labeled with near-infrared-emitting quantum dots (quantoplexes): imaging fast dynamics of distribution in living animals. *Molecular Therapy* **2009,** *17* (11), 1849-1856.
42. Wei, G.; Yan, M.; Ma, L.; Zhang, H., The synthesis of highly water-dispersible and targeted CdS quantum dots and it is used for bioimaging by confocal microscopy. *Spectrochimica Acta Part A: Molecular and Biomolecular Spectroscopy* **2012,** *85* (1), 288-292.
43. Zhang, Y.; Liu, J.-M.; Yan, X.-P., Self-assembly of folate onto polyethyleneimine-coated CdS/ZnS quantum dots for targeted turn-on fluorescence imaging of folate receptor overexpressed cancer cells. *Analytical chemistry* **2012,** *85* (1), 228-234.
44. Qi, L.; Cölfen, H.; Antonietti, M., Synthesis and characterization of CdS nanoparticles stabilized by double-hydrophilic block copolymers. *Nano Letters* **2001,** *1* (2), 61-65.
45. ACAR, H. Y.; DEMİR, F.; Hocaoglu, I.; Kiraz, A., Highly Luminescent and Cytocompatible Cationic Ag2S NIR-emitting Quantum Dots for Optical Imaging and Gene Transfection. *Nanoscale* **2015**.
46. Kronek, J.; Paulovičová, E.; Luston, J.; Paulovičová, L.; Kroneková, Z., *Biocompatibility and Immunocompatibility Assessment of Poly (2-Oxazolines)*. INTECH Open Access Publisher: 2013.
47. (a) Brus, L. E., Electron–electron and electron-hole interactions in small semiconductor crystallites: The size dependence of the lowest excited electronic state. *The Journal of chemical physics* **1984,** *80* (9), 4403-4409; (b) Brus, L., Electronic wave functions in semiconductor clusters: experiment and theory. *The Journal of Physical Chemistry* **1986,** *90* (12), 2555-2560.
48. Ehrlich, S., Spectroscopic studies of silver bromo-iodide crystals: Photoluminescence temperature dependence of iodide quantum clusters as tabular grain defects. *Journal of Imaging Science and Technology* **1997,** *41* (1), 13-29.
49. (a) Celebi, S.; Erdamar, A. K.; Sennaroglu, A.; Kurt, A.; Acar, H. Y., Synthesis and characterization of poly (acrylic acid) stabilized cadmium sulfide quantum dots. *The Journal of Physical Chemistry B* **2007,** *111* (44), 12668-12675; (b) Williams, A. T. R.; Winfield, S. A.; Miller, J. N., Relative fluorescence quantum yields using a computer-controlled luminescence spectrometer. *Analyst* **1983,** *108* (1290), 1067-1071.
50. Chan, CW. W.; Marwell, D. J.; Gao, X.; Bailey, E. R.; Han, M.; Nie, S., Luminescent quantum dots for multiplexed biological detection and imaging. *Current opinion in biotechnology*, **2002** *13*(1), 40-46.
51. Smith, A.; M., Nie, S., Chemical analysis and cellular imaging with quantum dots. *Analyst*, **2004** *129*(8), 672-677.

52. Fang Y. P., Topical delivery of DNA oligonucleotide to induce p53 generation in the skin via thymidine dinucleotide (pTT)-encapsulated liposomal carrier, *International Journal of Nanomedicine*, **2011** 6, 3373 –3381.
53. Zeng, X., Sun, Y.-X., Qu, W., Zhang, X.-Z., Zhuo, R.-X., Biotinylated transferrin/avidin/biotinylated disulfide containing PEI bioconjugates mediated p53 gene delivery system for tumor targeted transfection, *Biomaterials* **2010** 31, 4771-4780.

VITA

Didar Aşık was born in Bursa in 1990. She was graduated from Molecular Biology and Genetics department major and Chemistry in minor from Koç University in 2013. She was graduated from Materials Science and Engineering, Koç University in 2015.